Exploitation of host cellular pathways by *Chlamydia trachomatis*

D i s s e r t a t i o n

zur Erlangung des akademischen Grades
d o c t o r r e r u m n a t u r a l i u m
(Dr. rer. nat.)
im Fach Biologie

eingereicht an der
Mathematisch-Naturwissenschaftlichen Fakultät I
der Humboldt-Universität zu Berlin

von
Dipl.-Biol. Sebastian Banhart

Präsident der Humboldt-Universität zu Berlin
Prof. Dr. Jan-Hendrik Olbertz

Dekan der Mathematisch-Naturwissenschaftlichen Fakultät I
Prof. Dr. Andreas Herrmann

Gutachter: 1. Prof. Dr. Thomas F. Meyer
2. Prof. Dr. Thomas Sommer
3. Prof. Dr. Andreas Herrmann

Tag der mündlichen Prüfung: 19.12.2011

Todo começo é involuntário.
All beginnings are involuntary.

– Fernando Pessoa

Parts of this work have been or will be published under the following titles:

Banhart S.*, Mehlitz A.*, Mäurer A.P., Kaushansky A., Gordus A.G., Zielecki J., MacBeath G., Meyer T.F. 2010. Tarp regulates early *Chlamydia*-induced host cell survival through interactions with the human adaptor protein SHC1. *J Cell Biol*. 190(1):143-57. (* equal contribution)

Banhart S., Mehlitz A., Fuchs B., Schiller J., Heuer, D., Meyer, T.F. Global lipid analysis reveals essential role of cardiolipin synthase 1 for *Chlamydia* replication. (in preparation)

Table of contents

Abstract

The human pathogen *Chlamydia trachomatis* has evolved to strongly rely on the host due to its obligate intracellular replication and the acquisition of essential host cellular nutrients. This intimate relationship requires the efficient exploitation of both signaling and trafficking pathways of the host cell to ensure the pathogen's differentiation, replication, and protection from host immune responses, e.g., by inhibiting apoptosis.

Like many bacterial pathogens, *C. trachomatis* translocates effector proteins into the host cell to manipulate host cell functions. The early phase *C. trachomatis* effector protein Tarp harbors several N-terminal SH2 binding sites, which are rapidly tyrosine phosphorylated upon host cell entry, and a putative C-terminal SH3 binding site, both for the interaction with host cell proteins. To comprehensively and quantitatively assess these interactions, protein microarrays comprising virtually all human SH2 and SH3 domains were used. Numerous novel interactions between Tarp and human SH2 and SH3 domains were discovered. The adaptor protein SHC1 was among Tarp's strongest SH2-dependent interaction partners. Transcriptome analysis of SHC1-dependent gene regulation during infection indicated that SHC1 regulates apoptosis- and growth-related genes. SHC1-mediated cell survival and gene regulation was found to be controlled through both MEK/ERK-dependent and -independent signaling. SHC1 knockdown sensitized infected host cells to TNFα-induced apoptosis. These findings reveal a critical role for SHC1 in early *Chlamydia*-induced cell survival and suggest that Tarp functions as a multivalent phosphorylation-dependent and -independent signaling hub that is important during the early phase of chlamydial infection.

To acquire host-derived lipids such as cholesterol, sphingomyelin, glycerophospholipids, and neutral lipids, *C. trachomatis* hijacks both vesicular and nonvesicular trafficking pathways and modifies lipids during their translocation to the inclusion. To assess infection-dependent changes of the host cell lipid composition, infected cells were analyzed by MALDI-TOF mass spectrometry for their lipid content, providing a comprehensive list of lipid species existent in both infected and uninfected cells, as well as lipids only present in infected cells. Amongst these lipids, phosphatidylinositol and cardiolipin species were most prominently influenced by *C. trachomatis* infection, with infected cells harboring increased levels of lipids with comparably short fatty acids. Furthermore, phosphatidylinositol, phosphatidylethanolamine, phosphatidylglycerol, and cardiolipin species with a characteristic mass difference of 14 Da were detected during the course of infection, indicating the presence of *Chlamydia*-derived branched chain fatty acids and a role of cytosolic phospholipase A2 in this process. Accordingly, infection of cytosolic phospholipase A2 and cardiolipin synthase 1

knockdown cells resulted in a significantly reduced formation of infectious particles in these cells. These data demonstrate both the cardiolipin synthase 1 and the cytosolic phospholipase A2 to be key enzymes in the chlamydial lipid acquisition and emphasize the importance of cardiolipin and a functional nutrient supply for the successful propagation of *C. trachomatis*.

Taken together, the results of this work contribute to our knowledge of the pathogen's repertoire to exploit the host cell by actively subverting signaling and trafficking pathways.

Zusammenfassung

Das humanpathogene Bakterium *Chlamydia trachomatis* ist aufgrund seiner obligat intrazellulären Replikationsweise und der Gewinnung essentieller Nährstoffe aus der eukaryotischen Zelle in besonderem Maße auf seinen Wirt angewiesen. Diese enge Beziehung erfordert eine effiziente Nutzung von Signaltransduktionswegen und intrazellulären Transportrouten der Wirtszelle durch das Pathogen, um sowohl die eigene Differenzierung und Replikation sicherzustellen als auch die Immunantwort des Wirts zu umgehen, z.B. durch Apoptoseinhibierung.

Vergleichbar mit vielen bakteriellen Pathogenen überträgt auch *C. trachomatis* Effektorproteine in die Wirtszelle, um zelluläre Funktionen zu manipulieren. Das bereits zu Beginn der Infektion sekretierte Effektorprotein Tarp besitzt sowohl mehrere N-terminale SH2-Bindungsstellen, welche nach Translokation des Effektors in die Wirtszelle rasch tyrosinphosphoryliert werden, als auch eine putative C-terminale SH3-Bindungsstelle. Die Bindungsstellen dienen der Interaktion mit Wirtszellproteinen. Zur umfassenden Charakterisierung und Quantifizierung dieser Interaktionen wurden Protein-Microarrays verwendet, welche nahezu alle SH2- und SH3-Domänen humaner Proteine beinhalten. Dabei wurden zahlreiche neue Interaktionen zwischen Tarp und SH2- bzw. SH3-Domänen detektiert, wobei das Adaptorprotein SHC1 eine der stärksten SH2-abhängigen Interaktionen mit Tarp zeigte. Mittels Transkriptionsanalyse SHC1-abhängiger Genregulation während der Infektion konnten Gene identifiziert werden, welche an der Kontrolle von Apoptose- und Zellwachstumsprozessen beteiligt sind. Dabei zeigte sich, dass diese Gene sowohl über MEK/ERK-abhängige als auch -unabhängige Signaltransduktionswege reguliert werden. Infizierte Wirtszellen mit Knockdown von SHC1 wiesen eine erhöhte Apoptoserate nach Stimulation mit TNFα auf. Diese Ergebnisse offenbaren eine entscheidende Rolle von SHC1 im Kontext des frühen, Chlamydien-induzierten Überlebens der Wirtszelle und deuten darauf hin, dass Tarp als vielseitige, phosphorylierungsabhängige und -unabhängige Signaltransduktionsplattform dient, welche in der frühen Phase der Chlamydieninfektion von Bedeutung ist.

Um Wirtszelllipide – u.a. Cholesterol, Sphingomyelin, Glycerophospholipide und Neutrallipide – abzufangen und aufzunehmen, nutzt *C. trachomatis* sowohl vesikuläre als auch nicht vesikuläre intrazelluläre Transportrouten der Wirtszelle und modifiziert diese Lipide aktiv, bevor sie zur Inklusion transferiert werden. Zur Bestimmung dieser infektionsabhängigen Veränderungen der Lipidzusammensetzung der Wirtszelle wurde der Lipidgehalt infizierter Zellen mittels MALDI-TOF-Massenspektrometrie analysiert. Dies erlaubte eine umfassende Aufstellung der Lipidspezies, welche sowohl in infizierten und nichtinfizierten Zellen als auch ausschließlich in infizierten Zellen detektiert

wurden. Dabei hatte die Infektion den stärksten Einfluss auf bestimmte Phosphatidylinoslitol- und Cardiolipinspezies, wobei infizierte Zellen einen erhöhten Gehalt an Lipiden mit vergleichsweise kurzkettigen Fettsäureresten aufwiesen. Des Weiteren konnte im Infektionsverlauf ein Anstieg von Phosphatidylinositol-, Phosphatidylethanolamin-, Phosphatidylglycerol und Cardiolipinspezies mit einem charakteristischen Massenunterschied von 14 Da verzeichnet werden, was auf verzweigtkettige Fettsäurereste chlamydialen Ursprungs und eine Beteiligung der cytosolischen Phospholipase A2 hindeutet. Entsprechend zeigten infizierte Wirtszellen mit einem Knockdown der cytosolischen Phospholipase A2 oder der Cardiolipinsynthase 1 eine signifikant reduzierte Bildung infektiöser Bakterien. Dies zeigt, dass sowohl die Cardiolipinsynthase 1 als auch die cytosolischen Phospholipase A2 eine Schlüsselrolle in der chlamydialen Lipidaufnahme einnehmen und unterstreicht die Bedeutung von Cardiolipin und einer funktionsfähigen Nährstoffversorgung für die erfolgreiche Vermehrung von *C. trachomatis*.

Zusammenfassend erweitern die Ergebnisse dieser Arbeit unser Wissen über das Repertoire der Chlamydien bei der aktiven Nutzung von Signaltransduktionswegen und intrazellulären Transportrouten der Wirtszelle.

INTRODUCTION

1 Introduction

1.1 Chlamydiae

Chlamydiae are obligate intracellular, gram-negative bacteria, which exhibit a unique biphasic developmental cycle (Abdelraham and Belland, 2005). They infect a wide range of host organisms and account for a diversity of diseases in humans, such as infections of the urogenital tract, the eye, or the lung (Peeling and Brunham, 1996). Due to their intracellular lifestyle, chlamydiae have evolved to intimately interact with host cellular signaling and trafficking pathways to both acquire nutrients and ensure their own replication (Saka and Valdivia, 2010; Scidmore, 2011). Hence, the detailed investigation of chlamydiae and their close relationship to the host is of great biomedical relevance.

1.1.1 Taxonomy of *Chlamydia*

According to phylogenetic analyses based on 16S rRNA and 23S rRNA sequencing, the bacterial phylum Chlamydiae comprises the only order Chlamydiales consisting of the four families *Chlamydiaceae*, *Parachlamydiaceae*, *Waddliaceae*, and *Simkaniaceae* (Everett *et al.*, 1999; Bush and Everett, 2001). The family *Chlamydiaceae* harbors all human and animal pathogenic species and is subdivided into two genera, *Chlamydophila* and *Chlamydia*, which include the most important human pathogenic species, *Chlamydia trachomatis* and *Chlamydophila pneumoniae* (Figure 1-1).

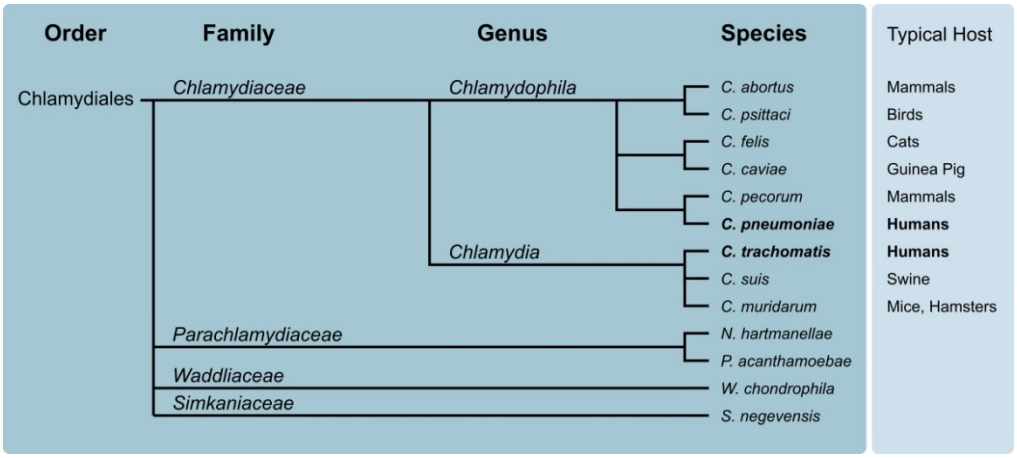

Figure 1-1. Taxonomy of the order *Chlamydiales*. Graphical representation showing the phylogenetic tree of the order Chlamydiales, which consists of four families: *Chlamydiaceae*, *Parachlamydiaceae*, *Waddliaceae*, and *Simkaniaceae*. The family *Chlamydiaceae* is divided into the two genera *Chlamydophila* and *Chlamydia*. Lines do not represent actual phylogenetic distances.

Recently, there have been efforts to reunite the family *Chlamydiaceae* into a single genus, *Chlamydia*, stating that this separation is neither widely used by the research community nor is it reflecting the natural history of the organism based on genome comparisons (Stephens *et al.*, 2009).

1.1.2 Pathology of *Chlamydia*

The species *C. trachomatis* is the leading cause of preventable blindness (trachoma) (Wright *et al.*, 2008) and responsible worldwide for up to 90 million cases per year of sexually transmitted disease (STD) (Brunham and Rey-Ladino, 2005). More than 15 serovars (serologically distinct variants) of *C. trachomatis* can be defined, showing different types of pathology, anatomical sites of infection, and tissue tropism (Grayston and Wang, 1975; Schachter, 1999; Stephens, 1999). The ocular serovars A to C infect mucosal epithelial cells of the conjunctiva, leading to trachoma. Transmission may occur by direct contact with eye, nose, and throat secretions from infected individuals, or by flies. Symptoms can range from mild inflammation to a strong inflammatory response. If not treated with antibiotics, chronic infection can lead to scarring of the eyelid and subsequent blindness through scratching of the cornea (Gambhir *et al.*, 2007). The urogenital serovars D to K cause STD by infecting mucosal epithelial cells of the urogenital tract. Most acute infections are asymptomatic and can lead to chronic inflammation of the urethra (urethritis), the rectum (proctitis), or the cervix (cervicitis) if not treated. Severe consequences of untreated ascending *Chlamydia* infections are pelvic inflammatory disease (PID), ectopic pregnancy, and infertility due to tubal scarring and occlusion. These complications are a main cause of preventable infertility in industrialized countries today (Schachter and Caldwell, 1980; Faro, 1985; Haggerty *et al.*, 2010). The more invasive serovars L1 to L3 cause Lymphogranuloma venereum (LGV), a sexually transmitted infection of lymphatics and lymph nodes. Comparable to urogenital serovars, the LGV serovars infect mucosal epithelial cells of the urogenital tract but additionally spread to regional lymph nodes by infecting macrophages, finally causing a systemic infection of lymphoid tissues. Symptoms of LGV are lymphadenopathy, including the retro-peritoneal lymph nodes in women or the inguinal lymph nodes in men. Chronic inflammation of these tissues can lead to lymphatic obstruction and lymphoid tissue destruction (Schachter and Osoba, 1983; Mabey and Peeling, 2002).

The species *C. pneumoniae* primarily infects epithelial cells of the upper and lower respiratory tract (Wreghitt, 1993). This airborne infection is mainly asymptomatic in the acute phase, though it accounts for approximately 10 % of community-acquired pneumonia and 5 % of pharyngitis, bronchitis, and sinusitis (Kuo *et al.*, 1995). *C. pneumoniae* infection has been associated with several

chronic diseases, e.g., asthma (Blasi *et al.*, 2009), artherosclerosis (Campbell and Kuo, 2004) or Alzheimer's disease (Shima *et al.*, 2010); however, these associations remain to be further clarified.

Once detected, *Chlamydia* infections can be effectively treated with antibiotics including tetracyclines, macrolides, and quinolones (Centers for Disease Control and Prevention, 2010). However, as infected people are frequently asymptomatic, the infection is often not diagnosed. Therefore, additional approaches, such as education on protected sexual intercourse or active screening for *Chlamydia* infections are of great importance (Belland *et al.*, 2004).

1.1.3 Developmental cycle of *Chlamydia*

All *Chlamydia* species exhibits a unique biphasic developmental cycle initiated by the infectious elementary bodies (EBs), which are metabolically inactive and have a diameter of up to 0.3 µm (Abdelraham and Belland, 2005). Infection starts with EBs attaching to the host cell (Figure 1-2, (1)). So far, attachment is described to be a two step process with a first reversible contact based on electrostatic interactions with heparan sulphate-like glycosaminoglycans, followed by a second, more specific attachment to a not specified host cell receptor (Dautry-Varsat *et al.*, 2005). Attachment is followed by uptake of the infectious particles via endocytosis or phagocytosis (Figure 1-2, (2)). Both clathrin-dependent and -independent pathways of bacterial entry are described (Dautry-Varsat *et al.*, 2005). Once engulfed by the host cell, EBs reside within a protective vacuole called the inclusion. The inclusion membrane is actively modified to prevent fusion with late endosomes or lysosomes, thereby avoiding lysosomal degradation (Ojcius *et al.*, 1997; Scidmore *et al.*, 2003). Among these modifications is the integration of bacterial Inc proteins into the membrane of the inclusion via a type III secretion system (Subtil *et al.*, 2001). The function of these proteins is widely unknown. However, IncA is described to be phosphorylated by host cell kinases and mediates the homotypic fusion of inclusions (Rockey *et al.*, 1997; Hackstadt *et al.*, 1999). IncG has been shown to recruit the protein 14-3-3β to the inclusion membrane (Scidmore and Hackstadt, 2001). The early inclusion gets translocated to a perinuclear, peri-Golgi site in the vicinity of the microtubule-organizing center (MTOC) within 6 h *post infectionem* (*p.i.*) (Hackstadt *et al.*, 1996; Grieshaber *et al.*, 2003). At 8 to 10 h *p.i.*, EBs differentiate into actively replicating reticulate bodies (RBs), the larger (1 µm diameter), metabolically active form of *Chlamydia*, which is not infectious (Mathews *et al.*, 1999) (Figure 1-2, (3)). The inclusion grows and RBs divide by binary fission (Abdelraham and Belland, 2005) (Figure 1-2, (5)). Sphingolipids, glycerophospholipids, and cholesterol are intercepted from the exocytic pathway between Golgi apparatus and host cell

membrane and guided to the inclusion (Hackstadt *et al.*, 1995; Wylie *et al.*, 1997; Carabeo *et al.*, 2003). The lipid acquisition was shown to be dependent on the activation of the cytosolic phospholipase A2 (cPLA2) via the mitogen-activated protein kinase (MAPK) pathway (Su *et al.*, 2004). Furthermore, *Chlamydia* induces fragmentation of the Golgi apparatus, thus leading to the formation of ministacks and supporting the efficient lipid acquisition (Heuer *et al.*, 2009). Apart from that, other essential nutrients like amino acids, nucleotides, and iron also have to be acquired (Karayiannis and Hobson, 1981; McClarty *et al.*, 1993; Al-Younes *et al.*, 2001).

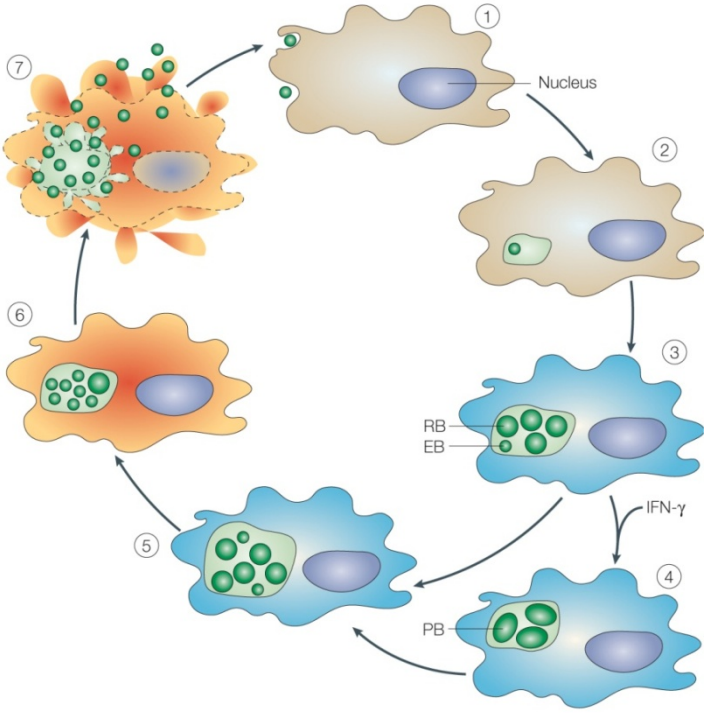

Figure 1-2. Developmental cycle of *Chlamydia*. The chlamydial developmental cycle starts with the attachment (1) and invasion of host cells (2), followed by the differentiation of EBs into RBs within the inclusion (3), intracellular replication of RBs (5), redifferentiation of RBs into EBs (6), and the final release of EBs from the host cell (7). An alternative pathway can occur during special environmental conditions (e.g., host cell activation by IFNγ), leading to the formation of PBs (4). Figure was modified from Byrne and Ojcius, 2004.

An alternative pathway can occur during special unfavorable environmental conditions (e.g., host cell activation by interferon gamma (IFNγ) or treatment with antibiotics), leading to the formation of persistent bodies (PBs) with a distinct change in morphology (de la Maza *et al.*, 1987) (Figure 1-2, (4)). This allows for a chronic long-term infection of the host cell. However, if the stimulus of persistence is omitted, *Chlamydia* can resume its developmental cycle of acute infection (Beatty *et al.*, 1993; Al-Younes *et al.*, 2001). Starting at 16 to 20 h *p.i.*, RBs eventually redifferentiate to form

EBs, a not synchronized process resulting in the presence of both bacterial forms in the chlamydial inclusion (Figure 1-2, (6)). Release of new infectious particles is achieved by lysis of the host cell (Abdelrahman and Belland, 2005) or a form of exocytosis (Beatty, 2007; Hybiske and Stephens, 2007) at 48 to 72 h *p.i.*, dependent on the chlamydial strain and species, and on growth conditions (Figure 1-2, (7)). Released EBs are then ready to infect new cells.

1.2 Protein secretion systems

Gram-negative bacteria are known to express and secrete host interactive proteins via type III or type IV secretion systems into the host cell cytoplasm to modulate host cell processes (Hueck, 1998; Christie *et al.*, 2005). These effector proteins enable the pathogen to undermine host cellular functions and pathways. Some of the effectors become phosphorylated upon host cell entry, such as the translocated intimin receptor (Tir) of enteropathogenic *Escherichia coli* (EPEC) (Kenny *et al.*, 1997) and the cytotoxicity associated gene A (CagA) of *Helicobacter pylori* (Asahi *et al.*, 2000).

1.2.1 Type III secretion system of *Chlamydia*

C. trachomatis uses a type III system to secrete numerous effector proteins (Valdivia, 2008). This needle-like structure enables *Chlamydia* to secret virulence-associated effector proteins into the host cell cytoplasm (Ghosh, 2004; Tampakaki *et al.*, 2004) (Figure 1-3).

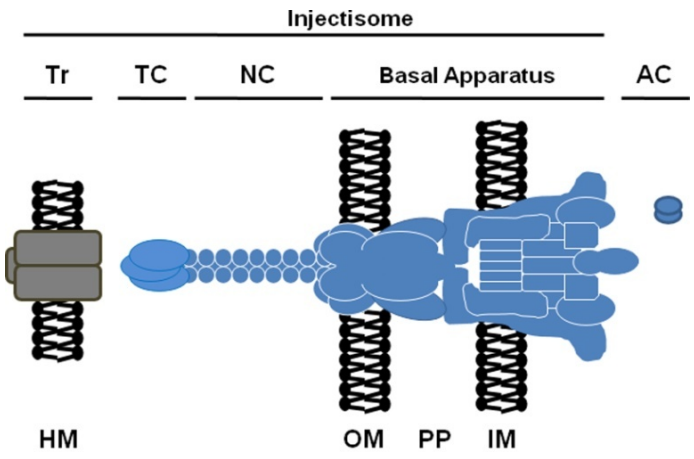

Figure 1-3. The type III secretion system. Scheme showing the components of the chlamydial type III secretion system (Tr, translocator complex; TC, tip complex; NC, needle complex; basal apparatus; AC, cytoplasmic ancillary proteins). The bacterial inner membrane (IM), periplasm (PP), and outer membrane (OM) are bridged by the basal apparatus (blue), while the secreted translocon components (gray) are localized at the host membrane (HM). Figure was modifed from Betts-Hampikian and Fields, 2010.

The most well characterized chlamydial effector, the translocated actin-recruiting phosphoprotein (Tarp), becomes tyrosine phosphorylated upon entry of *Chlamydia* into the host cell (Clifton *et al.*, 2004). To date, several host cell kinases have been implicated in Tarp phosphorylation including SRC, ABL, and SYK (Elwell *et al.*, 2008; Jewett *et al.*, 2008; Mehlitz *et al.*, 2008) and the number of Tarp phosphorylation sites varies between *Chlamydia* species and serovars (Jewett *et al.*, 2008).

1.2.2 The effector protein Tarp

Despite major difficulties in genetically manipulating *Chlamydia* species (Heuer *et al.*, 2007; Kari *et al.*, 2011), Tarp's function has been assessed using the heterologous type III secretion system of *Yersinia pseudotuberculosis* (Clifton *et al.*, 2004). This study revealed a critical role of Tarp in the actin-driven uptake of bacteria by host epithelial cells. Tyrosine phosphorylation of Tarp, however, appears to be uncoupled from actin polymerization because nonphosphorylated *C. pneumoniae* Tarp still induces actin polymerization (Clifton *et al.*, 2005). Furthermore, domain analysis of *C. trachomatis* Tarp based on truncated versions of the protein confirmed that actin recruitment and tyrosine phosphorylation involve distinct domains of Tarp (Jewett *et al.*, 2006). Actin polymerization is thought to be stimulated through oligomerization of a WAVE2-like actin binding domain in the C-terminus of the protein (Jewett *et al.*, 2006) and Tarp phosphorylation takes place at multiple N-terminal motifs (Jewett *et al.*, 2008). Phosphotyrosine-containing motifs are known to interact with SRC homology 2 (SH2) or phosphotyrosine binding (PTB) domains of signaling proteins (Schlessinger and Lemmon, 2003). Phosphorylation of Tyr179 and Tyr189 of Tarp has previously been implicated in recruiting the RAC guanine nucleotide exchange factor VAV2 and the regulatory subunit of phosphatidylinositol 3-kinase (PI3K) in an SH2-dependent manner (Lane *et al.*, 2008). These interactions are thought to participate in a redundant invasion mechanism. Nonetheless, a more comprehensive analysis of Tarp's interactions with host cellular proteins is necessary to establish the effector's functional repertoire and to further clarify the role of Tarp during the early phase of *Chlamydia* infection.

1.3 Host-pathogen interplay

Chlamydia has evolved a close relationship to its host, reflected by the efficient exploitation of host cellular signaling and trafficking pathways to ensure its intracellular replication and protection from host immune responses. This host-pathogen interplay has been investigated for major host cellular pathways, such as the MAPK pathway, the regulation of apoptosis, and the trafficking of lipids.

1.3.1 *Chlamydia* and the MAPK pathway

An important pathway modulating host cell apoptosis and survival is the RAS/RAF/MEK/ERK MAPK signaling cascade. This signaling cascade is one of the best studied signal transduction pathways and is connected with a variety of cellular functions. An initial extracellular signal is transmitted to the cell by the interaction of a ligand with its corresponding receptor tyrosine kinase (RTK). Upon this, the receptor's cytoplasmic domain is autophosphorylated and recruits adaptor proteins like the SRC homology-containing protein SHC1 via SH2 interactions (Figure 1-4).

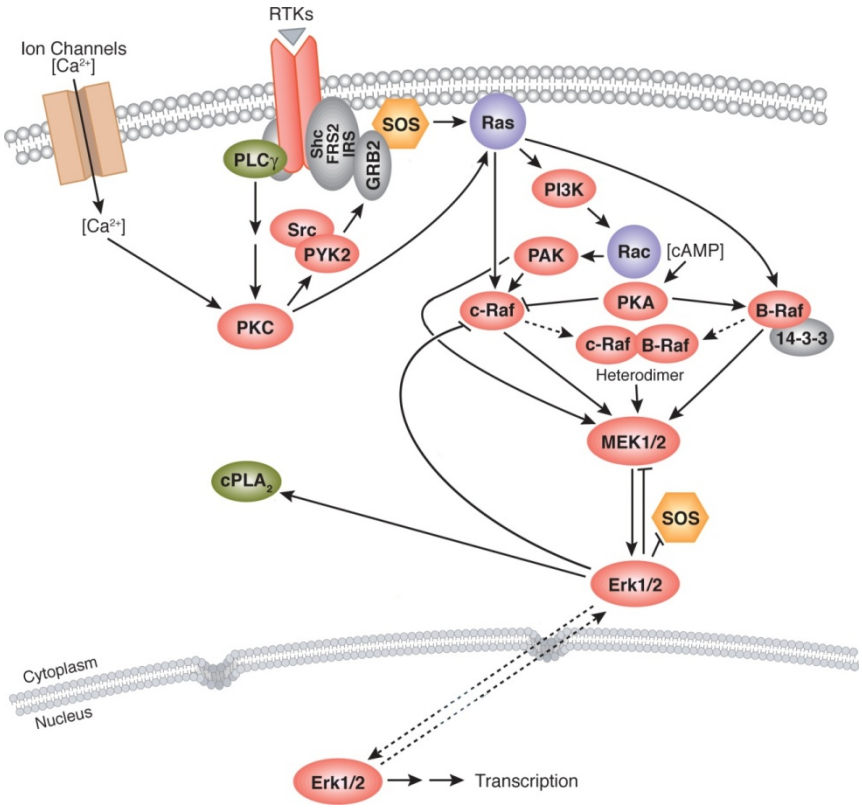

Figure 1-4. The MAPK pathway. Model representing the MAPK pathway, which starts with RTKs being activated by extracellular ligands, thus leading to tyrosine autophosphorylation of the receptor's cytoplasmic domain. Adaptor proteins like SHC1 bind to phosphorylated RTKs via SH2 interactions, recruiting other docking proteins such as GRB2. GRB2 activates the guanine nucleotide exchange factor SOS, which then drives the switch of inactive, GDP-bound RAS to active, GTP-bound RAS. Activated RAS promotes recruitment, heterodimerization, and activation of RAF, a kinase that phosphorylates and activates MEK. The kinase MEK then activates ERK, which controls gene transcription by regulating several transcription factors through phosphorylation. Figure was modified from Cell Signaling Technology, 2010.

The protein SHC1 represents a molecular adapter, linking extracellular signals to mitogenic responses (Pelicci *et al.*, 1992). SHC1 exists as three isoforms, all encoded by a single gene locus (Luzi *et al.*, 2000). The isoforms share a common domain composition: a C-terminal SH2 domain, an

N-terminal PTB domain, and a central collagen-homology domain (CH1) harboring several phosphorylation sites (Ravichandran, 2001). Interaction at these sites with growth factor receptor-bound protein 2 (GRB2), in conjunction with the RAS exchange factor SOS, activates the RAS/RAF/MEK/ERK pathway to induce a mitogenic response (van der Geer *et al.*, 1996). In detail, GRB2 activates the guanine nucleotide exchange factor SOS, which then drives the switch of inactive, GDP-bound RAS to active, GTP-bound RAS. Activated RAS promotes recruitment, activation, and heterodimerization of RAF, a kinase that activates the MAPK/ERK kinase MEK1/2 (Rushworth *et al.*, 2006; McCubrey *et al.*, 2007). Upon activation, MEK1/2 phosphorylates the extracellular signal-regulated kinase ERK1/2 at specific tyrosine/threonine residues, which then directly phosphorylates a variety of transcription factors including c-JUN, c-MYC, and nuclear factor κB (NF-κB).

Chlamydia infection was shown to activate ERK, followed by the downstream activation of cPLA2 (Su *et al.*, 2004), the induction of interleukin-8 (IL-8) (Buchholz and Stephens, 2008), TNF receptor 1 (TNFR1) shedding (Paland *et al.*, 2008), and stabilization of MCL-1 (Rajalingam *et al.*, 2008). Recent work has revealed that MEK/ERK activation is independent of RAS/RAF during mid and late *Chlamydia* infection (Gurumurthy *et al.*, 2010).

1.3.2 *Chlamydia* and apoptosis

Apoptosis is, among necrosis and autophagy, a type of cell death and fundamentally contributes to the balance between proliferation and the maintenance of constant cell numbers, e.g., during development and tissue homeostasis of multicellular organisms (Jaattela, 2002). Apoptosis occurs as a tightly defined process of irreversible effector caspase activation, resulting in the degradation of a series of substrates (Byrne and Ojcius, 2004). It is characterized by changes in cell morphology, such as cell shrinkage, pyknosis, plasma membrane blebbing, karyorrhexis, and formation of apoptotic bodies (Kerr *et al.*, 1972). During apoptosis, no neighboring cells are damaged and no inflammatory response is induced (Fink and Cookson, 2005). Two major pathways of apoptosis induction have been described: the extrinsic pathway (death receptor pathway) and the intrinsic pathway (mitochondrial pathway) (Figure 1-5).

In the extrinsic pathway, external death ligands like tumor necrosis factor alpha (TNFα) or FAS ligand (FASL) bind to their cognate receptors (members of the TNF receptor family), leading to caspase 8 activation (Locksley *et al.*, 2001). Type I cells show a high level of active caspase 8, which then directly activates effector caspase 3 (Hengartner, 2000). However, in type II cells, levels of active caspase 8 a comparably low. Therefore, these cells require the additional activation of the

mitochondrial pathway via Bid (Scaffidi *et al.*, 1999). The intrinsic pathway is triggered by intracellular stress, e.g., induced by radiation, toxins, hypothermia, or infections. BH3-only proteins act as stress sensors and trigger the activation of the BCL-2 family members Bax and Bak (Bouillet *et al.*, 2002). Bax and Bak oligomerize in the mitochondrial outer membrane, leading to the release of cytochrome c into the cytoplasm (Wei *et al.*, 2001; Willis and Adams, 2005). In type II cells, the activation of Bax and Bak is mediated by Bid, which itself gets cleaved by caspase 8 to form truncated Bid (tBid). Once cytochrome c is released, it binds to apoptosis activating factor-1 (APAF-1), forming a complex with caspase 9 (Hill *et al.*, 2004). This complex is called the apoptosome. Activated caspase 9 can now activate caspase 3, resulting in cellular apoptosis (Reed, 2000; Faherty and Maurelli, 2008). Substrates of active caspase 3 are, amongst others, cytokeratin 18 (CK18) or poly (ADP-ribose) polymerase (PARP).

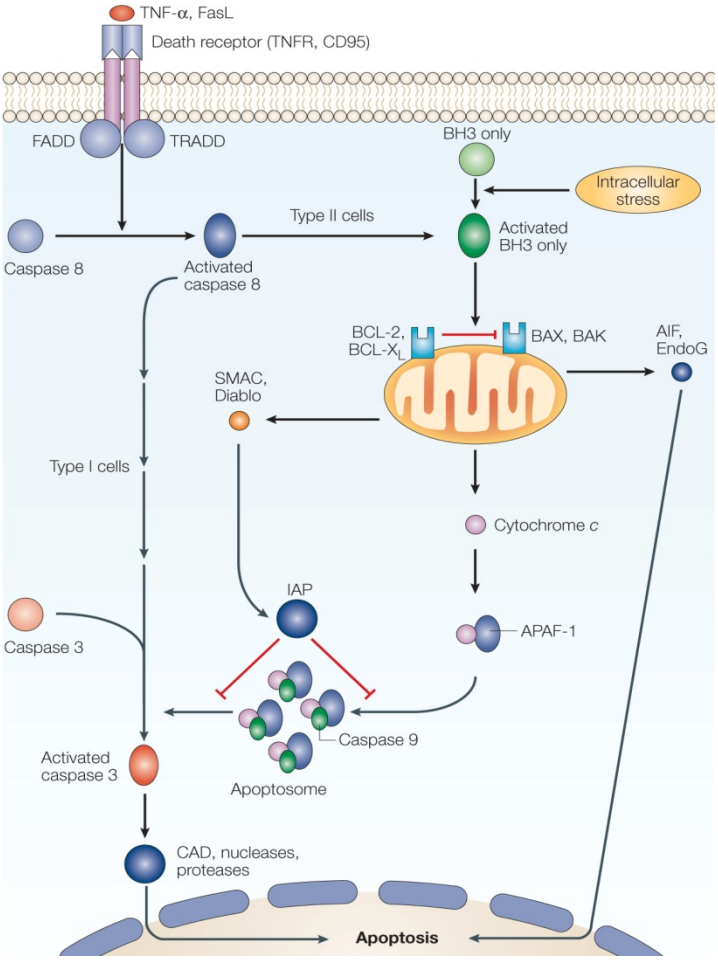

Figure 1-5. Major pathways of apoptosis induction. Model describing the two major apoptosis induction pathways: the extrinsic pathway (left side) and the intrinsic pathway (right side). While the extrinsic pathway (death receptor pathway) is triggered by external ligands, the intrinsic pathway (mitochondrial pathway) is caused by intracellular stress. Figure was modified from Byrne and Ojcius, 2004.

A prerequisite of *Chlamydia* replication is the pathogen's ability to prevent apoptosis of its host cell. *Chlamydia*-infected cells become resistant to numerous pro-apoptotic stimuli, including staurosporine, etoposide, TNFα, FAS antibody, and granzyme B/perforin (Fan *et al.*, 1998). Anti-apoptotic activity is thought to be conveyed by the proteolytic degradation of the pro-apoptotic BH3-only proteins BIM/BOD and PUMA, and by the mitochondrial sequestration of BAD during chlamydial infection (Fischer *et al.*, 2004). Alternatively, recent studies have implicated the anti-apoptotic BCL-2 family member MCL-1 as a key factor in preventing apoptosis (Rajalingam *et al.*, 2008). In addition, *Chlamydia* subverts the function of the pro-apoptotic protein kinase Cδ (PKCδ) by increasing diacylglycerol (DAG) levels in the chlamydial inclusion membrane (Tse *et al.*, 2005). Together, these observations suggest that *Chlamydia* prevents host cell apoptosis through a variety of mechanisms, likely acting sequentially as infection proceeds (Fan *et al.*, 1998; Perfettini *et al.*, 2002; Rajalingam *et al.*, 2008).

1.3.3 *Chlamydia* and nutrient acquisition

Due to the obligate intracellular lifestyle and extensive genome condensation of *Chlamydia*, the bacterium has evolved to rely on the host cell in acquiring lipids, amino acids, nucleotides, and other nutrients (Trentmann *et al.*, 2007; Saka and Valdivia, 2010) (Figure 1-5).

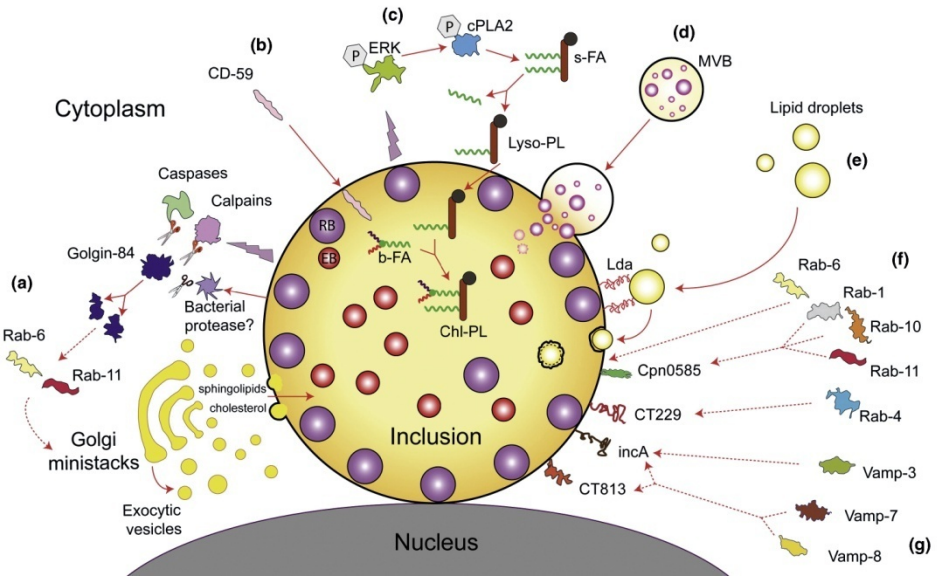

Figure 1-6. Host cell nutrient acquisition by *Chlamydia*. Model representing strategies of *Chlamydia* to exploit host cell pathways, including (a) Golgi fragmentation and subsequent association of Golgi ministacks with the inclusion, uptake of lipids via exocytic vesicles, (b) recruitment of CD59 to the inner side of the inclusion membrane, (c) cPLA2 activation and subsequent processing of host cell phospholipids to assist lipid translocation to the inclusion, (d) uptake of multivesicular

bodies via Lda, (e) translocation of lipids droplets, to the inclusion, (f) recruitment of Rab GTPases via Cpn0585 and CT229, and (g) recruitment of SNARE proteins (Vamp-3, Vamp-7, Vamp-8) via IncA and CT813. The following abbreviations are used: b-FA, *Chlamydia*-derived branched fatty acid; Lda, lipid droplet-associated protein; MVB, multivesicular body; PL, phospholipid. Figure was modified from Saka and Valdivia, 2010.

Recent findings reveal an intimate interaction between the inclusion and host cell organelles. Both Rab GTPases and SNARE proteins get recruited to the bacterial inclusion (Delevoye *et al.*, 2008; Paumet *et al.*, 2009; Rejman Lipinski *et al.*, 2009)). Further, lipids such as glycerophospholipids, sphingolipids, and cholesterol are acquired by re-routing Golgi-derived exocytic vesicles and multivesicular bodies (Wylie *et al.*, 1997; Beatty, 2006; Beatty, 2008; Moore *et al.*, 2008; Robertson *et al.*, 2009). This transport is based on the *Chlamydia*-induced fragmentation of the Golgi apparatus (Heuer *et al.*, 2009). Apart from this, Valdivia and colleagues were able to show the uptake of lipid droplets (neutral lipid storage vesicles) into the inclusion (Kumar *et al.*, 2006; Cocchiaro *et al.*, 2009).

1.3.4 *Chlamydia* and lipids

The acquisition of host-derived lipids such as cholesterol, sphingomyelin, glycerophospholipids, and neutral lipids is of major importance for the successful replication of *C. trachomatis*. For this purpose, the bacterium subverts both vesicular and nonvesicular trafficking pathways (Saka and Valdivia, 2010). Membranes of *Chlamydia* were shown to contain lipid classes that are associated with eukaryotic membranes and to reflect the host cell lipid composition (Hatch and McClarty, 1998a). Among these lipids are phosphatidylcholine (PC) and phosphatidylinositol (PI), which are normally derived from the endoplasmic reticulum, and cardiolipin (CL) (Wylie *et al.*, 1997). CL is a structural and functional component found exclusively in mitochondrial membranes (Hatch, 1998). It is linked with mitochondrial energy production, since several enzymes involved in energy metabolism require CL for full enzymatic function and structural stability (Eble *et al.*, 1990; Hatch, 1998; Gomez and Robinson, 1999). CL has also been associated with targeting tBid to mitochondria, thereby contributing to cytochrome c release during apoptosis (Lutter *et al.*, 2000). Formation of CL is catalyzed by the cardiolipin synthase 1 (CRLS1) from phosphatidylglycerol and CDP-diacylglycerol (Schlame, 2008). The enzyme is localized to the inner membrane of mitochondria and is expressed in HeLa cells (Chen *et al.*, 2006; Lu *et al.*, 2006). Interestingly, no homolog of CRLS1 can be found in *C. trachomatis*.

Furthermore, *Chlamydia* induces the modification of lipids during their translocation to the inclusion. Host-derived glycerophospholipids are deacylated at the *sn*-2 position of the glycerol backbone and

the remaining lysophospholipid gets modified by addition of a *Chlamydia*-derived branched chain fatty acid to the *sn*-2 position (Wylie *et al.*, 1997). The host enzyme cPLA2 was shown to be responsible for the *sn*-2 deacylation, and pharmacological cPLA2 inhibition reduces glycerophospholipid uptake and bacterial replication (Su *et al.*, 2004). Additionally, *Chlamydia* activates cPLA2 via the MAPK pathway (Su *et al.*, 2004; Vignola *et al.*, 2010).

Taken together, several studies demonstrate the modulation of host cell trafficking and lipid metabolism by *Chlamydia*, indicating that the pathogen is highly dependent on these components. However, the central mechanisms and key molecules of these processes remains to be investigated.

1.4 Aim of this study

The scope of this thesis was to further dissect the repertoire of *C. trachomatis* to exploit the host cell and actively subvert signaling and trafficking pathways – by identifying novel factors involved in both the invasion process and the pathogen's nutrient acquisition.

In the first part of this study, a systematic approach was performed to discover and quantify phosphorylation-dependent and -independent interactions between the bacterial effector protein Tarp and host cell SH2 and SH3 domain-containing proteins. To comprehensively assess these interactions, protein microarrays comprising virtually all human SH2 and SH3 domains were used. Detected interactions were validated by means of biochemical, microscopic, and computational methods and analyzed for their involvement in host cell signaling. Moreover, SH2 and SH3 interactome data were globally studied for their participation in major cellular processes. Combining the knockdown of interaction partners with subsequent transcriptional profiling during infection allowed for the identification of specifically regulated genes and their further functional characterization.

In the second part of this study, changes in host cell lipid composition during *C. trachomatis* infection were globally studied by mass spectrometry to gain a better understanding of their significance for the pathogen's survival and replication. Lipid species showing a prominent change during infection were selected for further analysis. The knockdown of genes involved in biosynthesis and trafficking of these lipids revealed their impact on chlamydial growth and progeny formation.

MATERIALS AND METHODS

2 Materials and methods

2.1 Materials and general methods

2.1.1 Cell lines and bacteria

HeLa (ATCC no. CCL-2) and End1/E6E7 (ATCC no. CRL-2615), both human cervical epithelial cells, and HEp-2 (ATCC no. CCL-23), human laryngeal epithelial cells, were grown in DMEM (Invitrogen, Germany) supplemented with 10 % (v/v) fetal calf serum (FCS), 5 mM L-glutamine, and 1 mM sodium pyruvate (Invitrogen, Germany). *Chlamydia trachomatis* LGV biovar strain L2/434/Bu (ATCC no. VR-902B, strain collection no. C2), *C. trachomatis* trachoma type D strain UW-3/Cx (ATCC no. VR-885, strain collection no. C4), and *Chlamydophila pneumoniae* TWAR strain CDC/CWL-029 (ATCC no. VR-1310, strain collection no. C1) were purified from confluent HeLa monolayers. In brief, HeLa cells were grown to 80 % confluency and were inoculated for 2 h with the respective *C. trachomatis* strain. For infections with *C. pneumoniae*, inoculated cells were incubated at 22°C for 1 h on a shaker, centrifuged (500 rpm at 35°C) for 1 h and then incubated for 2 h at 35°C. The medium was replaced by infection medium (DMEM, 5 % (v/v) FCS, 5 mM L-glutamine, 1 mM sodium pyruvate, 1 µg/ml cycloheximide) and growth was allowed for 48 h. Cells were mechanically detached and bacteria were released using 2-5 mm glass beads (Carl Roth, Germany). Low speed supernatant (5 min at 4000 *g* and 4°C) was subjected to high speed centrifugation (25 min at 40000 *g* and 4°C) to pellet the bacteria. Bacteria were washed twice with 10 ml SPG storage buffer (220 mM sucrose, 50 mM sodium phosphate, 5 mM glutamate, pH 7.4), aliquoted, and stored at -80°C in SPG.

2.1.2 Reagents, antibodies and constructs

Chemicals were obtained from Sigma-Aldrich (Germany). Recombinant human TNFα (554618) was obtained from BD Biosciences (USA). Antibodies against β-actin (sc-7210), cortactin (3503), ERK1/2 (9108), p-ERK1/2 (9106), MEK1/2 (9122), p-MEK1/2 (9121), PARP-1/2 (sc-7150), SHC (sc-967 and sc-288), p-SHC Tyr239/240 (sc-18074-R), p-Tyr PY99 (sc-7020), NCK1/2 (sc-290), cPLA2 (2832), and GST (sc-34072) were acquired from Santa Cruz (USA), or Cell Signaling (USA). Antibodies against the M30 epitope of cleaved CK18 (ALX-804-590-T200) and against bacterial Hsp60 (804-071-R100) were obtained from Enzo Life Sciences (USA). Secondary Cy2-conjugated antibodies against rabbit IgG (111-225-144), mouse IgG (115-225-146), and Cy5-conjugated antibodies against rabbit IgG (111-175-144) and mouse IgG (115-175-146) were obtained from Jackson ImmunoResearch Laboratories (USA). Alexa Fluor 532 phalloidin for staining of actin was obtained from Invitrogen

(Germany). Antiserum against Tarp was raised by immunization of rats with GST-Tarp fusion protein (Biogenes, Germany). Monoclonal anti-*Chlamydia* OMP1 was obtained from University of Washington (USA). GST-Tarp was constructed by PCR amplification of nucleotides 6-818 of *C. trachomatis* LGV L2 Tarp or 1-939 of *C. trachomatis* D Tarp and ligation of the product into pGEX4T-3 (GE Healthcare, USA) using dinucleotide sticky-end cloning (strain collection no. H3792 and H3838). Purification of GST-Tarp was performed according to the manufacturer's instructions using glutathione sepharose (GE Healthcare, USA). pEGFP-C1-RBD_{RAF-1} (strain collection no. H3972) and pmCherry-C1-HRAS (strain collection no. H3974) were obtained from Mark R. Phillips (NYU).

2.1.3 Infection time courses

For Western blot analysis, HeLa or End1/E6E7 cells were seeded into 12-well plates at a density of 60-70 %. Cells were serum starved for 24 h in serum-free growth medium before performing infection time course experiments. Infection was performed at indicated multiplicity of infection (MOI) with either bacteria or control mock infected cells (i.e., treated with SPG). *C. pneumoniae* infections were synchronized by centrifugation for 1 h at 500 *g* and 4°C and shifting to 35°C. Infection was stopped at the indicated time points by removing the medium, rinsing quickly with prewarmed PBS and immediately lysing in SDS loading buffer at 94°C for 5 min. For lipid analysis, HeLa or HEp-2 cells were seeded in T75 flasks at a density of 1.5 x 10^6 cells per flask. Infection was carried out with an MOI of 2.5 according to Figure 3-32. Prior to infection and prior to lipid analysis, cell numbers were counted manually.

2.1.4 Statistical analysis

Statistical significance was determined using Student's *t* test. In case of the gene enrichment analysis (Figure 3-23), Fisher's exact test was used to determine statistical significance. P-values below 0.05 were defined as significant.

2.2 DNA techniques

2.2.1 Transfections

siRNA transfection of HeLa cells was carried out using Lipofectamine 2000 (Invitrogen, Germany) according to the manufacturer's instructions. siRNA against SHC1, CRLS1 (both SMARTpool, Thermo Fisher Scientific, Germany), cPLA2 (QIAGEN, Germany), or luciferase (QIAGEN, Germany) were used.

Knockdown was confirmed via quantitative real-time PCR (qRT-PCR) or Western blotting 72 h after transfection. Plasmid transfection (pEGFP-C1-RBD_{RAF-1} and pmCherry-C1-HRAS) of HeLa cells was performed with Lipofectamine 2000 (Invitrogen, Germany) according to the manufacturer's instructions. Live-cell microscopy experiments were carried out 48 h after transfection.

2.2.2 DNA microarrays and analysis

RNA from infected, uninfected, or transfected (and infected) HeLa cells was isolated with the RNAeasy Kit (QIAGEN, Germany) according to the manufacturer's instructions. RNA integrity was analyzed using a Bioanalyzer 2100 (Agilent Technologies, USA). DNA microarray experiments were performed as two-color dye-reversal ratio hybridizations on arrays containing 44000 human genes (AMADID 010646, Agilent Technologies, USA) in biological duplicates. RNA labeling was performed with a Fluorescent Linear Amplification kit (Agilent Technologies, USA). Labeling efficiency was verified with a Nanodrop photometer (Kisker Biotech, Germany). Before hybridization, cDNA was fragmented and mixed with control targets and hybridization buffer according to the manufacturer's instructions (Agilent Technologies, USA). Hybridizations were performed overnight (~17 h) at 60°C. Slides were washed according to the manufacturer's instructions and scanning of microarrays was performed at 5 µm resolution using a microarray laser scanner (Agilent Technologies, USA).

Data analysis was performed on the Rosetta Resolver system 7.2 (Rosetta Biosoftware, USA). Ratio profiles were generated from raw scan data by a processing pipeline, which includes preprocessing (feature extraction) and postprocessing (Rosetta Resolver) of data and error model adjustments to the raw scan data. Ratio profiles were combined in an error-weighted fashion (Rosetta Resolver) to create ratio experiments. Expression patterns were identified using stringent analysis criteria of 1.6-fold expression cutoffs of the ratio experiments and an anti-correlation of the dye reversal ratio profiles. Anti-correlation was determined by using the compare function to match two different hybridizations pairs and to decide how similar or dissimilar they were. By combining the first and the second criteria of analysis, data points with a low p-value ($p < 0.01$) were filtered out, making the analysis robust and reproducible. Additionally, by using this strategy the data selection was independent of error models implemented in the Rosetta Resolver system.

2.2.3 qRT-PCR analysis

For qRT-PCR, mRNA from HeLa cells was isolated with the RNAeasy Kit (QIAGEN, Germany) according to the manufacturer's instructions. 10 µl mRNA was DNaseI digested with RNase-free DNaseI

(Fermentas, Germany) according to the manufacturer's instructions. Digested mRNA was phenol/chloroform purified. In brief, 180 µl of RNase free water (Synergy Ultrafiltration System, Millipore, USA) and 200 µl of phenol/chloroform (Carl Roth, Germany) were added to the 20 µl digestion reaction and vortexed. Samples were phase separated at 12000 *g* (4°C for 10 min) and the supernatant was combined with 200 µl of chloroform followed by vortexing. After repeated phase separation mRNA was precipitated using 0.1 vol. of 3 M sodium acetate and 2 vol. of 80 % (v/v) ethanol followed by centrifugation at 14000 *g* (4°C for 15 min). The supernatant was removed and the pellet was air dried in a clean bench environment and resuspended in 50 µl of RNase free water. mRNA was reverse transcribed using the Revert Aid First Strand Synthesis kit (Fermentas, Germany) according to the manufacturer's instructions and was diluted 1:10 with RNase free water. qRT-PCR was set up with Absolute QPCR SYBR Green Mix (Thermo Fisher Scientific, Germany) according to the manufacturer's instructions. qRT-PCR was performed on a Step One Plus device (Applied Biosystems, USA) and data were analyzed using the $\Delta\Delta C_t$ method, Step One Plus software package (Applied Biosystems, USA), and Microsoft Excel. Endogenous controls were GAPDH and L13a. Splice variant specific primers were designed using National Center for Biotechnology Information (NCBI) Primer Blast or Primer 3 (Rozen and Skaletsky, 2000) (Table 2-1).

Table 2-1. qRT-PCR primers. List shows the PCR primers used in this study for amplification in qRT-PCR. Primers were chosen as described above.

Primer	Sequence (5' to 3')	Length (bp)	Start (bp)	Stop (bp)	T_m (°C)	GC (%)	Product length (bp)
TEK forward	GTGCTGTTCCTTCTTGCCTC	20	300	319	60.0	55.0	117
TEK reverse	TCCACAAATGTGCATGAGGT	20	416	397	60.0	45.0	
BMF forward	AGTCAAACTTTGTGACCGGC	20	58	77	60.2	50.0	148
BMF reverse	AGTAGGCTCTGGGCAAACAG	20	205	186	59.5	55.0	
EGR1 forward	GACCGCAGAGTCTTTTCCTG	20	570	589	60.0	55.0	110
EGR1 reverse	AGCGGCCAGTATAGGTGATG	20	679	660	60.1	55.0	
FST forward	ATCTTGCAACTCCATTTCGG	20	969	988	60.1	45.0	115
FST reverse	CACTGAACACTTATAGAGAGTTTACCA	27	1083	1057	57.4	37.0	
PHLDA1 forward	GGCAAGACAAGGTTTTGAGG	20	176	195	59.7	50.0	139
PHLDA1 reverse	CGCCAAGTTGTTCAGTAGGG	20	314	295	60.7	55.0	
CXCL1 forward	GAAAGCTTGCCTCAATCCTG	20	325	344	60.0	50.0	107
CXCL1 reverse	CACCAGTGAGCTTCCTCCTC	20	431	412	60.0	60.0	
DKK1 forward	ATCATAGCACCTTGGATGGG	20	636	655	59.8	50.0	112
DKK1 reverse	CCTGAGGCACAGTCTGATGA	20	747	728	60.0	55.0	

SDC4 forward	GTCTGGCTCTGGAGATCTGG	20	220	239	60.0	60.0	139
SDC4 reverse	TAGTTTCTTGGGTTCGGTGG	20	358	339	60.0	50.0	
MAP2K3 forward	ATTAGTCAGGCAGGGCAGTG	20	81	100	60.3	55.0	105
MAP2K3 reverse	GGACTCCAGGGCCTTATCTC	20	185	166	60.0	60.0	
FLI1 forward	CGAGAGGAGAGTCATCGTCC	20	701	720	59.9	60.0	107
FLI1 reverse	TGTCGATCTCCATCAAGCTG	20	807	788	59.9	50.0	
CRLS1 forward	CCATGGACAATCCCGAATATG	21	470	490	50.7	47.6	75
CRLS1 reverse	TTCAATAATCAAATAGCCCAGAACTG	26	544	519	52.0	34.6	

2.3 Protein techniques

2.3.1 Peptide synthesis and protein microarrays

For SH2/PTB interactome analysis, peptides representing the Tarp phospho-sites were synthesized as described (Jones *et al.*, 2006), purified to > 95 % by preparative reverse phase high-performance liquid chromatography (HPLC), quality controlled via matrix-assisted laser desorption/ionization time-of-flight (MALDI-TOF) mass spectrometry (Thermo Fisher Scientific, Germany), and labeled on their N-termini with 5-(and 6)-carboxytetramethylrhodamine (5(6)-TAMRA) from Anaspec (San Jose, USA). For SH3 interactome analysis, peptides representing the Tarp SH3 binding site were synthesized, purified to > 95 %, and N-terminally biotinylated (Thermo Fisher Scientific, Germany).

MacBeath and colleagues have previously described cloning, expressing, and purifying virtually every human SH2 and PTB domain, as well as preparing microarrays of these domains on chemically-derivatized glass surfaces (MacBeath and Schreiber, 2000; Jones *et al.*, 2006). In brief, the coding regions for each domain were cloned from human cDNA and the corresponding proteins were produced recombinantly in *E. coli* using the T7 expression system. Each domain features an N-terminal His_6-tag, as well as a thioredoxin-tag to facilitate the high-level production of soluble protein. After purifying each domain from large-scale bacterial culture (0.5 l), purity was controlled by SDS-polyacrylamide gel electrophoresis (SDS-PAGE) and its aggregation state by size exclusion column chromatography. In the current version of the arrays, domains that were impure or did not contain soluble, monomeric protein were eliminated. Notably, SH2 domains derived from the signal transducers and activator of transcription (STAT) and suppressors of cytokine signaling (SOCS) families of proteins did not behave well. By cloning larger portions of STAT1 and STAT2 that included their entire SH2 domain-containing cores (Mao and Chen, 2005), soluble, monomeric material for these two proteins were obtained. In addition, the N-terminal domain of CBL (Meng *et al.*, 1999),

which contains a noncanonical SH2 domain was cloned, expressed, and purified. In total, 133 domains representing 103 proteins were used in this study.

To facilitate the rapid and automated processing of the SH2/PTB protein microarrays, a NanoPrint microarrayer (TeleChem International, USA) was used to spot the proteins in quadruplicate on aldehyde displaying glass substrates, cut to the size of a microtiter plate (112.5 mm x 74.5 mm x 1 mm) (Erie Scientific, USA). 96 separate arrays were prepared on each glass substrate, and the glass was attached to the bottom of a bottomless microtiter plate using an intervening silicone gasket (Grace Bio-Labs, USA). Two 16 × 17 microarrays were required to accommodate all 133 domains, as well as the appropriate controls (His_6-tagged thioredoxin and buffer). Proteins were spotted in quadruplicate at a high concentration (40-200 µM), and a low concentration (200 nM) of cyanine 5-labeled bovine serum albumin (BSA) was included in each sample to facilitate image analysis. Arrays were stored at -80°C before use.

Immediately before use, plates were quenched with buffer A (20 mM HEPES, 100 mM KCl, 0.1 % (v/v) Tween-20, pH 7.8) containing 1 % (w/v) BSA for 30 min at room temperature, followed by several rinses with buffer A. Arrays were probed with eight different concentrations of labeled peptides (5 µM, 3 µM, 2 µM, 1 µM, 500 nM, 200 nM, 100 nM, and 10 nM) dissolved in buffer A. Peptide solution was removed after a 1 h incubation at room temperature and arrays were washed with 150 ml of buffer A for 10 s. Arrays were rinsed briefly with double-distilled H_2O (ddH_2O) and spun upside down in a centrifuge for 1 min to remove residual water.

SH2/PTB protein microarrays were scanned at 10 µm resolution using an LS400 scanner (Tecan, Austria). Spots were defined using the Cy5 image and the mean fluorescence of each spot was calculated from the 5(6)-TAMRA image. It has previously been shown that probing a protein microarray with a single concentration of a labeled probe can produce very misleading results (Gordus and MacBeath, 2006). Therefore, the arrays were probed with eight concentrations of each peptide and fit the resulting spot intensities, F_{obs}, to the following equation:

(1)

where F_0 is the background fluorescence, F_{max} is the maximum fluorescence at saturation, [*pep*] is the total peptide concentration, and K_D is the equilibrium dissociation constant. This procedure was performed for each peptide/domain interaction. Interactions were considered specific if the data fit

well to equation (1) (R^2 > 0.9), with K_D < 2 µM and F_{max} at least twofold higher than the mean fluorescence of control spots (His_6-tagged thioredoxin). The resulting data were displayed graphically using the Cytoscape 2.1 software (Shannon *et al.*, 2003).

For SH3 interactome analysis, protein microarrays (TranSignal SH3 domain arrays, Panomics, USA) consistent of 117 SH3 domains in duplicate were acquired from Panomics (USA) and probed with peptides according to the manufacturer's instructions. In brief, 750 ng of biotin-conjugated peptide (wild type or mutated version) were mixed with 15 µg streptavidin-HRP conjugate (Amersham, USA) and incubated with the SH3 protein microarrays. Each SH3 domain was spotted in duplicate on the membrane. Signal detection was performed using ECL/Hyperfilm (Amersham, USA). Quantification was carried out using ImageJ (Girish and Vijayalakshmi, 2004) and Microsoft Excel. Interactions with at least 25 % of the signal intensity of the positive control (biotin) and a minimum signal decrease of 50 % between wild type and mutated peptide were defined as hits.

2.3.2 Pull-down assays and immunoblotting

GST-Tarp was phosphorylated while the beads coupled to glutathione sepharose (Pharmacia, USA). In brief, GST-Tarp beads were incubated for 30 min at 30°C with recombinant human c-SRC (Cell Signaling, USA) in kinase buffer (25 mM HEPES, pH 7.0, 150 mM NaCl, 10 mM $MgCl_2$, 1 % (v/v) Nonident P40, 5 mM dithiothreitol, 1 mM Na_3VO_4, 1x COMPLETE protease inhibitors, 6 mM ATP). GST-Tarp beads were washed three times with PBS and incubated with lysate from 10^7 cells (50 mM Tris, pH 7.5, 150 mM NaCl, 1 % (v/v) Nonident P40, 0.5 % (w/v) sodium deoxycholate, 1x COMPLETE protease inhibitors) for 2 h at 4°C. Proteins were eluted by incubation with 20 mM of reduced glutathione in 50 mM Tris, pH 8.0. Immunoprecipitation and Western blotting were performed according to standard procedures (Sambrook and Russel, 2001). Signal detection was performed using ECL/Hyperfilm (Amersham, USA). Quantification was carried out using ImageJ (Girish and Vijayalakshmi, 2004) and Microsoft Excel.

2.4 Lipid techniques

2.4.1 Lipid extraction

The method of lipid extraction is adopted from Folch *et al.*, 1957. In brief, cells were washed once with 10 ml PBS and scraped off in 5 ml PBS per flask. The cell suspension was centrifuged (20 min at 200 *g* and 4°C) in glass tubes and pellets were resuspended in 1 vol. chloroform/methanol (2:1).

After sonicating the cells for 20 min, tube walls were rinsed with 1 vol. chloroform/methanol (2:1) and the mixture was shaken vigorously for 4 h at RT. Subsequently to addition of 0.4 vol. ddH_2O, the mixture was again shaken several times and incubated overnight at 4°C. The lower phase was removed and 1 vol. chloroform/methanol (2:1) was added to the remaining upper phase. The mixture was shaken and centrifuged (20 min at 200 *g* and 4°C). Again, the lower phase was removed and the combined lower phases were washed with 0.2 vol. ddH_2O. After phase separation, the lower phase was transferred to a new glass tube and the solvent was evaporated under a stream of nitrogen. Extracted lipids were dissolved in 100 µl chloroform, transferred to small glass tubes and chloroform was evaporated using a SpeedVac concentrator system. Finally, the extracted lipids were dissolved in 15 µl chloroform.

2.4.2 MALDI-TOF mass spectrometry

Two approaches were applied: 1. the direct MALDI-TOF measurement of lipids in the crude lipid extract, and 2. the separation of lipids by normal phase thin-layer chromatography (TLC) according to their head group followed by MALDI-TOF measurement of lipids directly on the TLC plate. In case of direct measurement, lipid samples were mixed with an equal volume of matrix solution (0.5 M 2,3-dihydroxy benzoate, 0.1 % (v/v) trifluoroacetic acid in methanol) and 2 µl aliquots were spotted on gold-coated MALDI target plates. In the second approach, lipid samples and a lipid standard (containing phosphatidylglycerol (PG), phosphatidylethanolamine (PE), phosphatidic acid (PA), phosphatidylinositol (PI), phosphatidylserine (PS), phosphatidylcholine (PC), sphingomyelin (SM), and lysophosphatidylcholine (LPC)) were spotted on an aluminum base TLC plate (Merck, Germany). Normal phase TLC was performed using a mixture of chloroform/ethanol/ddH_2O/triethanolamine (30:35:7:35) as running buffer. Subsequently, the TLC plate was dried and stained with primuline. Spots were visualized with UV light, marked, and matrix solution (100 mg/ml 2,3-dihydroxy benzoate in acetonitril/ddH_2O (1:1)) was added. Finally, the TLC plate was fixed on a gold-coated MALDI target plate.

All MALDI-TOF mass spectra were acquired using a Bruker Autoflex workstation (Bruker Daltonics, Germany). This system uses a 337 nm pulsed nitrogen laser with an extraction voltage of 20 kV. For each mass spectrum, 128 single laser shots were averaged. Spectra were acquired in the reflector mode using delayed extraction conditions to improve the spectral resolution. Processing and analysis of the acquired spectra was done using the Flex Analysis software (Bruker Daltonics, Germany). More details on the methodology are given in Schiller *et al.*, 2004.

2.5 Microscopy

2.5.1 Immunofluorescence staining and microscopy

For immunofluorescence cells were either seeded in 24- or 12-well plates with or without coverslips and were infected in a humidified incubator at 35°C and 5 % (v/v) CO_2 with MOI indicated in the respective experiments. Cells were fixed at indicated time points with 4 % (w/v) PFA, washed once with PBS and stained. In brief, cells were permeabilized with 0.2 % (v/v) Triton X-100 or 0.1 % (v/v) saponin in PBS for 30 and 10 min, respectively, and were washed three times with PBS for 5 min at RT. Cells were blocked with 2 % (v/v) FCS in PBS for 45 min and were stained with primary antibodies diluted in 2 % (v/v) FCS in PBS for 1 h at RT. After three times washing with PBS, samples were incubated with secondary antibodies for 1 h in blocking solution at RT in the dark. After one short wash with ddH_2O, samples were mounted with Mowiol 4-88 (Carl Roth, Germany) and visualized at RT on a Leica TCS SPE confocal microscope (photomultiplier equipped) at 63x magnification (HCX Plan-Apochromat with a 63x/1.40-0.60 oil objective lens) using the Leica LAS AF TCS SPE acquisition software. Data were processed with Adobe Photoshop (adjustment of brightness and contrast identical for all images).

2.5.2 Live-cell fluorescence microscopy

HeLa cells were seeded in 3.5 cm^2 glass-bottom dishes (MatTek, USA) and transfected with pEGFP-C1-RBD_{RAF-1} and pmCherry-C1-HRAS as described above. After 24 h, cells were washed twice with PBS and incubated in serum-free medium overnight. The next day, fresh serum-free medium was added and cells were monitored in a humidified incubation chamber at 37°C and 5 % (v/v) CO_2. Image acquisition was done at 60x magnification (Olympus UPlanFL N 60x/1.25 NA lens) with an Olympus IX81 microscope equipped with a Hamamatsu C9100-02 CCD camera. Images were processed using the Metamorph software (Molecular Devices, USA).

2.6 Other methods

2.6.1 Invasion, inclusion formation, and progeny assays

For measurement of invasion efficiency, inclusion formation, and progeny formation, HeLa cells were seeded in 12-well plates and were siRNA transfected as described above. On day 2 cells were split into three separate wells and then infected on day 4 at MOI 50 for invasion assays or MOI 1 for

inclusion formation and progeny counts. Invasion assays were stopped at 1 and 10 h *p.i.*, cells were fixed with ice-cold methanol overnight at -20°C, stained for OMP1 and DNA (Hoechst 33342) and analyzed by automated microscopy (Olympus Scan^R system consisting of an Olympus IX81 inverted microscope, Hamamatsu charge-coupled device (CCD) camera (model C4742-80-12AG) and the Scan^R acquisition software) at 10x magnification (Olympus UPlanS Apo 10x/0.40 NA lens). Data were processed using ImageJ (Girish and Vijayalakshmi, 2004) and Microsoft Excel. Inclusion formation assays were stopped at 24 h *p.i.* For SHC1 knockdown, inclusion formation was quantified 24 h *p.i.* by manually counting the inclusion forming units (IFU) as inclusions per 40x field on a Leica DM-IL cell culture microscope. For cPLA2 or CRLS1 knockdown, cells were fixed with ice-cold methanol overnight at -20°C, stained for OMP1 and DNA (Hoechst 33342) and analyzed by automated microscopy (Olympus Scan^R system) at 10x magnification. Progeny infections were grown for 48 h before glass bead lysis of host cells to release infectious particles and titration of infectious particles on fresh HeLa monolayers. After another 24 h of infection, cells were processed as described for inclusion formation. Data were processed with Olympus Scan^R Analysis software and Microsoft Excel.

2.6.2 Apoptosis induction and detection, data acquisition and analysis

HeLa cells were seeded in 12-well plates and infected with *C. trachomatis* L2 at MOI 50 for 6 h, then apoptosis was induced by the addition of TNFα (25 ng/ml) and cycloheximide (10 µg/ml) for an additional 4 h (Figure 3-19). Infection with *C. pneumoniae* (MOI 50) was assisted by centrifugation (1 h at 500 *g* and 35°C), followed by 5 h of incubation before apoptosis induction as described for *C. trachomatis*. For the PARP cleavage assay, cells were directly lysed in 2x sample buffer (Laemmli) and heated at 95°C for 10 min. For quantification, Western blots were imaged using a LAS-3000 bioluminescence reader (Fujifilm, USA) and the Image Reader LAS-3000 software (Fujifilm, USA). Respective bands and their lane backgrounds were measured using the Advanced Image Data Analyzer (AIDA) software and the ratio of cleaved PARP to the total PARP amount was calculated. For the CK18 cleavage and the terminal deoxynucleotidyl transferase dUTP nick end labeling (TUNEL) assays cells were spun down before staining. CK18 staining was done as described in the immunofluorescence section, and TUNEL staining was performed according to manufacturer's instructions (DeadEnd Fluorometric TUNEL System, Promega, USA) with green fluorescence of apoptotic cells due to fluorescein-12-dUTP labeling. Nuclei were stained blue with Hoechst 33342. Images of stained PBS stored cells were acquired at RT using an automated microscope (Olympus Scan^R system consisting of an Olympus IX81 inverted microscope, Hamamatsu charge-coupled

device (CCD) camera (model C4742-80-12AG) and the Scan^R acquisition software) at 10x magnification (Olympus UPlanS Apo 10x/0.40 NA lens). Cells positive for cleaved CK18, TUNEL, and nuclei were counted using ImageJ (Girish and Vijayalakshmi, 2004) and the ratio (cells with cleaved CK18 / total nuclei or TUNEL positive cells / total nuclei) was calculated. An average of 10000 cells per condition was analyzed. Apoptosis inhibition was depicted as ratios from uninfected TNFα-stimulated and infected TNFα-stimulated cells.

2.7 Computational methods

2.7.1 Multiple sequence alignment

Alignment analysis of multiple protein sequences was performed using the ClustalW2 software (Larkin *et al.*, 2007) provided by the European Bioinformatics Institute (EMBL-EBI). Tarp protein sequences of *C. trachomatis* L2 and *C. trachomatis* D were retrieved from NCBI, uploaded to the ClustalW2 software, and analysis was performed with default settings.

2.7.2 Prediction of SH3 interactions

Online prediction software (SH3-Hunter) (Ferraro *et al.*, 2007) was used to recognize putative SH3 interaction sites within the Tarp protein sequence and predict putative SH3 domain-containing proteins as interaction partners. An interaction score between 0 and 1 is calculated to rank the probability of the predicted interaction.

2.7.3 Modeling of Tarp signaling

Interaction partners identified using the SH2/PTB protein arrays were analyzed for their participation in signaling pathways using Ingenuity Pathway Analysis (IPA) software (Ingenuity Systems, USA) and the Kyoto Encyclopedia of Genes and Genomes (KEGG) (Kanehisa *et al.*, 2010). Only signaling pathways associated with at least two Tarp interaction partners were considered in the model. Pathways involved in SHC1-dependent regulation of the 21 apoptosis and cell growth related genes were obtained by using IPA. In brief, all known transcriptional regulators upstream of the SHC1-dependently regulated genes were introduced into the model and then linked to SHC1 using the "Path Explorer" tool of IPA. Pathways were grouped for MEK/ERK dependency. Interaction partners identified with the SH3 protein arrays were grouped according their participation in major molecular and cellular functions based on IPA. The top five functional categories and annotations are given in

Table 3-2. Functional categories were further described by their detailed functional annotations, giving more information on the specific involvement of the interacting molecules.

2.7.4 Docking simulation

Docking simulations were performed using the AutoDock 4 software package and the AutoDockTools (ADT) interface (Sanner, 1999). This software runs an automated procedure to predict the interaction of ligands (I) with biomacromolecular targets (E) (equation 2).

$$\frac{}{} \quad (2)$$

For the computational docking experiment, structural data of the second SH3 domain of NCK2 were used (2FRW). The structure of the Tarp SH3 binding site was modeled by using the known structure of the paxillin SH3 binding site (2O9V). Several docking simulations were performed with varying degrees of freedom regarding the movement of residues of NCK2 facing the interaction interface. Each docking simulation led to a set of secondary structures of the Tarp SH3 binding site characterized by their individual equilibrium dissociation constant K_D and free energy of binding ΔG (equation 3).

(3)

Among these, one structure had both a minimal dissociation constant K_D and a minimal free energy of binding ΔG, thus representing the most likely secondary structure of the Tarp SH3 binding site interacting with NCK2.

RESULTS AND DISCUSSION

3 Results and discussion

3.1 Preface

The human pathogen *Chlamydia trachomatis* has developed versatile strategies of subverting host cell signaling and trafficking pathways to ensure its intracellular replication and efficiently acquire nutrients. To broaden the current knowledge of the pathogen's repertoire in manipulating the host cell, two approaches were followed. One project, presented in the first part of this thesis, concentrates on the invasion phase of *C. trachomatis* and the interactions of the type III secreted effector protein Tarp with host cellular SH2 and SH3 domain-containing proteins. Another project, illustrated in the second part of this thesis, investigates changes in lipid composition of infected host cells and thereby explores lipid trafficking pathways affected by *C. trachomatis*. Taken together, both parts administer to a better understanding of *Chlamydia* infection from two different perspectives.

3.2 Part I: Interactions of host cell proteins with the effector protein Tarp

3.2.1 Peptide design of Tarp interaction sites

The *C. trachomatis* effector protein Tarp shows high homology among different serovars. Comparison of the Tarp amino acid sequences from serovar L2 and D identifies differences mainly in the number and sequence of N-terminal tyrosine phosphorylation sites (Figure 3-1 and Figure 3-2).

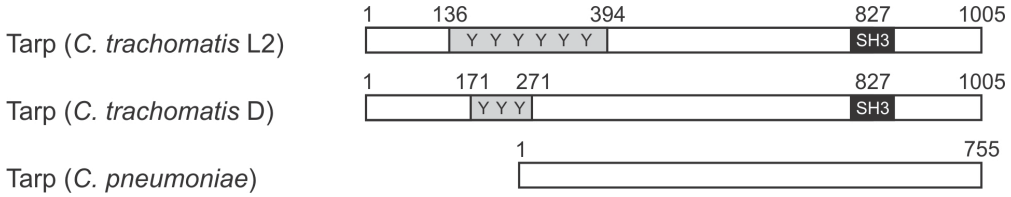

Figure 3-1. Graphical representation of Tarp. Tarp amino acid sequences from *C. trachomatis* L2 and D differ in the number and motif of N-terminal tyrosine phosphorylation sites (gray region). Both serovars have the identical sequence for a putative C-terminal SH3 binding site (black region). Tarp from *Chlamydophila pneumoniae* is devoid of both types of interaction sites.

C. trachomatis D Tarp features three identical ENIYE motifs at tyrosine residues Tyr171, Tyr221, and Tyr271 (Figure 3-2 and Figure 3-3 A), whereas *C. trachomatis* L2 Tarp has nine sites of tyrosine phosphorylation at residues Tyr136, Tyr140, Tyr189, Tyr239, Tyr242, Tyr291, Tyr341, Tyr390, and Tyr394 (Figure 3-2 and Figure 3-3 B). Six of these nine *C. trachomatis* L2 phosphorylation sites – Tyr136/140, Tyr238/242 and Tyr390/394 – are double-phosphorylation sites of the primary sequence ENIYENIYESI (Figure 3-2 and Figure 3-3 B). The C-terminal region of Tarp harbors a putative SH3 binding site with the primary sequence SVQTLLPSPPPTPSTTTLRT consisting of two overlapping core motifs (consensus sequence PxxP (Mayer, 2001)) (Figure 3-2). The sequence of this SH3 binding site is identical for Tarp from *C. trachomatis* L2 and D, and is also shared by other serovars, e.g., serovars A, B, C, and G. In contrast, *Chlamydophila pneumoniae* Tarp neither shows N-terminal tyrosine phosphorylation sites nor a C-terminal SH3 binding site (Clifton *et al.*, 2005) (Figure 3-1).

```
Tarp (C. trachomatis L2)      MTNSISGDQPTVTTFTSSTTSASGASGSLGASSVSTTANATVTQTANATNSAATSSIQTT 60
Tarp (C. trachomatis D)       MTNSISGYQPTVTTSTSSTTSASGASGSLGASSVSTTANATVTQTANATNSAATSSIQTT 60
                              ******* ****** ********************************************

Tarp (C. trachomatis L2)      GETVVNYTNSASAPTVTVSTSSSSTQATATSNKTSQAVAGKITSPDTSESSETSSTSSSD 120
Tarp (C. trachomatis D)       GETVVNYTNSASAPNVTVSTSSSSTQATATSNKTSQAVAGKITSPDTSESSETSSTSSSD 120
                              **************.********************************************

Tarp (C. trachomatis L2)      HIPSDYEPISTTENIYENIYESIDDSSTSGPENTSGGAAALNSLRGSSYSNYDDAAADYE 180
Tarp (C. trachomatis D)       HIPSDYDDVGSNSGDISNNYDDVG-----------------SNNGDISSNYDDAAADYE 162
                              ******: :.:...  .* *:.:.               * .*.  *********** 

Tarp (C. trachomatis L2)      PISTTENIYESIDDSSTSDPENTSGGAAALNSLRGSSYSNYDDAAADYEPISTTENIYEN 240
Tarp (C. trachomatis D)       PIRTTENIYESIGGSRTSGPENTSG----------------------------------- 187
                              ** *********..* **.******
```

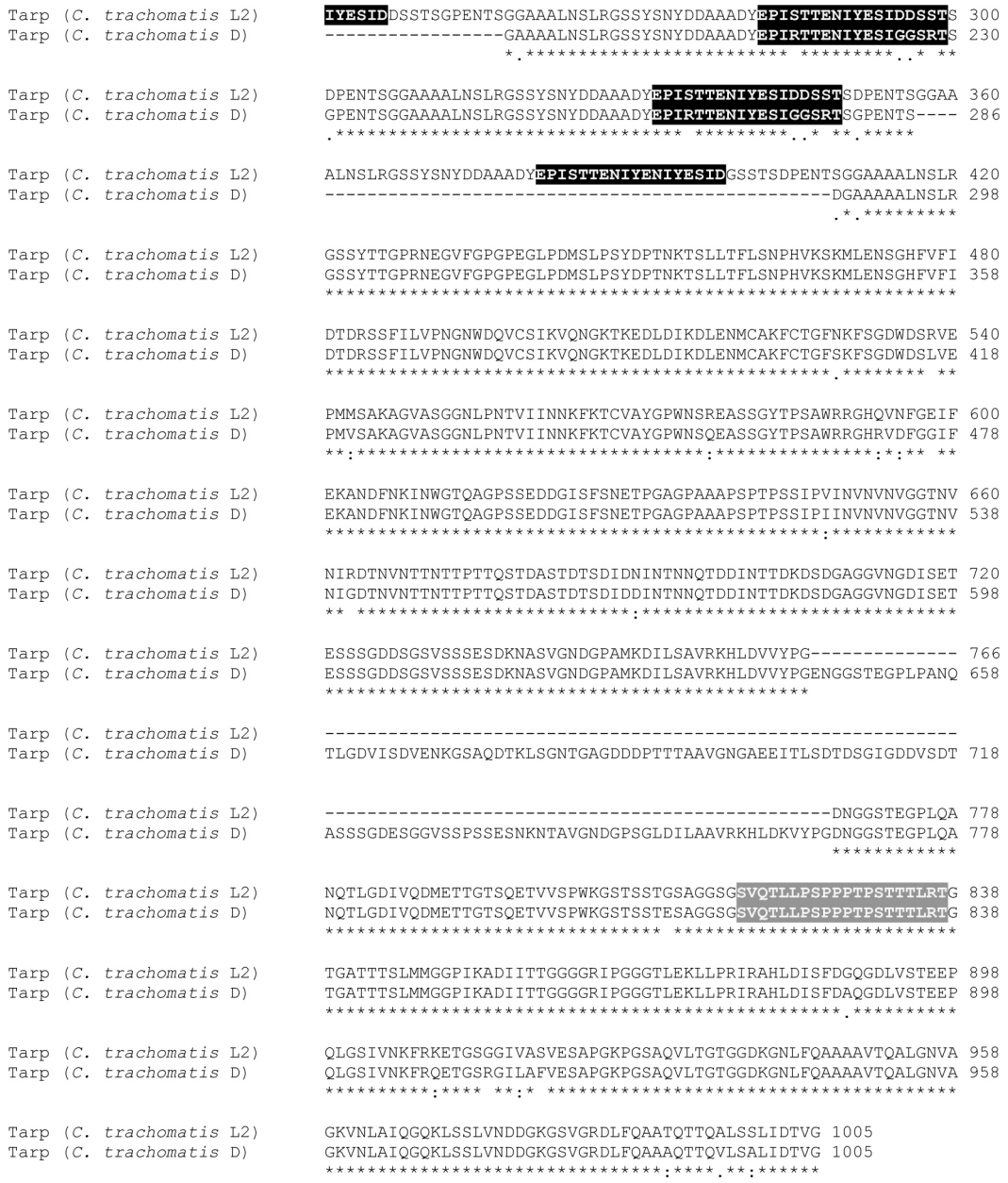

Figure 3-2. Multiple alignment of Tarp sequences. Multiple sequence alignment of the Tarp protein sequences of *C. trachomatis* L2 and D. Alignment was calculated using the ClustalW2 software (Larkin *et al.*, 2007) provided by the EMBL-EBI. Tyrosine phosphorylation sites are highlighted in black. Tarp from *C. trachomatis* D and L2 share three single-phosphorylation sites, whereas Tarp from *C. trachomatis* L2 additionally harbors three double-phosphorylation sites. The putative SH3 binding site is marked in gray.

To identify cellular interaction partners of the Tarp N-terminus, fluorescently labeled peptides representing the N-terminal sites of tyrosine phosphorylation on Tarp were synthesized. Eight peptides, each comprising 18 amino acids surrounding the respective phosphorylation sites, were synthesized in their non-, singly, or doubly phosphorylated states (Table 6-1). A fluorescent dye was coupled to the N-terminus of each peptide for detection purposes. These peptides were then used

to investigate interactions with human SH2 and PTB domains. For analysis of interactions between cellular SH3 domains and the Tarp C-terminus, wild type (SVQTLLPSPPPTPSTTTLRT) and mutated (SVQTLLDSPDPTDSTTTLRT) versions representing the putative SH3 binding site and the surrounding amino acids were synthesized and, for further detection, N-terminally biotinylated. Mutation was achieved by replacing respective proline residues with aspartic acid, rendering the binding site nonfunctional (Saksela *et al.*, 1995; Collette *et al.*, 2000; Antoku *et al.*, 2008).

3.2.2 Quantitative SH2/PTB interactome analysis of Tarp N-terminus

To identify and quantify interactions between Tarp-derived peptides representing the N-terminal tyrosine phosphorylation sites and human signaling proteins, protein microarrays comprising 133 SH2 and PTB domains were probed in duplicate with eight concentrations of each Tarp-derived peptide and the observed fluorescence data, F_{obs}, was fit to an equation that describes saturation binding, as described previously (Jones *et al.*, 2006). By this, binding affinities between every peptide and every recombinant domain were measured. From the resulting quantitative dataset, a graphical representation of biophysical interactions with phospho-sites of the D and L2 serovariants of Tarp was constructed (Figure 3-3). Three Tarp phosphorylation states were defined: nonphosphorylated (Figure 3-3, A and B), singly phosphorylated (Figure 3-3, C and D), and doubly phosphorylated (Figure 3-3 E). Because not all SH2/PTB domain-containing proteins are expressed at appreciable levels in every cell type or at every subcellular location, these diagrams should be viewed as quantitative maps of potential Tarp interactions in the context of particular cell expression patterns.

Nonphosphorylated peptides derived from both Tarp D and Tarp L2 exhibited very few interactions with human SH2 and PTB domains, as anticipated. Most notably, the tyrosine kinase ABL2 (ARG) and the GTPase activating protein RASA1 interacted with Tarp peptides (Figure 3-3, A and B, and Table 6-1). By probing the arrays with the singly phosphorylated version of the Tarp D peptide, the affinity of its interaction with ABL2 increased and several new interactions appeared, including a high affinity interaction with the SH2 domain of SHC1 (K_D < 200 nM) and interactions with the SH2 domains of CRKL, ABL1, SHC3, and RASA1. Even more prominent changes were observed with phosphorylated Tarp L2 peptides. Numerous high affinity interactions occurred, most notably with the SH2 domains of ABL1, ABL2, FGR, SYK, HCK, YES1, GRB2, CRKL, NCK2, SHB, TENC1, RASA1, VAV2, and SHC1; and with all three isoforms of the regulatory subunit of PI3K (Figure 3-3 D). Interestingly, the incremental effect of introducing the doubly phosphorylated peptide was minimal: only minor changes in affinities for some interaction partners (e.g., VAV2, PI3KR2, SYK, and HCK) were observed

(Figure 3-3 E and Table 6-1). This result is consistent with previous findings that doubly phosphorylated peptides derived from a variety of human RTKs behave similarly as compared to their singly phosphorylated counterparts (Jones *et al.*, 2006).

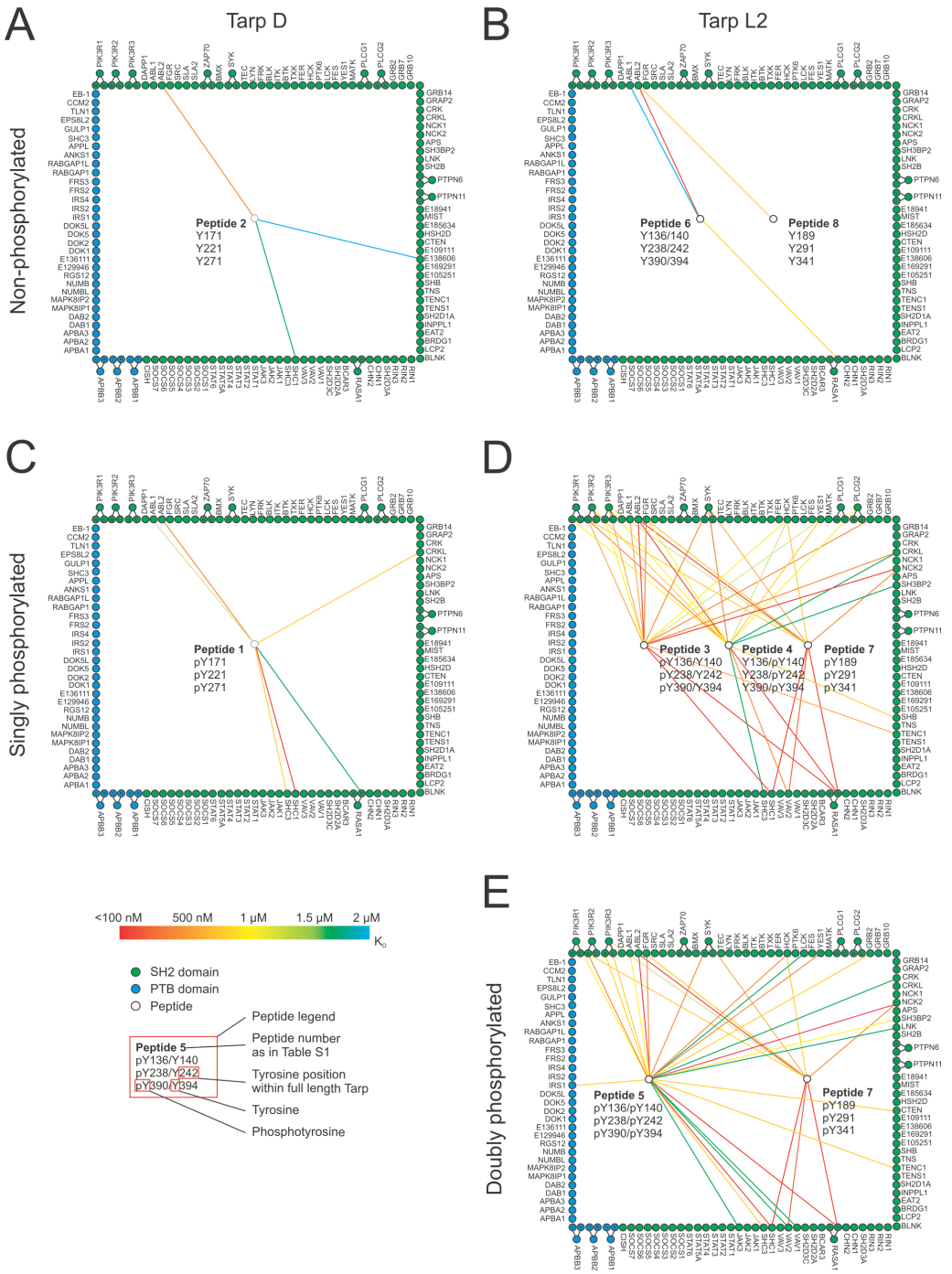

Figure 3-3. Quantitative protein interaction mapping. Quantitative data were obtained by probing SH2/PTB domain microarrays with fluorescently labeled Tarp peptides (performed by MacBeath and colleagues). The resulting data were used to construct quantitative protein interaction maps. White circles within the square represent peptides derived from *C. trachomatis*. Peptide allocation can be derived from Table 6-1 and the peptide legend, which shows phosphorylation

status and position within the full length protein. For example, peptide 2 in Figure 3-1 A mimics the three identical ENIYE repeats of serovar D Tarp in the nonphosphorylated state. Green and blue circles around the square represent individual SH2 and PTB domains, respectively. Circles outside the square indicate tandem domains (corresponding spot on the protein array contains both domains), which are connected to their individual domains (i.e., full length SYK is in possession of two SH2 domains located either N- or C-terminally). A color coded line is used to reflect the measured interaction strength between each domain-peptide pair (n = 2). Exact values are provided in Table 6-1. Interactions with $K_D \geq 2$ µM are omitted. (A and B) Interaction maps of nonphosphorylated Tarp D and L2. (C and D) Interaction maps of singly phosphorylated Tarp D and L2. (E) Interaction map of doubly phosphorylated Tarp from *C. trachomatis* serovar L2.

Notably, no PTB domains recognized any of the Tarp-derived peptides, except the PTB domain of IRS1, which recognized the doubly phosphorylated peptide derived from Tarp L2 (Figure 3-3 E). These data suggest that Tarp proteins may have been evolutionarily optimized to recognize SH2 domains that preferentially bind sequences C-terminally of phosphotyrosines (Sudol, 1998).

To highlight differences in binding affinities, the interaction maps for Tarp D, Tarp $L2_1$ (singly phosphorylated), and Tarp $L2_2$ (doubly phosphorylated) were prepared using three different affinity thresholds (Figure 3-4, A-C).

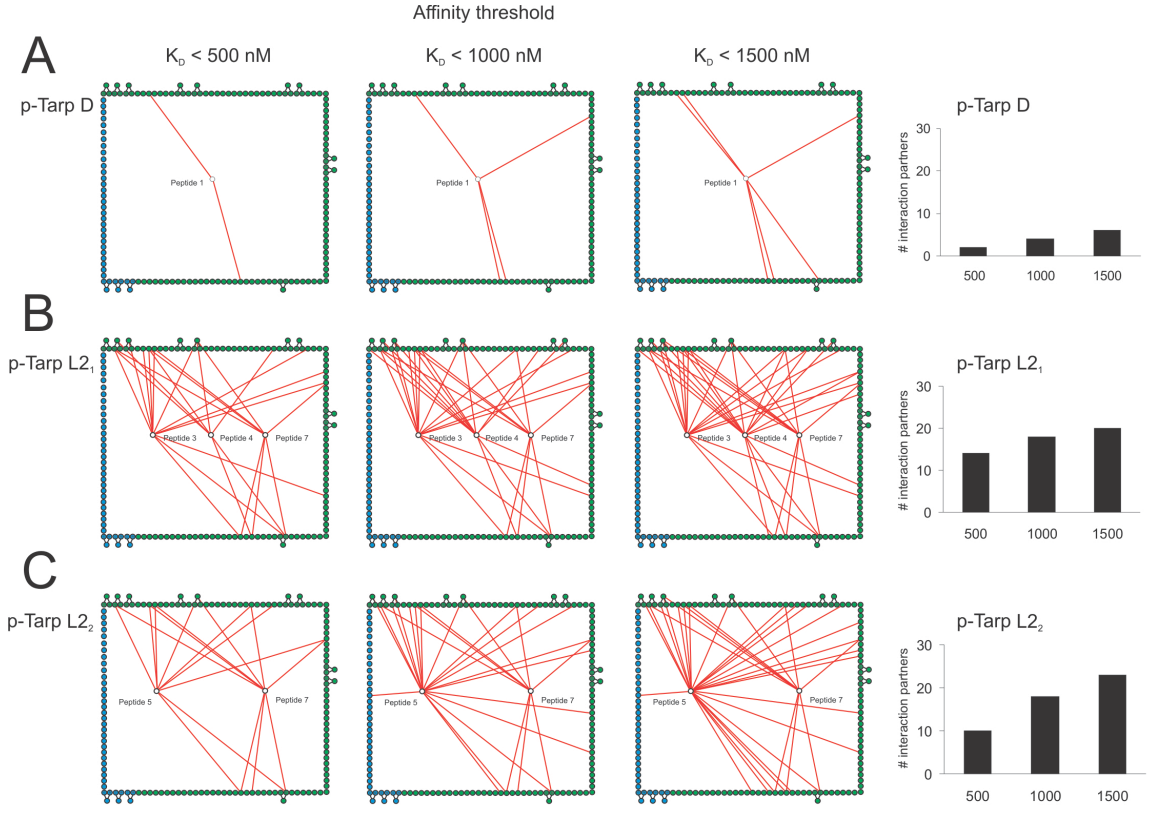

Figure 3-4. Quantitative analysis of the phospho-interactome. Interaction networks of the phospho-states from Figure 3-3 were binned using three different affinity thresholds (K_D < 500 nM, K_D < 1000 nM, and K_D < 1500 nM). In A-C, only

peptide/domain interactions below the stated threshold are shown (red lines). p-Tarp D refers to phosphorylated Tarp from *C. trachomatis* serovar D; p-Tarp $L2_1$ and $L2_2$ refer to singly and doubly phosphorylated Tarp from serovar L2, respectively. (A) Tarp D is less promiscuous than Tarp L2 and has few interaction partners at all affinity thresholds. (B) Tarp $L2_1$ exhibits highly promiscuous binding even at the highest affinity threshold (K_D < 500 nM). (C) Tarp $L2_2$ has fewer high-affinity interaction partners (K_D < 500 nM) than Tarp $L2_1$, but the number of interactors increases sharply as the affinity threshold is relaxed. To the right, the number of Tarp interaction partners at each affinity threshold is depicted in bar diagrams. Multiple domains from proteins interacting with more than one phospho-site are only counted once.

Tarp D exhibited high affinity interactions (K_D < 500 nM) with only two proteins, increasing to six as the threshold was relaxed to 1500 nM (Figure 3-4 A). In contrast, Tarp $L2_1$ (singly phosphorylated) exhibited promiscuous binding even at the highest affinity threshold (Figure 3-4 B). Surprisingly, hyperphosphorylation of Tarp L2 decreased the number of high affinity interactions, but the overall number of interaction partners for Tarp $L2_2$ sharply increased as the affinity threshold was relaxed (Figure 3-4 C).

Comparison of the different sets of interaction partners for both Tarp serovariants (Tarp D and L2) revealed two common interaction partners in the nonphosphorylated state (Figure 3-5 A) and a core set of six proteins in the phosphorylated state (Figure 3-5, B and C). This set included the adaptor protein SHC1, which bound both serovariants with high affinity. Tarp $L2_1$ and $L2_2$ were both found to interact with all of the phospho-Tarp D binding partners (Figure 3-5, B and C), which suggests that signaling initiated by the Tarp D serovariant constitutes a subset of the signaling initiated by Tarp L2. Tarp $L2_1$ and $L2_2$ were very similar, with 17 interaction partners in common (Figure 3-5 D).

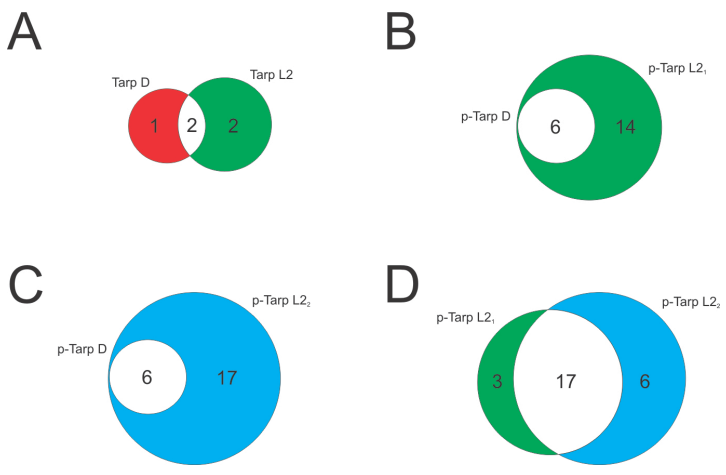

Figure 3-5. Comparison analysis of the phospho-interactome. Venn diagrams showing the number of overlapping interactions (white) between nonphosphorylated Tarp D (red) and L2 (green) (A), singly phosphorylated Tarp D (red) and $L2_1$ (green) (B), singly phosphorylated Tarp D (red) and doubly phosphorylated $L2_2$ (blue) (C), and singly phosphorylated Tarp $L2_1$ (green) and doubly phosphorylated $L2_2$ (blue) (D).

Overall, these results show that phosphorylation of Tarp enables multiple high affinity interactions with human SH2 domains; that a core set of proteins involved in MAPK signaling is able to interact with both serovariants of Tarp; and that signaling initiated by Tarp D likely constitutes a subset of the signaling initiated by Tarp L2.

3.2.3 Quantitative SH3 interactome analysis of Tarp C-terminus

To validate the functionality of the putative C-terminal SH3 binding site and to further investigate interactions of Tarp with cellular SH3 domain-containing proteins, protein arrays (TranSignal SH3 domain arrays, Panomics, USA) consistent of 117 SH3 domains in duplicate were used. The arrays were incubated with both wild type and mutated version of the peptide representing the C-terminal SH3 binding site (Figure 3-6).

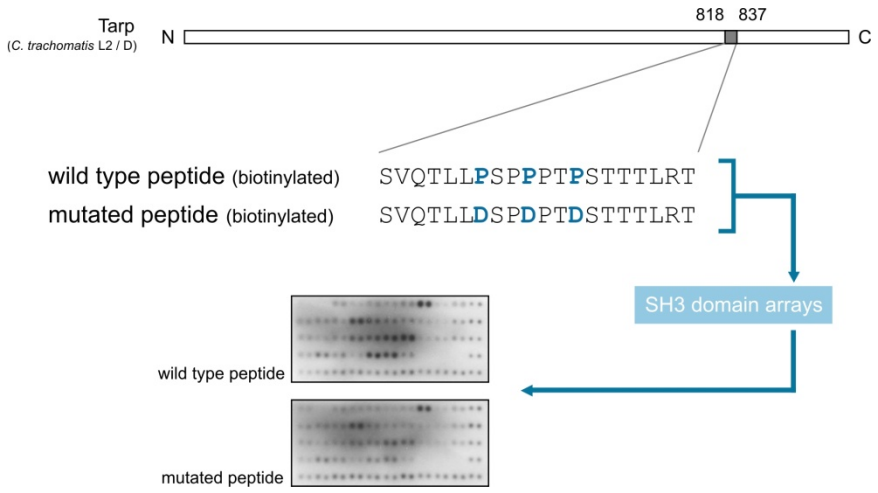

Figure 3-6. Workflow scheme of quantitative SH3 interactome analysis. Peptides representing the C-terminal SH3 binding site of *C. trachomatis* Tarp were synthesized and incubated with protein arrays comprising 117 SH3 domains. A mutated peptide version serving as negative control was processed in parallel.

Interaction intensities of the biotinylated peptides were quantified using HRP labeled streptavidin and normalized to biotin (positive control) and GST (negative control). Interactions with at least 25 % of the positive control signal intensity and a minimum signal decrease of 50 % between wild type and mutated peptide were defined as hits. These selection criteria lead to a set of 34 interactions (Figure 3-7 and Table 3-1). Among these interactions were high affinity interactions with a dissociation constant comparable to the biotin/streptavidin interaction ($K_D \approx 100$ nM) (Chivers *et al.*, 2010), most notably with the SH3 domains of CRK, CSK, VAV3, SRC, FYB, ABL2, NCK2, HCK, and YES1 (Figure 3-7 and Table 3-1).

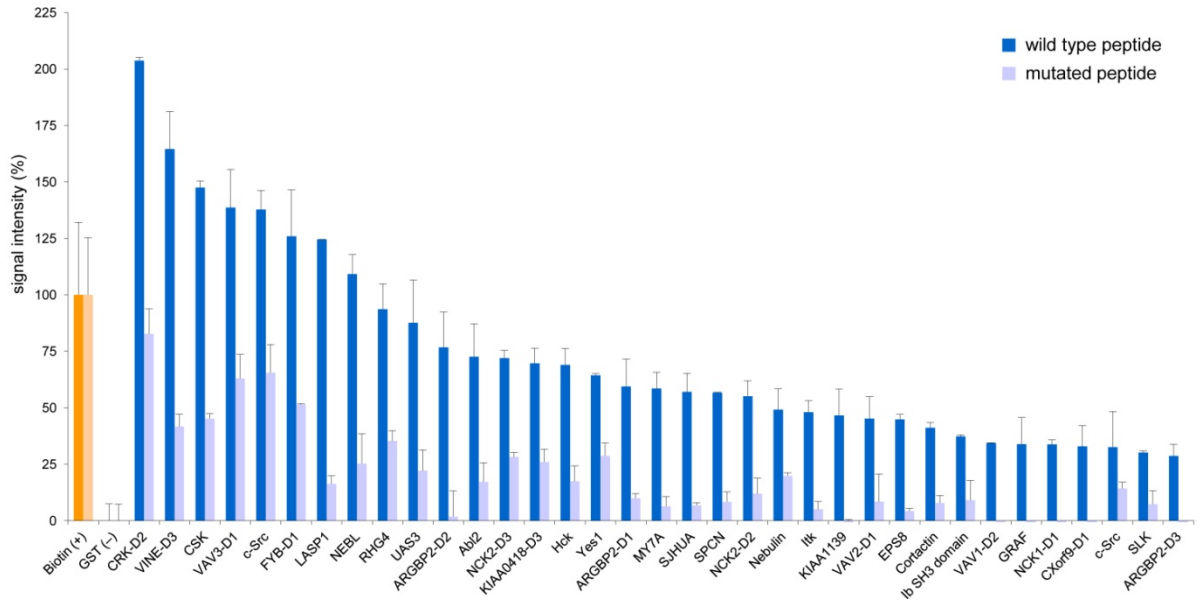

Figure 3-7. Quantitative SH3 interactome analysis. Bar diagram showing relative signal intensities of selected interactions between the respective SH3 domain and the peptide representing the Tarp SH3 binding site. Signals are sorted by intensity and normalized to positive and negative controls (orange). Interactions with wild type and mutated peptide are given in dark blue and light blue, respectively.

Interestingly, several of the measured interactions with Tarp's C-terminus were also detected to interact with the N-terminus of Tarp. These molecules, namely ABL2, CRK, HCK, NCK2, VAV1, VAV2, and YES1 all harbor both SH2 and SH3 domains, making them capable of interacting with both Tarp interaction sites (Figure 3-3, Figure 3-7, and Table 3-1). Amongst these, NCK2 and VAV2 showed the strongest interaction with both SH2 and SH3 binding sites of Tarp.

Table 3-1. Interaction partners of the Tarp SH3 binding site. Interaction strength is given relative to the positive control (biotin (+)) and the negative control (GST (-)). Peptides were synthesized representing the primary sequence of the putative SH3 binding site. Amino acid sequence of peptides is given in the footnotes. Additionally, interaction scores based on computational prediction (Ferraro *et al.*, 2007) and measured interaction with the Tarp N-terminus are listed.

Gene name[a]	Relative signal (wild type) (%)[b]	SD (%)	Relative signal (mutant) (%)[c]	SD (%)	Signal decrease (wild type vs. mutant) (%)	SD (%)	Interaction prediction score[d]	N-terminal SH2 interaction[e]
CRK-D2	203.7	1.4	82.7	11.0	59.4	6.2	0.977	Tarp L2
VINE-D3	164.5	16.5	41.6	5.5	74.7	11.0		
CSK	147.5	2.9	45.1	2.2	69.4	2.6		
VAV3-D1	138.6	16.9	62.9	10.7	54.6	13.8		

C-SRC	137.7	8.5	65.5	12.4	52.4	10.4	0.990	
FYB-D1	125.9	20.5	51.4	0.4	59.2	10.5		
LASP1	124.5	0.1	16.3	3.6	86.9	1.8		
NEBL	109.2	8.6	25.2	13.2	76.9	10.9		
RHG4	93.6	11.2	35.2	4.6	62.4	7.9		
UAS3	87.6	19.0	22.1	9.3	74.8	14.1		
ARGBP2-D2	76.7	15.6	1.8	11.3	97.6	13.5		
ABL2	72.6	14.4	17.2	8.5	76.3	11.4	0.990	Tarp L2, D
NCK2-D3	72.0	3.4	28.2	2.0	60.8	2.7	0.968	Tarp L2
KIAA0418-D3	69.6	6.7	26.0	5.7	62.7	6.2		
HCK	69.0	7.3	17.4	6.9	74.7	7.1	0.990	Tarp L2
YES1	64.4	0.7	28.6	5.7	55.5	3.2	0.991	Tarp L2
ARGBP2-D1	59.4	12.1	9.9	2.0	83.3	7.1		
MY7A	58.6	7.1	6.3	4.3	89.3	5.7		
SJHUA	57.0	8.3	6.8	1.2	88.1	4.7		
SPCN	56.6	0.2	8.4	4.3	85.3	2.3		
NCK2-D2	55.1	6.8	11.9	6.9	78.3	6.8	0.982	Tarp L2
NEBULIN	49.2	9.2	19.8	1.3	59.6	5.2	0.773	
ITK	48.0	5.1	5.1	3.4	89.4	4.2	0.986	
KIAA1139	46.6	11.6	-7.8	8.4	116.8	10.0		
VAV2-D1	45.2	9.6	8.4	12.3	81.5	10.9	0.984	Tarp L2
EPS8	44.8	2.2	4.3	1.1	90.5	1.7	0.988	
CORTACTIN	41.1	2.3	7.8	3.3	81.0	2.8	0.965	
CLASS IB SH3 DOMAIN	37.3	0.7	9.0	8.8	75.9	4.8		
VAV1-D2	34.4	0.0	-27.1	5.6	178.7	2.8	0.975	Tarp L2
GRAF	33.9	11.8	-23.5	3.1	169.3	7.5		
NCK1-D1	33.8	1.9	-43.5	2.9	228.5	2.4	0.973	
CXORF9-D1	32.9	9.2	-24.7	3.3	175.1	6.2		
C-SRC	32.5	15.7	14.2	2.8	56.3	9.3	0.990	
SLK	30.2	0.7	7.3	6.0	75.9	3.4		
ARGBP2-D3	28.6	5.2	-19.3	6.9	167.2	6.0		
Biotin (+)	100.0	32.1	100.0	25.2	0.0	28.7		
GST (–)	0.0	7.4	0.0	7.3	0.0	7.4		

[a] D1, D2, D3 specifies the respective SH3 domain of the protein

[b] wild type peptide, amino acid sequence SVQTLLPSPPPTPSTTTLRT

[c] mutated peptide, amino acid sequence SVQTLLDSPDPTDSTTTLRT

[d] according to SH3 prediction software (SH3-Hunter) (Ferraro *et al.*, 2007)

[e] detected interactions based on SH2/PTB protein microarrays (Figure 3-2 and Table 6-1)

3.2.4 Pathway analysis of N-terminal interactome

To identify signaling pathways that are potentially activated by the N-terminal interactome of Tarp, IPA software and KEGG (Kanehisa *et al.*, 2010) were used. Signaling pathways associated with at least two Tarp interaction partners were used to construct a qualitative model of Tarp-mediated signaling (Figure 3-8).

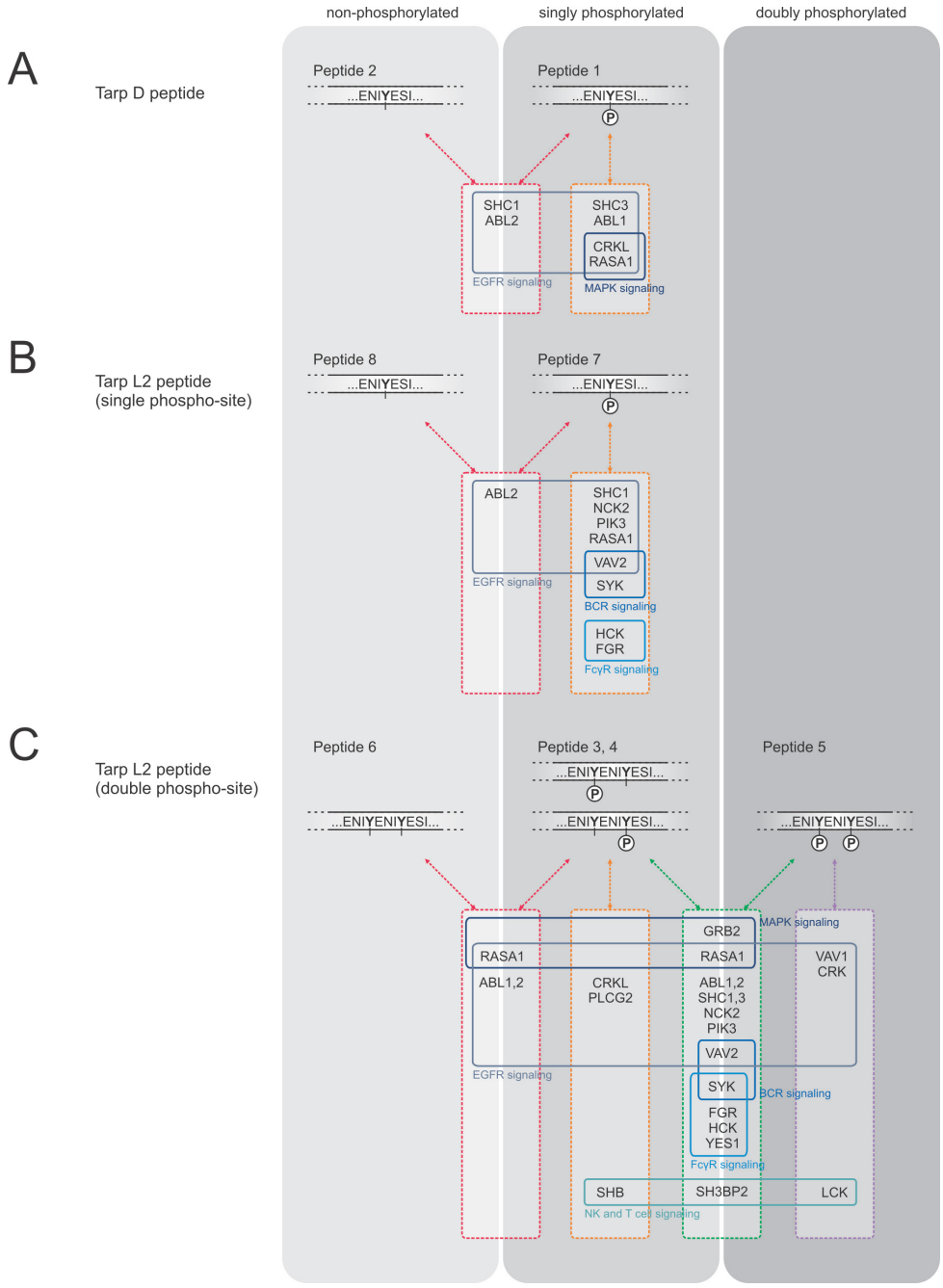

Figure 3-8. Tarp phospho-interactome and putative signaling. Model showing interaction partners and possible downstream signaling pathways of a single-phosphorylation site of Tarp D (A), a single-phosphorylation site of Tarp L2 (B),

or a double-phosphorylation site of Tarp L2 (C). Interacting proteins are listed in columns corresponding to the different phosphorylation states of the respective site (highlighted by dashed colored lines). Interaction partners were analyzed for their participation in signaling pathways (marked by continuous colored lines) using IPA software and KEGG (Kanehisa *et al.*, 2010). Only signaling pathways with involvement of at least two Tarp interactions identified on the SH2/PTB protein microarrays were included in the model.

Both serovariants of Tarp were found to interact with proteins commonly associated with EGF receptor (EGFR) signaling and MAPK signaling (Figure 3-8, A-C). Interestingly, Tarp L2 also interacted with proteins associated with immune signaling pathways of B and T cells, as well as with innate immune responses of natural killer (NK) cells, macrophages, and neutrophils (Figure 3-8, B and C). Connection of Tarp L2 with these additional signaling pathways involved in modulation of the immune response derives mainly from interactions mediated by its doubly phosphorylated state (Figure 3-8, B and C).

3.2.5 Pathway analysis of C-terminal interactome

To further functionally analyze the C-terminal interaction partners of Tarp, the measured interactions were grouped according to their involvement in major molecular and cellular functions based on IPA software. The major categories are ranked based on the number of interaction partners involved and are further specified by their detailed functional annotations, while only the top five annotations are given for each category (Table 3-2).

Table 3-2. Functional categories of Tarp SH3 interactions. Table lists top five functional categories of the 34 interaction partners of Tarp's C-terminal SH3 binding site and the respective number of molecules involved. Each functional category is subdivided by the top five functional annotations, giving information on the specific involvement of the interacting molecules. Interaction partners were analyzed for their participation in major functional categories using IPA software.

Category of molecular and cellular function[a]	Number of molecules	Function annotation[a]	Number of molecules involved	p-value	Molecules
Cellular assembly and organization	22	Formation of lamellipodia	8	1.61E-11	CRK, LASP1, NCK1, NCK2, C-SRC, VAV1, VAV2, VAV3
		Formation of cellular protrusions	10	2.51E-10	CRK, CORTACTIN, HCK, LASP1, NCK1, NCK2, C-SRC, VAV1, VAV2, VAV3
		Organization of cytoskeleton	9	1.18E-09	ABL2, RHG4, CRK, EPS8, ITK, NCK1, NCK2, SPCN, VAV1
		Organization of actin filaments	6	2.45E-09	ABL2, RHG4, CSK, NCK1, NCK2, SJHUA
		Organization of actin cytoskeleton	7	1.31E-08	ABL2, CRK, EPS8, NCK1, NCK2, SPCN, VAV1

Cellular function and maintenance	18	Organization of cytoskeleton	9	1.18E-09	ABL2, RHG4, CRK, EPS8, ITK, NCK1, NCK2, SPCN, VAV1
		Organization of actin filaments	6	2.45E-09	ABL2, RHG4, CSK, NCK1, NCK2, SJHUA
		Organization of actin cytoskeleton	7	1.31E-08	ABL2, CRK, EPS8, NCK1, NCK2, SPCN, VAV1
		Phagocytosis of cells	6	2.45E-07	CRK, CSK, HCK, MY7A, VAV1, VAV2
		Phagocytosis of eukaryotic cells	5	2.89E-06	CSK, HCK, MY7A, VAV1, VAV2
Cellular development	13	Development of transitional B lymphocytes	3	1.47E-08	VAV1, VAV2, VAV3
		Maturation of lymphocytes	4	2.01E-05	CSK, ITK, VAV1, VAV2
		Cell spreading of eukaryotic cells	5	2.10E-05	CRK, HCK, C-SRC, VAV2, VAV3
		Development of cells	11	2.33E-05	ABL2, CRK, CSK, HCK, ITK, NCK2, SJHUA, C-SRC, VAV1, VAV2, VAV3
		Shape change of eukaryotic cells	6	3.05E-05	CRK, HCK, NCK2, C-SRC, VAV2, VAV3
Cellular growth and proliferation	17	Proliferation of eukaryotic cells	16	4.33E-08	CRK, CSK, EPS8, FYB, HCK, ITK, NCK1, NCK2, CXORF9, SLK, SPCN, C-SRC, UAS3, VAV1, VAV2, VAV3
		Proliferation of lymphocytes	10	5.05E-08	FYB, HCK, ITK, NCK1, NCK2, CXORF9, UAS3, VAV1, VAV2, VAV3
		Proliferation of cells	17	1.27E-07	CRK, CSK, EPS8, FYB, HCK, ITK, LASP1, NCK1, NCK2, CXORF9, SLK, SPCN, C-SRC, UAS3, VAV1, VAV2, VAV3
		Proliferation of normal cells	13	4.50E-07	CSK, FYB, HCK, ITK, NCK1, NCK2, CXORF9, SLK, C-SRC, UAS3, VAV1, VAV2, VAV3
		Proliferation of T lymphocytes	7	1.68E-05	FYB, ITK, NCK1, NCK2, CXORF9, UAS3, VAV1
Cell-to-cell signaling and interaction	19	Turnover of focal adhesions	3	7.35E-08	ABL2, CSK, NCK2
		Phagocytosis of cells	6	2.45E-07	CRK, CSK, HCK, MY7A, VAV1, VAV2
		Activation of leukocytes	9	5.05E-07	CSK, HCK, ITK, NCK1, CXORF9, C-SRC, VAV1, VAV2, VAV3
		Phagocytosis of eukaryotic cells	5	2.89E-06	CSK, HCK, MY7A, VAV1, VAV2
		Activation of lymphocytes	7	3.94E-06	CSK, ITK, NCK1, CXORF9, C-SRC, VAV1, VAV2

[a] functional sorting according to IPA software

As stated above, the molecules interacting with the C-terminal SH3 binding site of Tarp are mainly involved in cellular assembly and organization, cellular function and maintenance, cellular development, cellular growth and proliferation, and cell-to-cell signaling and interaction. Interestingly, a major proportion of putative interaction partners is involved in processes of phagocytosis, cytoskeletal rearrangement, and proliferation.

3.2.6 Validation of interactions between Tarp's N-terminus and selected host cell proteins

To test whether the identified protein interactions have relevance for chlamydial infection, the strongest interaction partner of both serovariants of Tarp, SHC1, and a serovariant L2-specific interaction partner, NCK2, were selected for further experimental validation. Heterologously expressed GST fused to Tarp from *C. trachomatis* serovars D and L2 (Figure 3-9 A) was coupled to

beads, phosphorylated *in vitro* by SRC kinase, and incubated with host cell lysate. Truncated versions of N-terminal Tarp were used to avoid the actin nucleating activity of the C-terminal region (Jewett *et al.*, 2006) and additional interaction of cellular proteins with any noncharacterized Tarp motifs such as the C-terminal SH3 binding site.

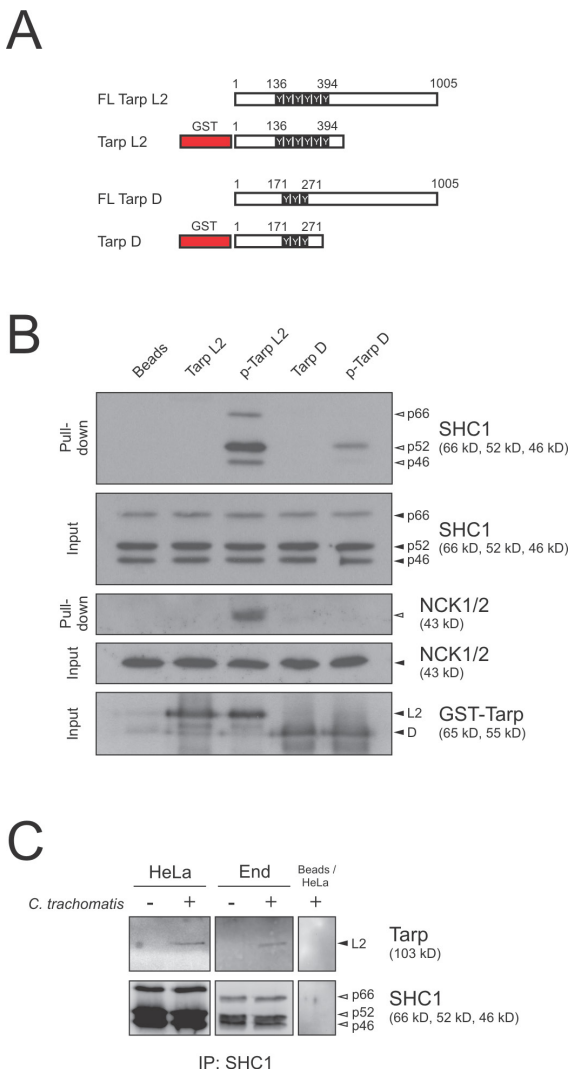

Figure 3-9. Validation of Tarp/SHC1 interaction. (A) Graphical representation of Tarp D, Tarp L2, and the respective GST-Tarp fusion proteins including all phospho-sites. Truncated versions of Tarp were used to avoid the actin nucleating activity of the C-terminus (Jewett *et al.*, 2006) and any unknown binding regions. (B) Western blot showing pull-down of SHC1 and NCK2 from HeLa cell lysate using bead coupled phospho-GST-Tarp. The fusion protein was phosphorylated *in vitro* with recombinant human SRC. Input shows Tarp loading (bead coupled, black arrowheads) and SHC1 and NCK2 loading in HeLa cell lysate (black arrowheads). Pulled down SHC1 and NCK2 are indicated by open arrowheads. SHC1 was only pulled down in lanes where Tarp was phosphorylated (indicated as p-Tarp). NCK2 was only pulled down with p-Tarp L2. As a control, beads were phosphorylated in the absence of GST-Tarp and did not pull down SHC1. (C) Western blot showing coimmunoprecipitation of SHC1 (white arrowheads) and Tarp (black arrowhead) after infection of HeLa or End1/E6E7 cells (*C. trachomatis* L2, MOI 500) for 60 min (performed by A. Mehlitz).

Both phosphorylated Tarp D and Tarp L2 bound SHC1 and showed a strong preference for the SHC1^{p52} isoform (Figure 3-9 B). In contrast, only phosphorylated Tarp L2 was capable of precipitating NCK2 (Figure 3-9 B). This is consistent with the array data because peptides derived from phospho-sites on Tarp L2, but not Tarp D, were recognized by the SH2 domain of NCK2. Focussing on SHC1, the common interaction partner of both serovariants, a coimmunoprecipitation experiment revealed, that endogenous SHC1 and Tarp L2 coprecipitated from two separate *C. trachomatis*-infected cell types (Figure 3-9 C). These experiments show that the interactions with SHC1 and NCK2 highlighted by the SH2/PTB protein microarrays are also observed with full-length proteins.

3.2.7 Analysis of the interaction between Tarp's C-terminus and NCK2

The interactions of the C-terminal SH3 binding site of Tarp were further investigated focussing on NCK2, an interaction partner with both a high interaction signal and predication score. To assess the ability of NCK2 to bind the Tarp SH3 motif, a computational docking experiment was performed. This automated procedure uses the Protein Data Bank (PDB) file format describing the three-dimensional structures of molecules to predict interactions of ligands with macromolecular targets (Figure 3-10).

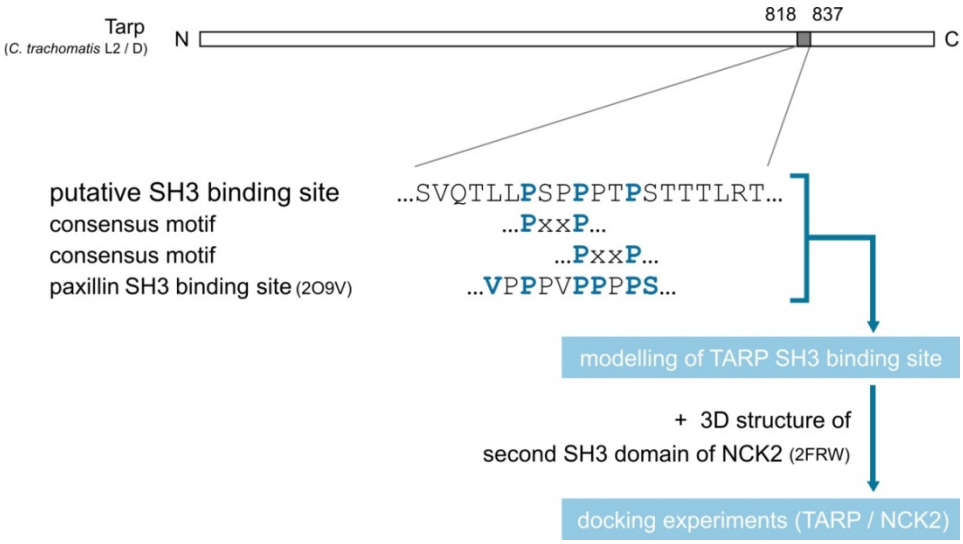

Figure 3-10. Workflow scheme of docking experiments. The C-terminal SH3 binding site of *C. trachomatis* Tarp shows high homology to the paxillin SH3 binding site. Docking experiments of NCK2 and the Tarp SH3 binding site were carried out using structural data of paxillin (2O9V) and the second SH3 domain of NCK2 (2FRW).

While structural data of the second SH3 domain of NCK2 (PDB ID number 2FRW) were available, the three-dimensional structure of Tarp is not described so far. Therefore, the structure of the Tarp SH3 binding site was modeled by using the known structure of the paxillin SH3 binding site, which shows

high homology to the Tarp SH3 sequence. The structural data file 2O9V (PDB ID number) describes the left-handed polyproline II helix of the paxillin SH3 binding site bound to the SH3 domain of its interaction partner ponsin. The structure file also contains information about the general orientation of binding site and binding domain. Subsequently, all structural data were uploaded to the AutoDock 4 software package using the ADT interface. Several docking simulations were performed with varying degrees of freedom regarding the movement of NCK2 residues facing the interaction interface. Each docking simulation led to a set of secondary structures of the Tarp SH3 binding site with one structure having both a minimal dissociation constant K_D and a minimal free energy of binding ΔG, representing the most likely secondary structure of the Tarp SH3 binding site interacting with NCK2 (Figure 3-11).

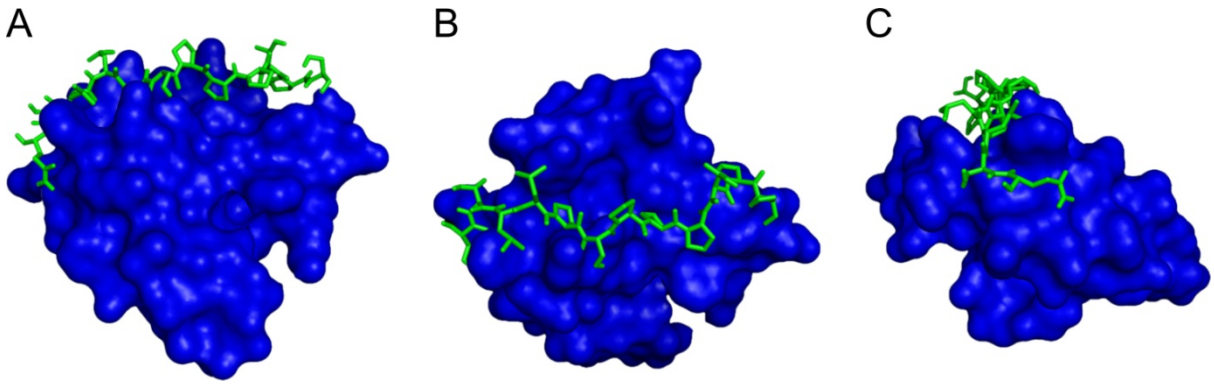

Figure 3-11. Model of Tarp/NCK2 interaction. The C-terminal Tarp SH3 binding site is highlighted in green, the second SH3 domain of NCK2 is colored blue. In this docking simulation, two residues of NCK2 facing the binding pocket (Phe7, Tyr51) were allowed to move freely during the automated docking procedure, resulting in an estimated free energy of binding ΔG of -6.90 kcal/mol, equivalent to a dissociation constant K_D of 8.80 µM. Different angles of view are given in (A), (B), and (C) with a 90 degree horizontal rotation from (A) to (B) and a 90 degree vertical rotation from (A) to (C).

In this docking simulation, two residues of NCK2 facing the binding pocket (Phe7, Tyr51) were allowed to move freely during the computational procedure, resulting in a secondary structure model with a minimal estimated free energy of binding ΔG of -6.90 kcal/mol, equivalent to a dissociation constant K_D of 8.80 µM. This is in the lower range of expected values for SH3 interactions in general (1-200 µM) (Li, 2005). A second docking simulation with six freely moving residues of NCK2 (Phe7, Tyr9, Asp15, Trp35, Asn50, Tyr51) resulted in a secondary structure with a minimal estimated free energy of binding of -10.46 kcal/mol, equivalent to a dissociation constant K_D of 21.69 nM. Interestingly, both secondary structure models of the Tarp SH3 binding site were nearly identical (data not shown). This fact additionally supports the validity of the observed Tarp/NCK2 interaction via Tarp's C-terminal SH3 binding site.

3.2.8 SHC1 activation and influence on MEK/ERK signaling during *Chlamydia* cell entry

Next, the influence of Tarp/SHC1 interaction on major downstream signaling pathways was assessed by investigating the activation of the MEK/ERK cascade upon phosphorylation of SHC1. As previously shown, recruitment of SHC1 to endogenous human receptors leads to its phosphorylation on Tyr239/240 and Tyr317 (van der Geer *et al.*, 1996). To test SHC1 activation during *C. trachomatis* infection, time course experiments were performed in HeLa cells. All three SHC1 isoforms were phosphorylated on Tyr239/240 during invasion of *C. trachomatis* (Figure 3-12 A) and for up to 5 h *p.i.* (Figure 3-12 B). In contrast, during infection with *C. pneumoniae*, which translocates a Tarp homolog (Cpn0572) lacking the phosphorylation sites (Clifton *et al.*, 2005), SHC1 phosphorylation was only marginally increased (Figure 3-12 C). Quantification of Western blotting data revealed that SHC1 phosphorylation was significantly increased during infections with *C. trachomatis*, but not *C. pneumoniae* (Figure 3-12 D).

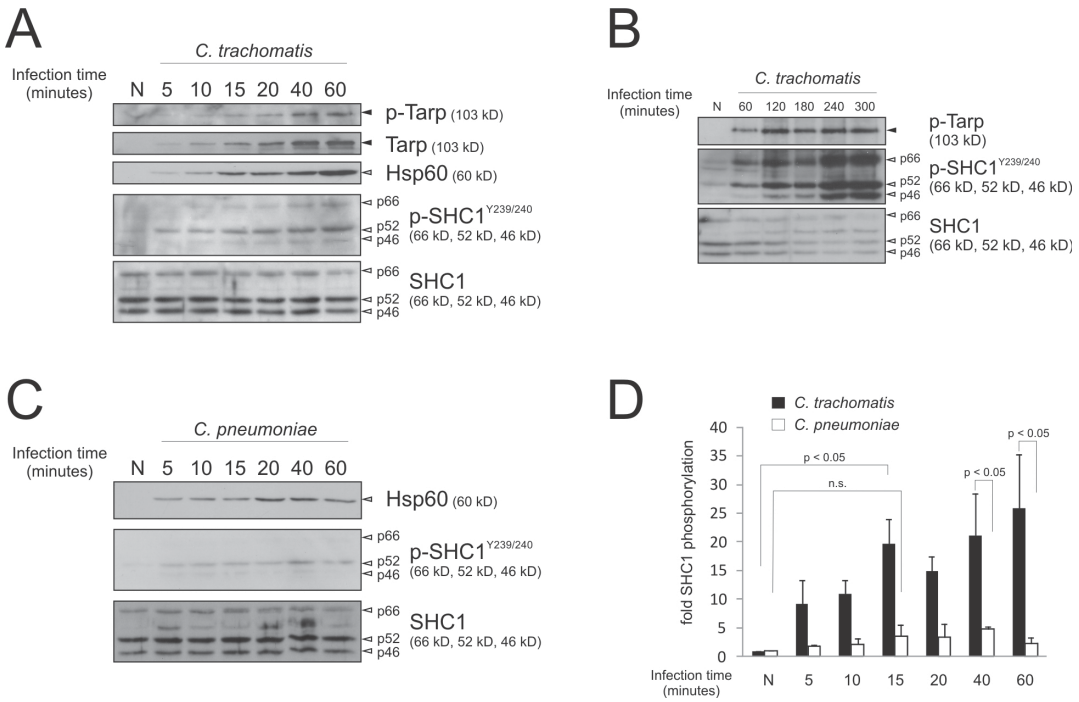

Figure 3-12. SHC1 activation during early chlamydial infection. Western blots showing SHC1 phosphorylation on tyrosine residues Tyr239/240 (p-SHC1$^{Y239/240}$, white arrowheads) and Tarp phosphorylation (p-Tarp, black arrowheads) during a time course infection experiment (*C. trachomatis* L2, MOI 200; HeLa cells) for 120 min *p.i.* (A) and up to 5 h *p.i.* (B) (performed by A. Mehlitz). Control experiment using *C. pneumoniae* (MOI 200, HeLa cells) showed only marginal SHC1 phosphorylation on tyrosine residues Tyr239/240 (p-SHC1$^{Y239/240}$, white arrowheads) (C). Tarp phosphorylation was determined with a tyrosine phosphorylation specific antibody. Hsp60 was used as an infection control (gray arrowhead). Controls (N) were mock infected with SPG for 60 min. (D) Densitometric quantification of SHC1 p52 Tyr239/240 phosphorylation. Values were calculated from Figure 3-12, A and C, and normalized to total SHC1 p52 (n = 2, error bars indicate standard error (SE)).

Interestingly, the SHC1^{p52} isoform was most rapidly and most strongly phosphorylated by *C. trachomatis* infection (Figure 3-12 A), which is consistent with the observed binding preference of Tarp L2 and D (Figure 3-9 B). Furthermore, immunofluorescence staining experiments showed that SHC1 activation was accompanied by recruitment of the protein to bacteria during host cell entry (Figure 3-13, A and B).

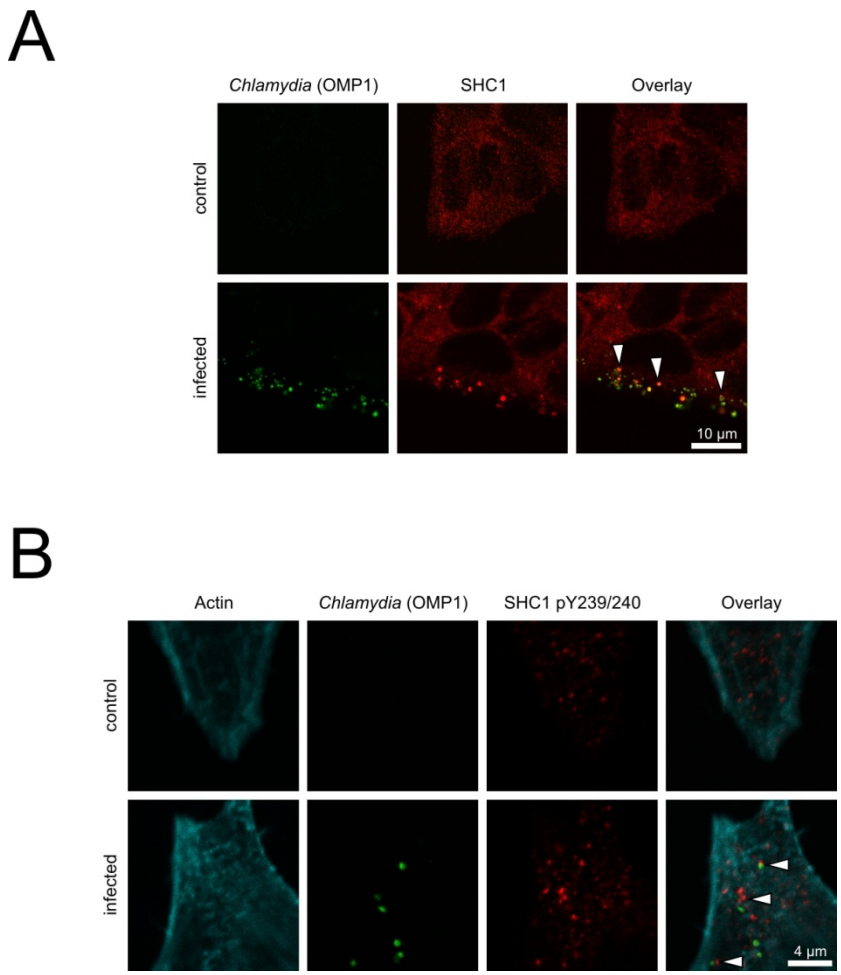

Figure 3-13. SHC1 phosphorylation and subcellular localization upon infection. Immunofluorescence staining of SHC1 (red, white arrowheads) (A) and p-SHC1 (red, white arrowheads) (B) after infection of HeLa cells for 60 min (*C. trachomatis* L2, green, MOI 200) (performed by A. Mehlitz). Vesicular structures of SHC1 and p-SHC1 were located in close proximity to *Chlamydia* EBs. These structures were not observed in control cells.

Both SHC1 phosphorylation (van der Geer *et al.*, 1996) and *Chlamydia* infection (Su *et al.*, 2004) have been shown to activate the MEK/ERK cascade via RAS and RAF; however, *Chlamydia*-induced MEK/ERK activation has mainly been demonstrated at later infection time points, e.g., from 12 h *p.i.* (Paland *et al.*, 2008). Because Tarp is secreted within minutes after attachment, RAS, MEK, and ERK activation was investigated during this early phase of infection.

To examine RAS activation, HeLa cells were transfected with a reporter construct for activated RAS. This construct, GFP-RBD_{RAF-1}, consists of GFP fused to the RAS binding domain (RBD) of RAF-1 and selectively binds to the active, GTP-bound form of RAS (Bivona *et al.*, 2006). It has previously been shown that endogenous levels of RAS are not sufficient to recruit detectable amounts of the GFP reporter (Bivona *et al.*, 2006). Therefore, cells were cotransfected with mCherry-tagged H-RAS for the overexpression of RAS. HeLa cells were infected with *C. trachomatis* L2 (phase contrast, MOI 100). RAS activation at the plasma membrane could be detected from 2 min after addition of infectious particles to the cells, decreasing to basal levels after 12 min (Figure 3-14).

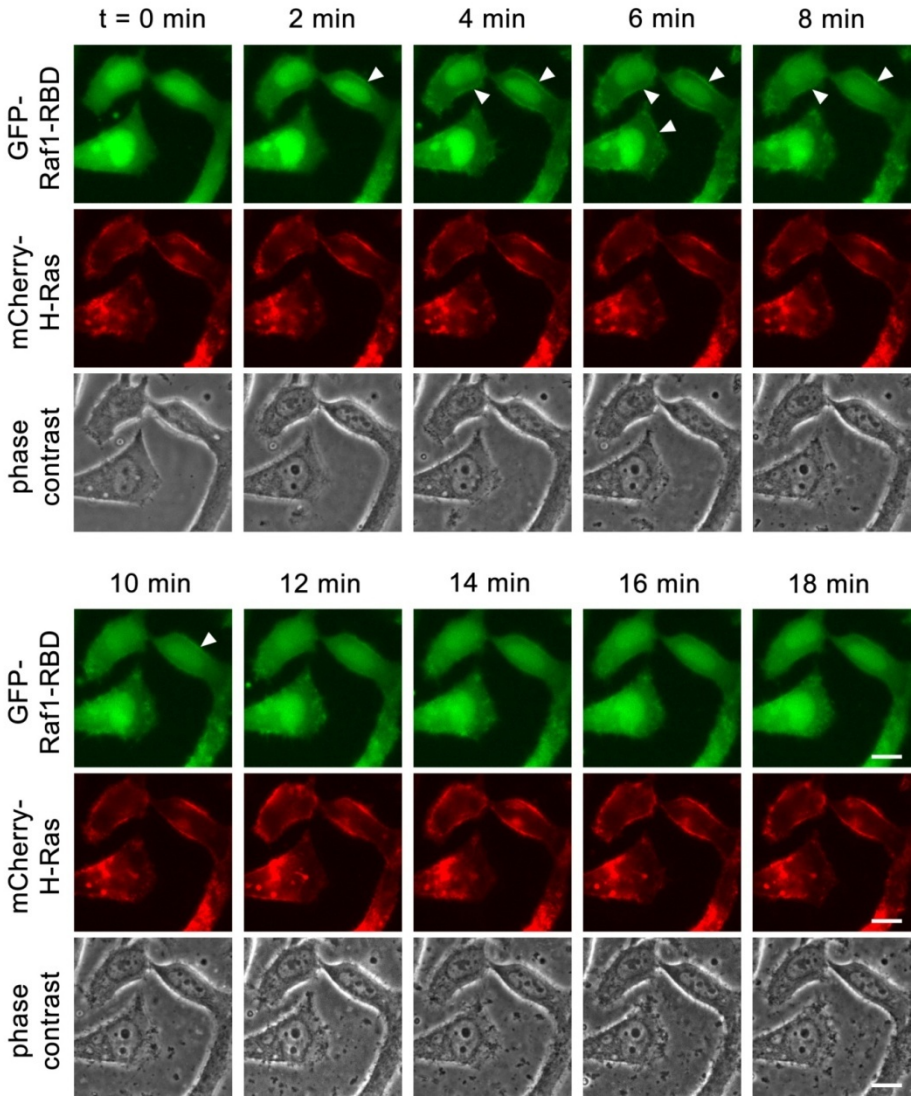

Figure 3-14. RAS activation during early chlamydial infection. Live-cell imaging of HeLa cells transfected with GFP-RBD_{RAF-1} (green), a reporter for RAS activation, and mCherry-tagged H-RAS (red) after infection with *C. trachomatis* L2 (phase contrast, MOI 100). Cells show recruitment of the GFP construct to the plasma membrane starting at 2 min after addition of *C. trachomatis* EBs. White arrowheads mark activated cells. White bar equals 10 µm.

Further downstream RAS activation, both MEK and ERK phosphorylation increased sharply 5-10 min *p.i.* in HeLa (Figure 3-15) and End1/E6E7 cells (primary immortalized endocervical cells; data not shown), then decreased to ~20 % and ~10 % above basal levels for MEK and ERK, respectively, after 1 h. MEK/ERK activation was dependent on MOI (data not shown).

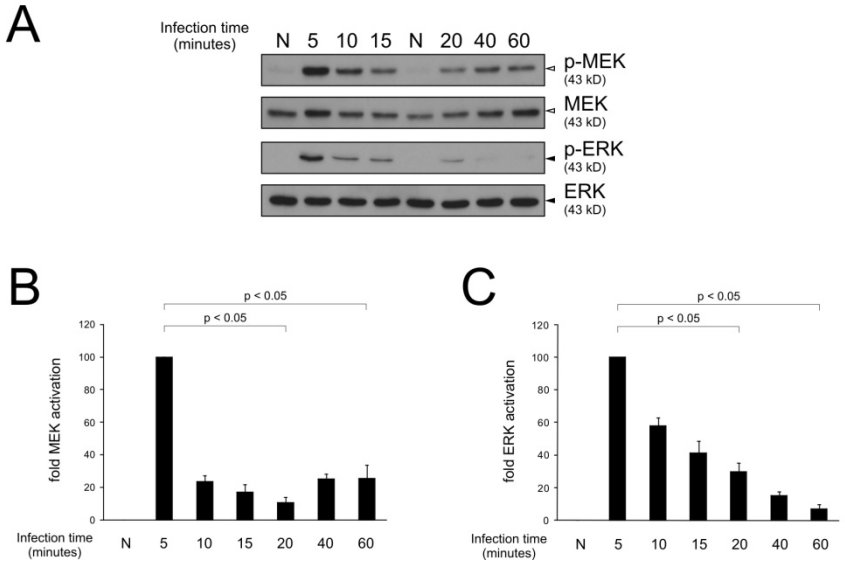

Figure 3-15. MEK/ERK activation during early chlamydial infection. (A) Western blots showing MEK (white arrowheads) and ERK (black arrowheads) phosphorylation during a time course infection experiment (*C. trachomatis* L2, MOI 200; HeLa cells), peaking at ~5 min (performed by A. Mehlitz). Densitometric quantification of MEK (B) and ERK phosphorylation (C). Values were calculated from Figure 3-15 A and normalized to total MEK or ERK (n = 2, error bars indicate SE). All values are normalized to the "5 min" infection time point. Controls (N) were mock infected with SPG for 60 min.

The role of SHC1 in infection and *Chlamydia*-induced early MEK/ERK activation was further examined by siRNA-mediated knockdown of SHC1. Upon *Chlamydia* infection, SHC1 knockdown reduced MEK and ERK phosphorylation (Figure 3-16, A and B).

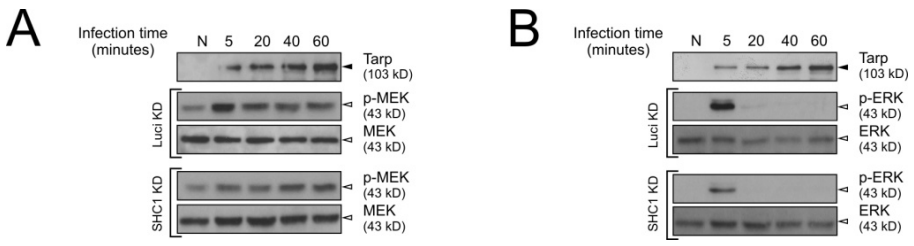

Figure 3-16. MEK/ERK activation and SHC1 dependency. Western blots showing MEK (A) and ERK (B) phosphorylation during an infection time course (*C. trachomatis* L2, MOI 200; HeLa cells) of a representative experiment (performed by A. Mehlitz). Cells were either treated with siRNA against luciferase (control) or SHC1. MEK and ERK activation were reduced upon infection. Controls (N) were mock infected with SPG for 60 min.

A similar degree of reduction occurred after stimulation of uninfected SHC1 knockdown cells with inducers of MEK/ERK phosphorylation such as TNFα and EGF (Figure 3-17, A and B).

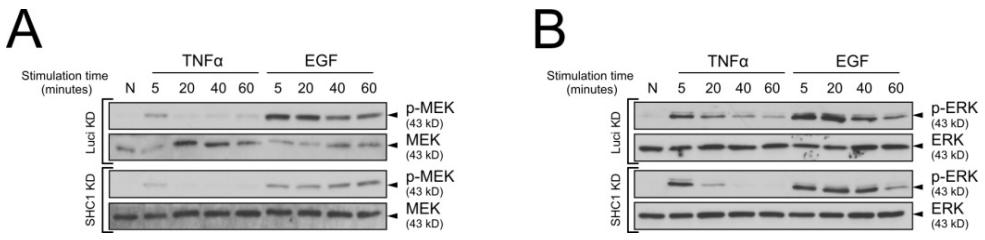

Figure 3-17. MEK/ERK activation in SHC1 knockdown cells. Western blots showing MEK (A) and ERK (B) phosphorylation during a time course after stimulation of cells with 25 ng/ml TNFα or 50 ng/ml EGF (performed by A. Mehlitz). HeLa cells were either treated with siRNA against luciferase (control) or SHC1. Controls (N) were mock infected with SPG for 60 min.

SHC1 knockdown resulted in a 90-95 % reduction at the protein level (Figure 3-18 A) and did not affect adhesion, invasion, inclusion formation, or numbers of progeny (Figure 3-18 B).

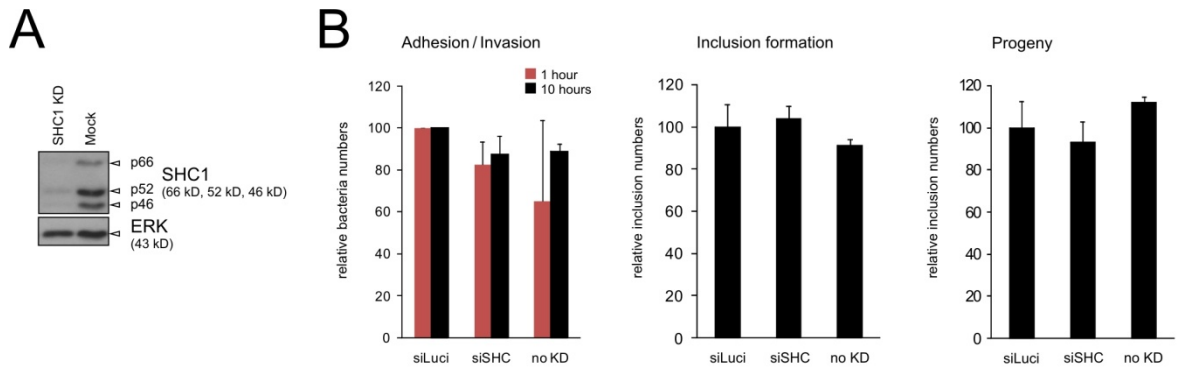

Figure 3-18. Chlamydial invasion, inclusion formation, and progeny after SHC1 knockdown. (A) Western blot showing nearly complete knockdown of all three SHC1 isoforms after siRNA-mediated gene silencing. (B) Bar diagrams showing adhesion/invasion efficiency, inclusion formation, and progeny formation after knockdown with luciferase (siLuci) or SHC1 (siSHC) siRNA or transfection reagent only (no KD). Adhesion/invasion efficiency was determined by automated microscopy detecting particle numbers associated with host cells at 1 or 10 h (n = 2, ~8000 cells per experiment and condition). Inclusion and progeny formation were determined by counting the number of inclusions per 40x field at 24 h *p.i.* and after transfer of end-cycle bacteria to fresh HeLa monolayers (n = 2, 10 fields per experiment and condition). SHC1 knockdown did not result in significant regulation of *C. trachomatis* invasion, inclusion formation, and progeny (error bars indicate SE).

These results show that SHC1 phosphorylation during early infection is Tarp-dependent. Furthermore, SHC1 is recruited immediately after infection where it is not directly needed for adhesion, invasion, inclusion formation, or bacterial propagation. Rather, SHC1 plays a prominent role in early *Chlamydia*-induced activation of the MAPK pathway.

3.2.9 SHC1 activation and its transcriptional regulation during infection

SHC1 activation is known to modulate survival, proliferation, and migration by transcriptional regulation, depending on the stimulus (Guo and Giancotti, 2004). Thus, the influence of SHC1 activation on transcription upon *C. trachomatis* cell entry was further investigated. Because of the expected delay between MEK/ERK activation and its transcriptional response, experiments were performed at 4 h *p.i.* (Figure 3-19), a time point at which the host cell exhibits a strong transcriptional response, but bacteria are still largely metabolically inactive (EB to RB conversion takes place at 8-10 h *p.i.*) (Mathews *et al.*, 1999).

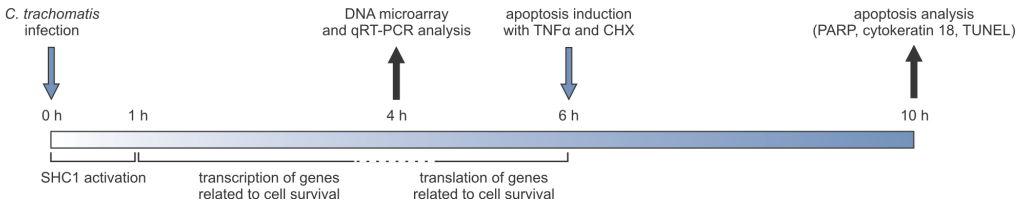

Figure 3-19. Workflow scheme of DNA microarray, qRT-PCR, and apoptosis experiments. Experimental time-scale of DNA microarray, qRT-PCR, and apoptosis experiments in this study. Blue bar shows time course of infection up to 10 h *p.i.* Arrows indicate treatment of cells (blue) and sample collection (black).

Using human DNA microarrays, genes that were differentially expressed during infection of either control cells (without knockdown) or SHC1 knockdown cells were determined. Data from two biological replicates were combined and only correlated genes were used for further analysis (Figure 3-20, green spots).

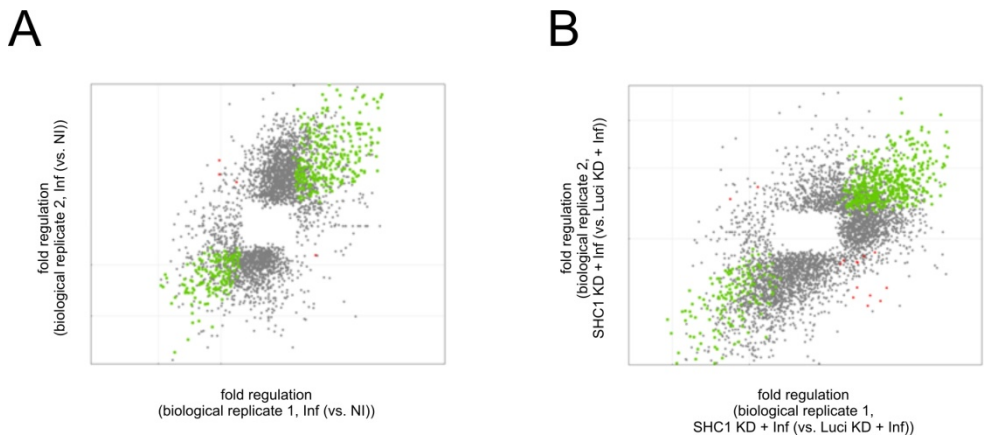

Figure 3-20. Correlation analysis of DNA microarrays. Comparison plots showing regulated genes from two independent biological experiments during infection (A) or SHC1 knockdown and infection (B). Correlated genes are highlighted in green, anti-correlated genes in red.

First, infected and uninfected HeLa cells at 4 h *p.i.* were compared, revealing 182 differentially regulated genes: 76 genes were down-regulated (Figure 3-21, upper left green circle, and Table 6-2) and 106 genes were up-regulated (Figure 3-21, lower right red circle, and Table 6-2) in response to infection. Second, infected SHC1 knockdown and infected luciferase (control) knockdown HeLa cells were compared, indicating regulation of 449 SHC1-dependent genes: 332 genes were down-regulated (Figure 3-21, upper right green circle, and Table 6-3), whereas 117 genes were up-regulated (Figure 3-21, lower left red circle, and Table 6-3) following SHC1 knockdown in infected cells.

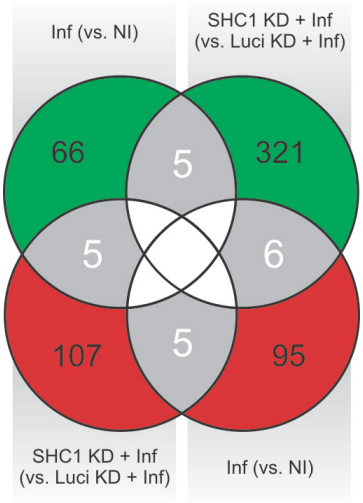

Figure 3-21. SHC1- and infection-dependent genes. Venn diagram showing differentially regulated genes during either infection alone or SHC1 knockdown and infection and genes regulated in both conditions. HeLa cells were infected for 4 h (*C. trachomatis* L2, MOI 20) before RNA isolation and array hybridization. Gene expression profiles of infected versus uninfected cells (Inf (vs. NI)) were compared to infected SHC1 knockdown versus infected luciferase knockdown cells (SHC1 KD + Inf (vs. Luci KD + Inf)) to determine infection- and SHC1-dependently regulated genes (n = 2, each with dye-reversal). In total, 21 genes are regulated in a both SHC1- and infection-dependent manner (up-regulated genes are marked in red, down-regulated genes in green).

The observed approximately threefold increase of down-regulated genes as compared with up-regulated genes upon infection of SHC1 knockdown cells indicates a strong activating potential of SHC1 on gene expression during infection (Figure 3-21, lower left red circle and upper right green circle). Interestingly, infection of SHC1 knockdown cells down-regulated approximately fourfold more genes than infection of control (no knockdown) cells alone (Figure 3-21, green circles), most likely due to more genes being SHC1- rather than infection-dependently regulated. A comparison of genes regulated between all conditions identified a total of 21 SHC1- and infection-dependent genes (Figure 3-21, gray overlapping areas, and Table 3-3).

Table 3-3. SHC1- and infection-dependently regulated genes. List of 21 genes regulated in an infection- and SHC1-dependent manner. Genes are grouped according to regulation pattern and functional sorting by IPA software. Full gene names and a short functional description including references are additionally provided.

Group[a]	Gene identifier	Gene name	Full name	Function	Reference	Regulation array 1[b]	p-value array 1[b]	Regulation array 2[c]	p-value array 2[c]	Apoptosis[d]	Cell growth[d]	MEK/ERK dependent[d]
1	NM_000459	TEK	tyrosine kinase, endothelial	receptor signaling, angiogenesis	Jones and Dumont, 2000	-1.90	3.00E-05	1.87	9.24E-07	-	+	-
1	BU729607	HMGB2	high mobility group box 2	DNA binding, formation of nucleoprotein complexes, V(D)J recombination, trans-cription initiation, DNA repair	Thomas and Travers, 2001	-1.73	1.64E-03	2.21	5.58E-08	-	-	+
1	NM_001964	EGR1	early growth response 1	transcription factor, suppression of trans-formation, up-regulation of proapoptotic genes	Arora *et al.*, 2008	-1.89	1.79E-07	2.32	7.84E-42	+	+	+
1	NM_153032	FLJ32065	hypothetical protein	-.	-	-1.97	2.13E-07	2.41	2.94E-16	-	-	-
1	NM_033503	BMF	Bcl2 modifying factor	BH3 only protein, inhibits pro-survival proteins	Willis and Adams, 2005	-2.44	2.01E-09	3.15	6.73E-14	+	+	-
2	AF086541	DAPL1	death associated protein-like 1	apoptosis and cell differentiation	Ashburner *et al.*, 2000	-1.61	9.43E-03	-1.72	5.50E-04	-	-	-
2	NM_024859	MAGIX	MAGI family member, X-linked	tight junction PDZ protein, caspase substrate	Gregorc *et al.*, 2007	-1.87	7.03E-03	-1.61	2.55E-03	-	-	-
2	NM_139241	FGD4	F+VE, RhoGEF and PH domain containing 4	guanine nucleotide exchange factor specific for Cdc42	Chen *et al.*, 2004	-2.00	1.59E-08	-1.82	5.34E-10	-	-	-
2	NM_001956	EDN2	endothelin 2	21 AA peptide, activates endothelin receptors, raises blood pressure, induces vascular and myocardial hypertrophy	Goraca, 2002	-2.94	0.00E+00	-2.05	1.76E-02	-	-	-
2	AL833897	AL833897	cDNA clone	-	-	-1.65	8.03E-07	-1.68	9.47E-03	-	-	-
3	NM_012242	DKK1	dickkopf homolog 1	Wnt inhibitor	Zhao *et al.*, 2009	3.53	0.00E+00	-1.99	4.67E-11	+	-	+
3	NM_002017	FLI1	Friend leukemia virus integ. 1	ETS transcription factor, proto-oncogene	Juban *et al.*, 2009	1.81	7.00E-05	-1.95	1.57E-09	+	+	+
3	BC033310	GDA	guanine deaminase	converts guanine to xanthine	-	1.65	2.82E-11	-1.70	2.73E-03	-	-	+
3	NM_005556	KRT7	cytokeratin 7	cytoskeletal component	-	1.62	2.66E-08	-2.13	0.00E+00	-	-	-
3	NM_145110	MAP2K3	mitogen-activated protein kinase kinase 3	stress signaling, activates p38MAPK, pro-apoptotic	Dhanasekaran and Premkumar Reddy, 1998	1.72	1.26E-12	-1.96	4.00E-10	+	+	-
3	NM_002999	SDC4	syndecan 4	transmembrane heparan sulfate proteoglycan, regulation of cytoskeleton, proliferation	Oh and Couchman, 2004	1.64	1.57E-14	-1.66	2.64E-10	+	-	+
4	NM_001511	CXCL1	chemokine (C-X-C motif) ligand 1 (melanoma growth stim. activity, alpha)	neutrophil attraction, cytoskeletal control	Reutershan and Ley, 2004	1.67	5.88E-24	1.75	1.18E-09	-	+	+

4	NM_013409	FST	follistatin	Activin binding protein, proliferation, differentiation and apoptosis	McDowall *et al.*, 2008	2.32	1.38E-33	1.98	1.04E-09	+	+	-
4	NM_005114	HS3ST1	heparan sulfate (glucosamine) 3-O-sulfo-transferase 1	Heparin sulfate biogenesis, sulfotransferase	Munoz *et al.*, 2006	2.29	2.75E-19	1.75	1.77E-28	-	-	+
4	BC037430	PHLDA1	pleckstrin homology-like domain, family A, member 1	expression increases basal apoptosis, regulation of cell growth and apoptosis	Neef *et al.*, 2002	2.23	6.38E-10	1.67	6.92E-14	+	+	+
4	NM_203349	SHC4	SHC (Src homology 2 domain cont.) family, member 4	cell migration and growth regulation	Fagiani *et al.*, 2007	1.65	4.50E-02	1.91	1.22E-17	-	-	-

[a] groups according to Figure 3-21

[b] array 1 (Inf. vs. NI)

[c] array 2 (SHC1 KD + Inf. vs. Luci KD + Inf.)

[d] functional sorting according to IPA

Functional analysis of these 21 differentially regulated genes using the IPA software revealed genes associated with apoptosis and cell growth regulation, with eight genes assigned to each category (Figure 3-22 and Table 3-3).

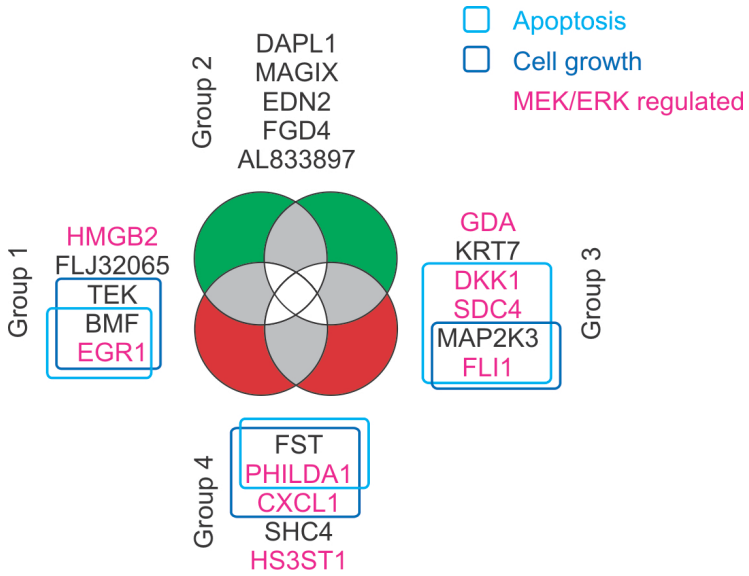

Figure 3-22. SHC1-dependent regulation of apoptosis and cell growth genes. Venn diagram showing color coded circles from Figure 3-21 with more detailed information on the 21 differentially regulated genes. The genes correlating with both infection and SHC1 signaling were further analyzed using the IPA software. Of these, eight genes are grouped into the functional category “apoptosis” and another eight genes are assigned to the category “cell growth”.

Indeed, these functional gene types were significantly enriched ($p < 0.01$) in this gene subset in comparison with the extended gene set, i.e., ~10 % of the 610 genes versus ~40 % of the 21 genes were apoptosis related (Figure 3-23).

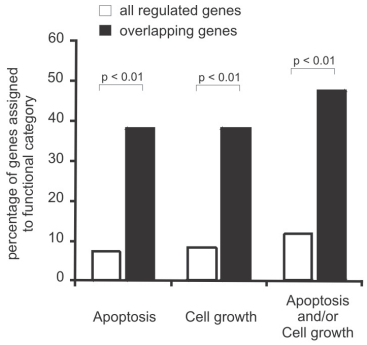

Figure 3-23. Gene enrichment analysis. Gene enrichment analysis of the overlapping genes (21) compared with all regulated genes (610). Both functional categories "apoptosis" and "cell growth" are significantly enriched in the 21 overlapping genes (as determined by Fisher's exact test).

Surprisingly, IPA analysis also indicated that, among these 21 genes, nine genes are associated with MEK/ERK signaling, whereas 12 genes are controlled by other pathways (Figure 3-22, magenta colored genes, Figure 3-24, and Table 3-3).

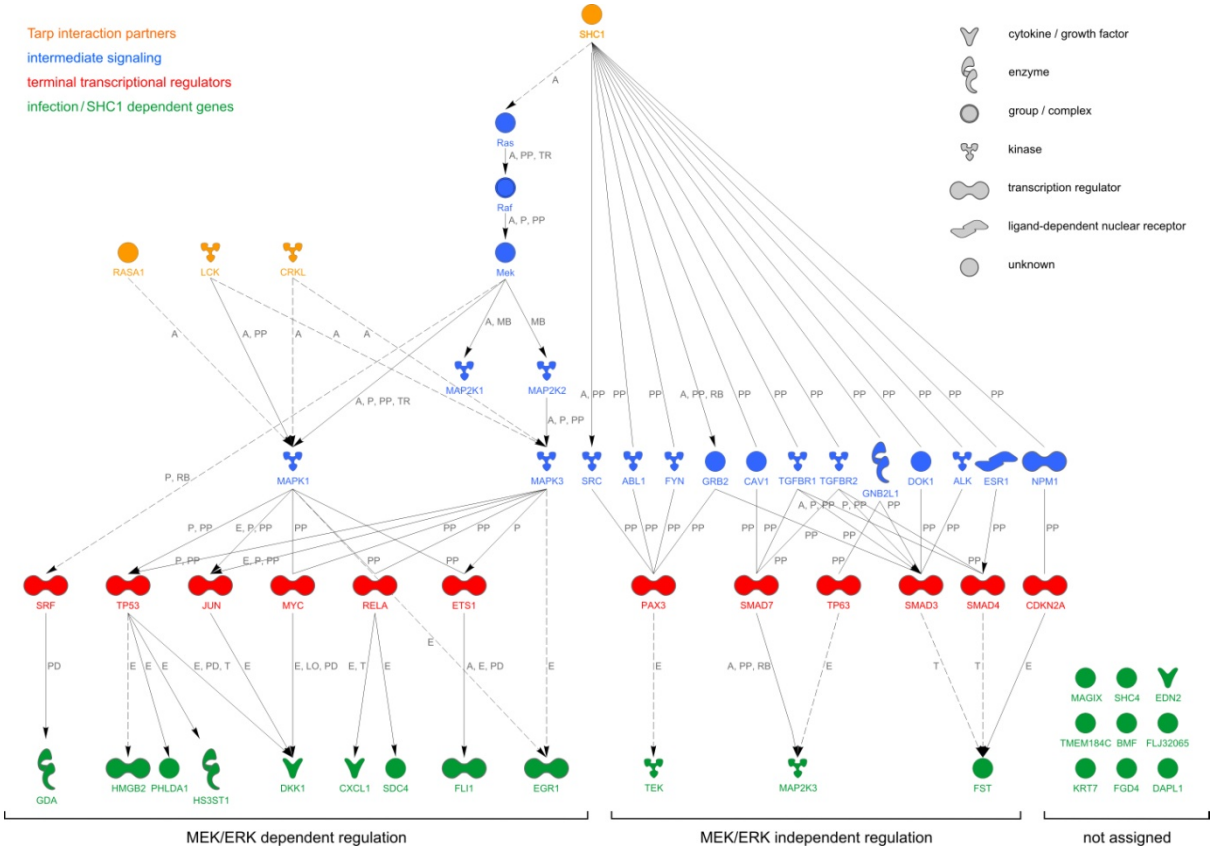

Figure 3-24. Putative SHC1 signaling. Model showing different pathways of SHC1 signaling in connection with the 21 SHC1-dependently regulated apoptosis and cell growth genes. Genes are grouped into the three categories "MEK/ERK-dependent regulation", "MEK/ERK-independent regulation" and "not assigned". Among the 21 genes (depicted in green),

only nine genes were MEK/ERK-dependently regulated, whereas 12 genes are controlled by other pathways. Relationships were analyzed using IPA software (straight line, direct relationship; dashed line, indirect relationship; A, activation; E, expression; LO, localization; MB, group/complex membership; P, phosphorylation/dephosphorylation; PD, protein-DNA binding; PP, protein-protein binding; RB, regulation of binding; T, transcription; TR, translocation). Color coding is as follow: yellow, potential Tarp interactions; blue, intermediate signaling molecules; red, terminal transcriptional regulators; and green, 21 infection- and SHC1-dependently regulated genes.

The regulation of the majority of the 21 infection- and SHC1-dependent genes was confirmed using qRT-PCR (Figure 3-25 and Table 6-4).

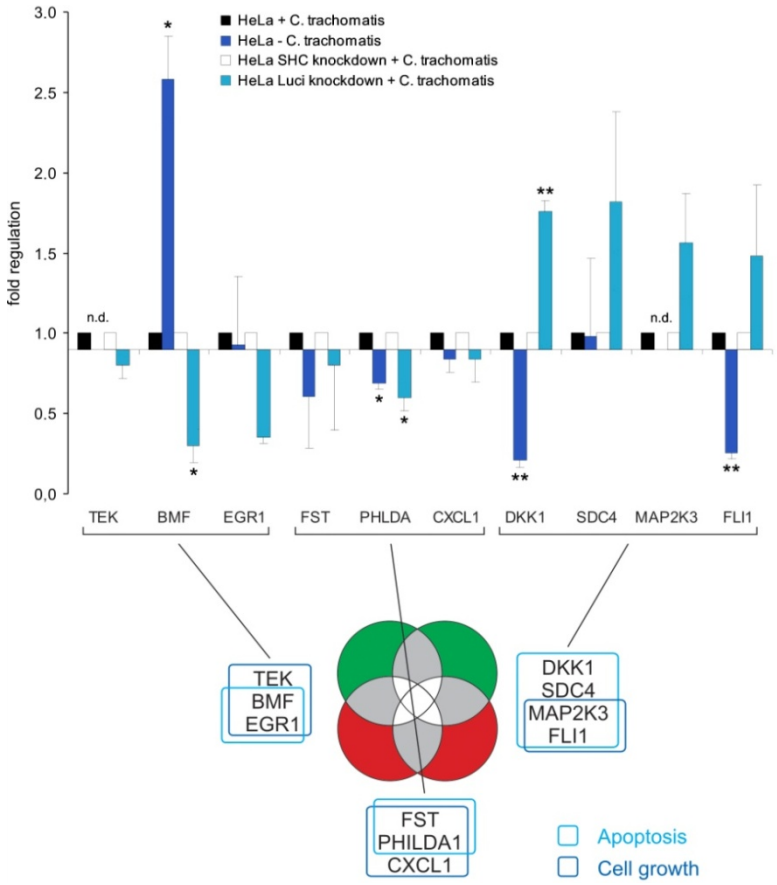

Figure 3-25. qRT-PCR confirmation of SHC1-dependent gene regulation. Bar diagrams showing gene expression of infected versus uninfected cells (black vs. dark blue bars) and infected SHC1 knockdown versus infected luciferase knockdown cells (white vs. light blue bars) (n = 2, error bars indicate SE, * denotes $p < 0.05$, ** denotes $p < 0.01$). HeLa cells were infected for 4 h (*C. trachomatis* L2, MOI 20). 10 genes identified in the array experiments and classified into apoptosis or growth regulation were selected for experimental verification by qRT-PCR. Figure shows comparison of qRT-PCR results with the Venn diagram (bottom); Table 6-4 confirms regulatory tendency of all genes tested.

Thus, the transcriptional data suggest that Tarp-mediated SHC1 activation after *C. trachomatis* infection is involved in the regulation of apoptosis and cell growth related genes.

Further analysis of the 21 gene subset revealed four distinct groups (Figure 3-22 and Table 3-3). Group 1 comprises transcripts less abundant upon infection and more abundant in infected SHC1 knockdown cells (Figure 3-26). Therefore, expression of the genes in group 1 is likely inhibited by SHC1 activation. In contrast, group 3 comprises transcripts more abundant upon infection and less abundant in infected SHC1 knockdown cells (Figure 3-26). Consequently, expression of genes in group 3 is likely enhanced by SHC1 activation.

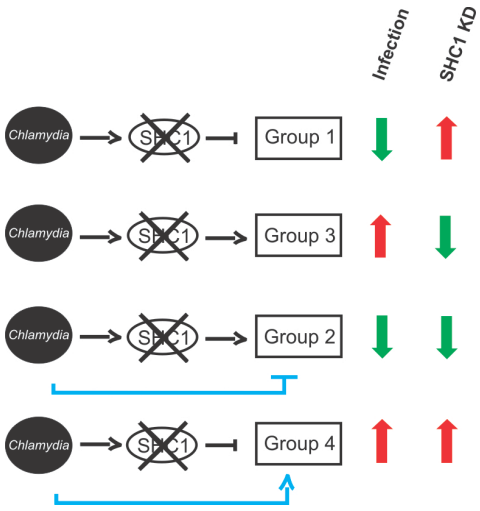

Figure 3-26. Model of the role of SHC1 during early infection-mediated gene regulation. *C. trachomatis* activates SHC1 leading to four groups of regulated genes. Expression of group 1 genes is likely inhibited by SHC1 activation, explaining their up-regulation after SHC1 knockdown in infected cells. In contrast, gene expression in group 3 is likely enhanced by SHC1 activation, causing a down-regulation of group 3 genes after SHC1 knockdown in infected cells. Genes of group 2 and 4 show an additional regulation by infection-independent of SHC1, remaining after SHC1 knockdown in infected cells.

Groups 2 and 4 include transcripts either less abundant (group 2) or more abundant (group 4) after both infection and SHC1 knockdown in infected cells (Figure 3-26). This can be explained by infection-dependent regulation of these genes in an SHC1-independent manner, counteracted by an SHC1-dependent regulation. Consequently, knockdown of SHC1 in infected cells leads to an enforced regulation due to the remaining SHC1-independent effects. Thus, the data have identified opposing gene regulatory circuits during *Chlamydia* infection – being dependent or independent of SHC1.

3.2.10 SHC1 activation and its role as a survival stimulus

To further examine the role of SHC1 in early *Chlamydia*-induced cell survival, the effect of SHC1 knockdown on host cell apoptosis after *Chlamydia* entry was investigated. For this purpose, TNFα was added to SHC1 or luciferase (control) knockdown cells at 6 h *p.i.* for a duration of 4 h, i.e., 2 h

after the observed transcriptional regulation changes (Figure 3-19). Apoptosis induction levels in a combination of SHC1 or luciferase knockdown cells infected with either *C. trachomatis* or *C. pneumoniae* were determined using three different readouts: PARP cleavage (Figure 3-27), CK18 cleavage (Figure 3-28, A-C), and terminal deoxynucleotidyl transferase activity using the TUNEL assay (Figure 3-28, D-F).

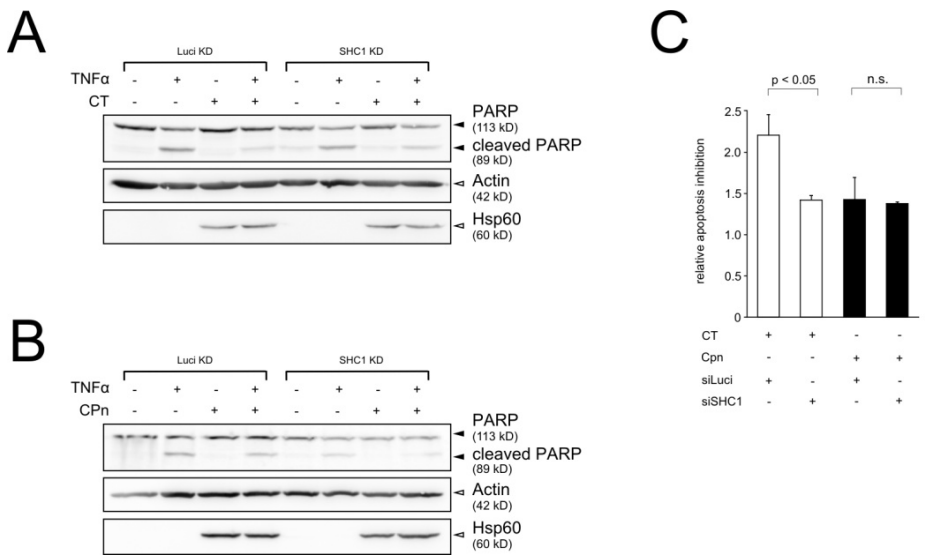

Figure 3-27. Apoptosis in early infected SHC1 knockdown cells (PARP cleavage). Western blots showing TNFα-induced PARP cleavage (black arrowheads) in HeLa cells with luciferase or SHC1 knockdown after *C. trachomatis* L2 infection (MOI 50) (A) or *C. pneumoniae* infection (MOI 50) (B) for 6 h and an additional induction of apoptosis for 4 h (25 ng/ml TNFα and 10 µg/ml cycloheximide). Actin and Hsp60 were used as loading control (white arrowheads). Infection with *C. trachomatis* L2 blocks PARP cleavage in infected luciferase transfected HeLa cells, whereas SHC1 knockdown sensitizes infected cells to apoptosis as indicated by PARP cleavage. (C) Quantification of PARP cleavage in *C. trachomatis* L2 and *C. pneumoniae* infection from chemiluminescence imager recorded blots (data from A and B, n = 3, error bars indicate SE). Band signals from PARP and cleaved PARP were measured using the AIDA software, and the ratio was calculated. The ratio of apoptosis inhibition in uninfected TNFα-stimulated versus infected TNFα-stimulated cells is depicted. *C. trachomatis* L2 infected control cells show a high degree of apoptosis resistance, which is significantly reduced upon SHC1 knockdown. In contrast, *C. pneumoniae* infected cells exhibit a diminished apoptosis resistance, independent of SHC1.

C. trachomatis-infected cells displayed the highest degree of apoptosis resistance under luciferase (control) knockdown conditions. This inhibitory phenotype was significantly reduced under SHC1 knockdown conditions using all three assays (Figure 3-27 C and Figure 3-28, C and F). Although SHC1 dependency was apparent for *C. trachomatis* at the early stages of infection, evidence was lacking for *C. pneumoniae*, which exhibited a comparably diminished degree of apoptosis resistance (Figure 3-27 C and Figure 3-28, C and F) and, notably, expresses a Tarp protein devoid of SHC1 phospho-binding sites (Clifton *et al.*, 2005).

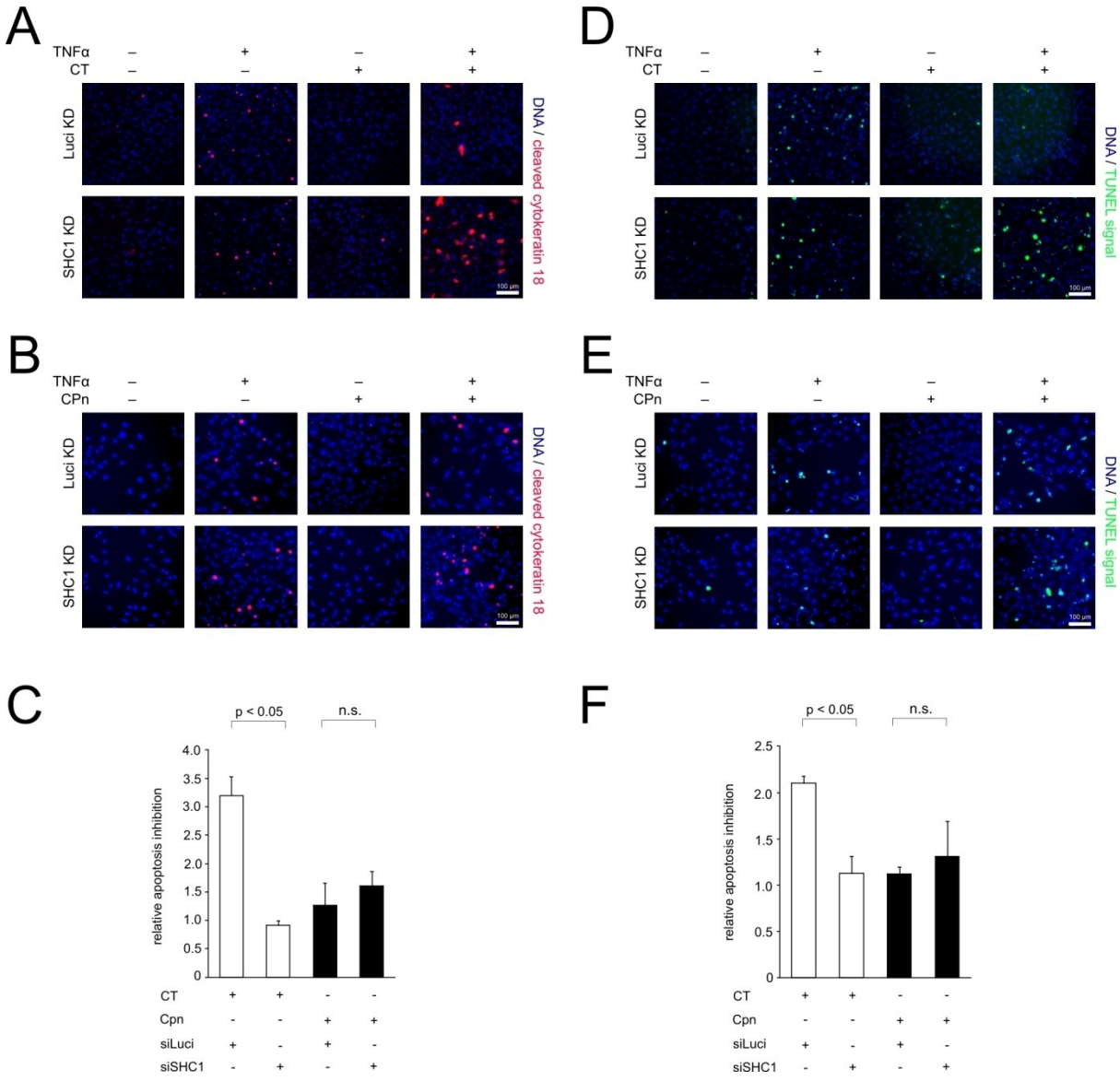

Figure 3-28. Apoptosis in early infected SHC1 knockdown cells (CK 18 cleavage, TUNEL assay). Immunofluorescence staining showing TNFα-induced apoptosis in HeLa cells with luciferase or SHC1 knockdown after infection with *C. trachomatis* L2 (A and D) or *C. pneumoniae* (B and E) and apoptosis induction (identical conditions to Figure 3-27). SHC1 knockdown sensitizes infected cells to apoptosis, whereas apoptosis is blocked in infected control cells. Apoptosis induction was assessed by CK18 cleavage (red) and TUNEL assay (green). Nuclei are stained blue with Hoechst 33342. Image area: 450 µm x 450 µm. Quantification of cells positive for (C) CK18 cleavage (data from A and B; n = 2, error bars indicate SE) and (F) TUNEL (data from D and E; n = 2, error bars indicate SE). An average of 10000 cells per condition was analyzed. Apoptosis inhibition is depicted as in Figure 3-27 C. *C. trachomatis* L2 infection leads to apoptosis inhibition in control cells, but not in SHC1 knockdown cells. In contrast, *C. pneumoniae* fails to block apoptosis in both control and SHC1 knockdown cells.

Thus, these data demonstrate that *C. trachomatis*, but not *C. pneumoniae*, is able to confer early apoptosis resistance to infected host cells in an SHC1-dependent manner.

3.2.11 Discussion

Here, protein microarrays comprising nearly every human SH2, PTB, and SH3 domain were used to quantitatively assess Tarp-mediated interactions with host cellular proteins. Tarp was found to have the capacity to interact with many different SH2 and SH3 domain-containing proteins, which suggests that Tarp contributes substantially to phosphorylation-dependent and -independent signaling. In total, 23 novel SH2 binding partners and 34 novel SH3 binding partners of Tarp were discovered *in vitro*, while two interactions (Tarp/VAV2 and Tarp/PI3K) were confirmed that had previously been identified. High-affinity SH2 interactions with two proteins, the serovariant L2 specific protein NCK2 and the serovariant D and L2 common interaction partner SHC1, were experimentally validated and the interaction of Tarp with SHC1 was studied in greater detail. The Tarp/SHC1 interaction was found to play a direct role in conferring resistance to apoptosis in infected cells. Together, these data extend our understanding of how Tarp modulates host cell functions.

In the nonphosphorylated state, the Tarp N-terminus showed serovariant-dependent affinity for host SH2 domain-containing proteins. ABL2 (ARG) was found to be the strongest interaction partner shared by both serovariants (D and L2). Furthermore, ABL2 and other SRC family kinases (HCK and YES1) were among the strongest interaction partners of the Tarp C-terminal SH3 binding site. ABL kinases can be activated through interaction of their SH2 domains with cellular substrates (Lewis and Schwartz, 1998; Barila *et al.*, 2000). Additionally, kinase activity is regulated via the interaction of their SH3 domain with a substrate SH3 binding site, as reported for ABL kinases and SRC kinases (Lerner and Smithgall, 2002; Smith *et al.*, 2003). While an intramolecular SH3 interaction inhibits ABL kinase activity (Barila and Superti-Furga, 1998), mutation or deletion of the SH3 domain leads to increased ABL kinase activity *in vivo* (Franz *et al.*, 1989; Jackson and Baltimore, 1989). The HIV-1 Nef protein, which is a high-affinity ligand for the SH3 domain of the SRC family kinase HCK (Saksela *et al.*, 1995), has been demonstrated to activate HCK by competing with and disrupting the intramolecular SH3 interaction of HCK, a mechanism described as SH3 domain displacement (Moarefi *et al.*, 1997).

ABL1 and ABL2 have been shown to be among the human kinases that phosphorylate Tarp (Elwell *et al.*, 2008; Jewett *et al.*, 2008; Mehlitz *et al.*, 2008). Consequently, the SH2 and the SH3 interaction between nonphosphorylated Tarp and ABL, leading to subsequent activation of ABL, may constitute an initial trigger for Tarp phosphorylation (Hantschel *et al.*, 2003; Nagar *et al.*, 2003) (Figure 3-29, (1) and (2)). It has previously been reported that infection of ABL/ARG$^{-/-}$ knockout mouse fibroblasts

leads to a ~50 % reduction of Tarp phosphorylation, which suggests that ABL could be the initial Tarp kinase (Elwell *et al.*, 2008). Interestingly, phosphorylation of the *H. pylori* protein CagA and the EPEC effector Tir was also shown to involve ABL (Swimm *et al.*, 2004; Poppe *et al.*, 2007). Furthermore, CagA, ABL, and CRKII have been shown to physically interact (Tammer *et al.*, 2007).

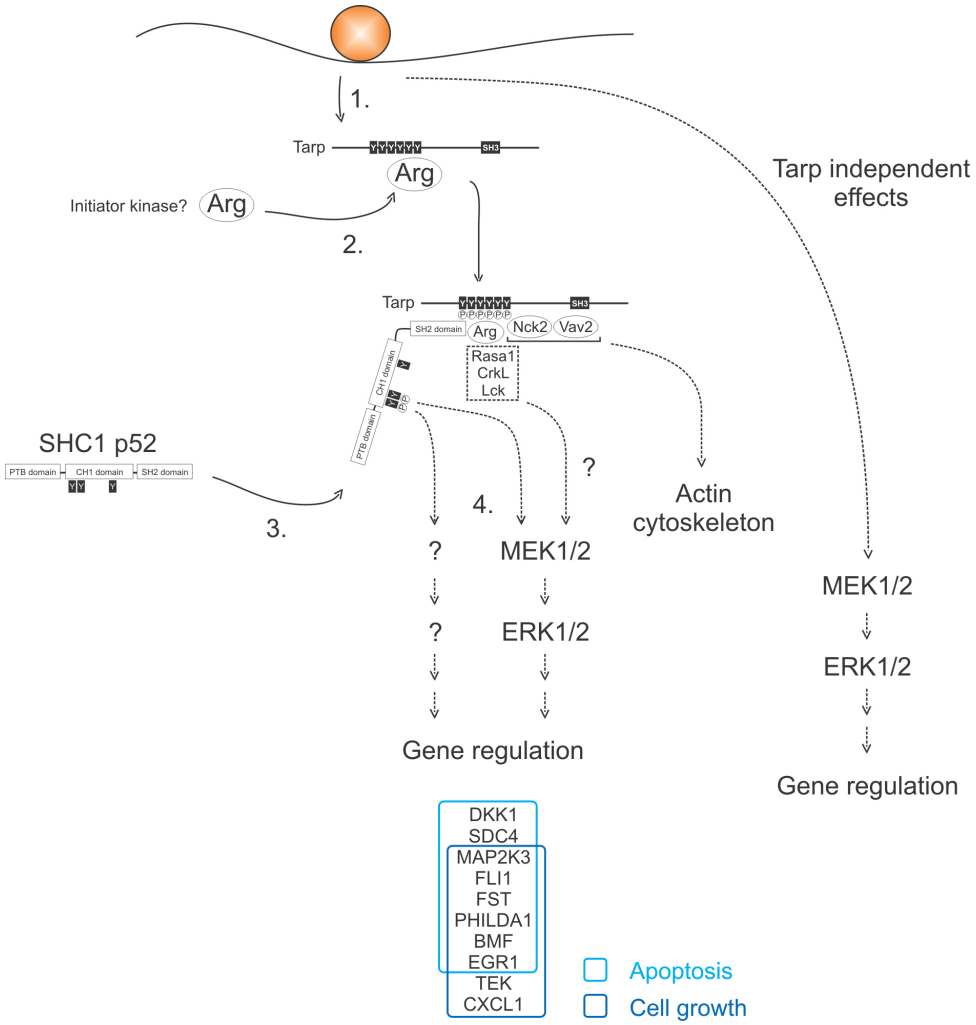

Figure 3-29. The role of Tarp in host cell signaling. (1) *Chlamydia* injects Tarp via its type III secretion system into the host cell. (2) Tarp becomes phosphorylated by an initiator kinase, e.g., ABL/ARG kinases, probably through SH2- and SH3-dependent interaction of the kinase to nonphosphorylated Tarp. Subsequently, phosphorylated Tarp is able to bind to a plethora of host SH2 and SH3 domain-containing proteins, which indicates that it functions as a signaling hub. SHC1 was validated as a serovariant D and L2 common interaction partner. (3) SHC1 binds Tarp through its C-terminal SH2 domain and becomes tyrosine phosphorylated on residues Tyr239/240. Other effectors are likely able to bind Tarp either in a timely or spatially regulated manner. NCK2 was validated as a serovariant L2 specific interaction partner and protein arrays indicate further interaction partners like VAV2 (which has previously been shown to interact with Tarp via immunoprecipitation) (Lane *et al.*, 2008), RASA1, CRKL, and LCK. (4) SHC1 was found to be an important regulator of anti-apoptotic and growth related genes and knockdown of SHC1 sensitized host cells for apoptosis induction via TNFα. Activation of MEK/ERK was not solely dependent on SHC1. The exact role of the MEK/ERK regulators RASA1 and CRKL in

gene regulation and *Chlamydia* growth and the redundancy with SHC1 in MEK/ERK activation needs further investigation. Additionally, Tarp-independent effects such as TLR signaling might influence the activation state of MEK/ERK.

The nonphosphorylated state of the Tarp C-terminus is short-lived as Tarp is phosphorylated immediately after translocation into the host cell (Clifton *et al.*, 2004). This phosphorylation leads to a dramatic increase of SH2 domain-mediated interactions, as demonstrated in this thesis. Accordingly, the Tarp phospho-interactome has a degree of complexity similar to that of the ERBB family of RTKs (Jones *et al.*, 2006). For example, Tarp D and L2 show similar numbers of interaction partners as ERBB4 and ERBB3, respectively. Previously, only VAV2 and the regulatory subunit of PI3K have been identified as interaction partners of phosphorylated Tarp (Lane *et al.*, 2008). Here, these interactions were confirmed using the SH2/PTB domain microarrays, approving the biological validity of the approach. Moreover, it was found that Tarp L2 interacts with several host cell kinases previously implicated in Tarp phosphorylation, corroborating Tarp L2 as a promiscuous phosphorylation substrate (Elwell *et al.*, 2008; Jewett *et al.*, 2008; Mehlitz *et al.*, 2008).

In addition to Tarp's C-terminal interactions mediated by its SH2 binding motifs, the N-terminal SH3 binding site expands and probably fine-tunes the capacity of Tarp to interact with host cellular proteins. This interaction site has so far not been described. Previous studies have focussed on a proline-rich domain in the N-terminal region of Tarp (Ser625 to Asn650), suggesting it promotes Tarp oligomerization and is required for Tarp-dependent nucleation of new actin filaments (Jewett *et al.*, 2006; Jewett *et al.*, 2010). However, this domain is distinct from the SH3 binding site investigated in the study presented here, which is located between Ser818 and Tyr837. Protein microarrays revealed a large set of Tarp interactions with cellular SH3 domain-containing proteins, mainly involved in processes like phagocytosis, cytoskeletal rearrangement, and proliferation. Furthermore, as stated above, SH3-mediated interactions with host cell kinases like ABL2, HCK, and YES1 were detected. These interactions might contribute to kinase activation (Moarefi *et al.*, 1997), thereby triggering initial phosphorylation of the Tarp N-terminus.

To validate the functionality of the putative SH3 binding site, the interaction with NCK2, an interaction partner with a high interaction signal, was chosen for further investigation. Both Tarp and NCK2 were structurally modeled and docking experiments were performed, demonstrating the previously detected interaction of Tarp and NCK2 *in silico*. Moreover, the calculated dissociation constant K_D for the Tarp/NCK interaction is within the lower range of values expected for SH3 interactions (Li, 2005). This further supports the observation of a Tarp/NCK2 interaction via the C-terminal SH3 binding site and approves the functionality of this newly described SH3 binding site.

Taken together, the detected interactions with host cellular SH2 and SH3 domain-containing proteins suggest that Tarp operates as a phosphorylation-dependent and -independent signaling hub comparable to receptor-mediated signaling. Furthermore, Tarp interactions are likely to occur in a timely or spatially regulated manner.

Comparison of the SH2 interactions of Tarp D and L2 revealed SHC1 as one of the strongest partners for both serovariants, which suggests a general role for SHC1 in *C. trachomatis* infections. SHC1, which has not previously been shown to interact with Tarp, is also involved in EGFR signaling, leading to MEK/ERK activation upon stimulation with EGF or TNFα. MEK/ERK activation, an emerging theme in the chlamydial infection process, was first shown to be involved in glycerophospholipid acquisition by *Chlamydia* (Su *et al.*, 2004) and more recently as an important anti-apoptotic mechanism (Paland *et al.*, 2008). Here, pronounced activation of MEK and ERK was found shortly after infection coincident with phosphorylation of Tarp and SHC1. Previous work suggested that rapid phosphorylation of ERK during chlamydial infection is linked to up-regulation of the anti-apoptotic protein MCL-1 (Rajalingam *et al.*, 2008), which was demonstrated to be independent of SHC1 in the study presented here (data not shown). Moreover, activation of both MEK and ERK was previously shown to be necessary for *C. trachomatis* at an advanced stage of infection, however, this activation was uncoupled from upstream signaling by RAS and RAF (Gurumurthy *et al.*, 2010). MEK activation is thought to be crucial during infections with *H. pylori* (Hatakeyama, 2008) and has been shown to be initiated through interaction of CagA with SHP-2 (Higashi *et al.*, 2002), CRK (Suzuki *et al.*, 2005), GRB2 (Mimuro *et al.*, 2002) and c-MET (Churin *et al.*, 2003).

Here, the direct recruitment of SHC1 and the subsequent activation of RAS and the MAP kinase family members MEK and ERK in the early stages of a *C. trachomatis* infection is described (Figure 3-29, (3)). However, *Chlamydia* Tarp may very well trigger additional pathways causing MEK/ERK activation (see Figure 3-24). Candidate molecules are the adaptor protein CRKL, which is capable of activating ERK through b-RAF upon integrin signaling (Guo and Giancotti, 2004); the GTPase RASA1, directly activating b-RAF (Schubbert *et al.*, 2007); and p56LCK, which bypasses RAS/RAF/MEK and activates ERK in a PKCε-dependent manner during *Mycobacterium leprae* infection (Tapinos and Rambukkana, 2005). All three factors were found to recognize phospho-Tarp in this thesis (Figure 3-1, Figure 3-29, and Table 6-1). Still, the exact role of CRKL, RASA1, and LCK on gene regulation and *Chlamydia* growth and the redundancy with SHC1 in MEK/ERK activation need to be further investigated. Additionally, Tarp-independent effects such as TLR signaling might influence the activation state of MEK/ERK.

SHC1 knockdown led to significant changes in the expression of anti-apoptotic and growth related genes in the context of *C. trachomatis* infection (Figure 3-29, (4)). As deduced from knowledge-based pathway analysis, SHC1 signaling depends only partially on the MEK/ERK cascade, whereas the remaining genes are regulated by additional signaling pathways (Figure 3-24 and Figure 3-29, (4)). This is consistent with the observation of a significant reduction in *C. trachomatis*-induced cell survival upon SHC1 knockdown despite a residual activation of MEK and ERK. It is tempting to argue that this SHC1-mediated gene regulation is a MEK/ERK-independent branch of the EGFR-mediated signaling cascade. In *H. pylori* infection, a major outcome of CagA translocation appears to be regulation of growth-dependent genes (Keates *et al.*, 1999; Mimuro *et al.*, 2002). Thus, induction of growth signaling seems to be an important function of tyrosine phosphorylated effectors. Future investigations are required to clarify whether this also holds true for other effectors like EPEC Tir, *Anaplasma phagocytophilum* AnkA or *Vaccinia* virus A36R (Backert *et al.*, 2008). Collectively, these observations support a model in which activation of both MEK/ERK-dependent and -independent growth signaling cascades plays a central role in *C. trachomatis*-induced cell survival. This assigns an important anti-apoptotic function to the interaction between phospho-Tarp and SHC1 during the early stage of infection.

An alternative approach to assess protein interactions with tyrosine-phosphorylated peptides from CagA, Tir, Tarp, and BepD-F used differential mass-spectroscopy (SILAC) (Selbach *et al.*, 2009). This study revealed only a few of the Tarp SH2 interaction partners reported here, notably the previously reported interaction with PI3K. Differences in methodological approach are most likely responsible for this small degree of overlap. The protein array analysis provides a list of all possible direct interaction partners. In contrast, immunoprecipitation coupled with mass spectrometry does not discriminate between direct and indirect interactions, owing to secondary protein contacts in signaling complexes. In addition, the approach used in this thesis provides a global view of biophysical interactions, whereas the approach of Selbach and colleagues focussed on a specific cell type and hence was dependent on the proteins being expressed in their cell of interest (Selbach *et al.*, 2009). Nonetheless, both approaches provide important and complementary information on the complexity of host-pathogen interactomes.

This thesis has shown that global interactome studies provide a powerful approach to uncover host cell counterparts of bacterial effector proteins, helping to increase our understanding of the mechanisms of host-microbe interactions. This work presents a comprehensive interactome study of a phosphorylated bacterial effector protein using SH2/PTB and SH3 domain microarrays. The study

not only confirmed several known interactions but also revealed an extensive repertoire of novel high- and low-affinity interactions with phosphorylated and nonphosphorylated versions of *C. trachomatis* Tarp. In addition, these interactions varied substantially between serovars. The focus of this thesis was on just one of the many possible Tarp-cellular protein interactions to substantiate the hypothesis of early Tarp-mediated host cell signaling. The remaining data reported here provide a wealth of additional hypotheses to test regarding Tarp-mediated signaling induced by chlamydial infection.

3.3 Part II: Changes in lipid composition induced by *Chlamydia*

3.3.1 Analysis of lipids using MALDI-TOF mass spectrometry

The acquisition of host cell lipids plays a crucial role for the successful establishment and growth of *Chlamydia* (Saka and Valdivia, 2010). By subverting host cellular trafficking pathways, *Chlamydia* actively interferes with the host cell lipid composition (Wylie *et al.*, 1997; Hatch and McClarty, 1998a). To globally investigate changes in lipid composition induced by *C. trachomatis* infection, lipid extracts obtained from uninfected and infected (24 h *p.i.*) HeLa cells were analyzed by MALDI-TOF mass spectrometry. For this purpose, two approaches were applied: 1. the direct measurement of lipids in the crude lipid extract without further intermediate experimental steps, and 2. the separation of lipid extracts by normal phase TLC based on the properties of their head groups followed by lipid measurement directly on the TLC plate (Figure 3-30). While the first method reduces experimental procedures to a minimum and thereby avoids degradation of lipids, the second approach allows for a higher sensitivity to detect less abundant lipid species within the lipid extracts (Schiller *et al.*, 2004).

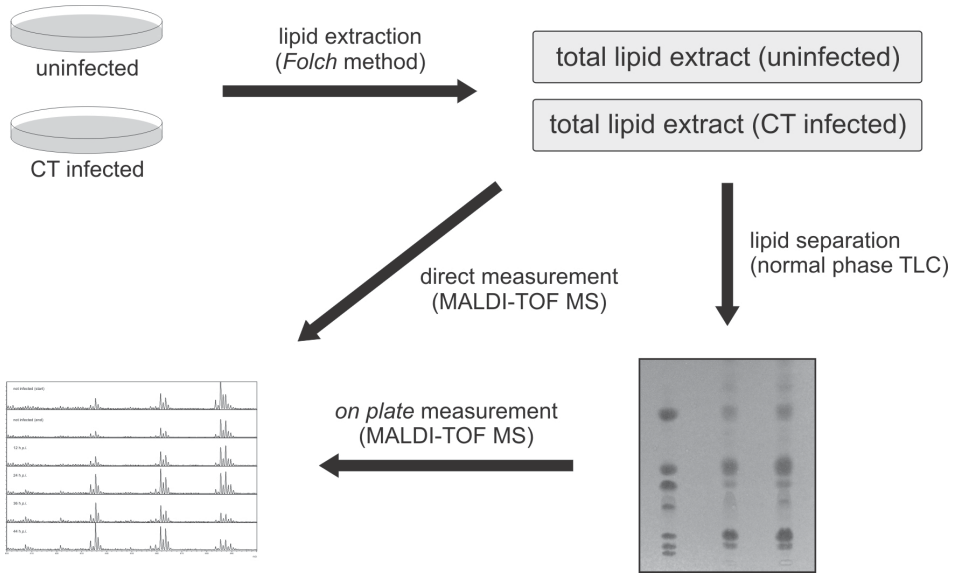

Figure 3-30. Workflow scheme of MALDI-TOF lipid analysis. Lipids were extracted from uninfected and infected HeLa cells (*C. trachomatis* L2, MOI 2.5, 24 h *p.i.*) according to Folch *et al.*, 1957 and subsequently analyzed by MALDI-TOF mass spectrometry. Two methods were applied: 1. the direct MALDI-TOF measurement of crude lipid extracts, and 2. the separation of lipid classes by normal phase TLC prior to MALDI-TOF measurement.

Normal phase TLC provided a separation of different lipid classes, such as PG, PE, PA, PI, PS, PC, SM, and LPC (Figure 3-31). A standard solution comprising these major lipid classes was spotted on the

TLC plate and separated in parallel to the lipid extracts of uninfected and infected HeLa cells. This allowed for the identification of lipid class spots within the extracts. After spots were marked, matrix solution was added to the spots and lipids were measured by MALDI-TOF mass spectrometry directly on the TLC plate.

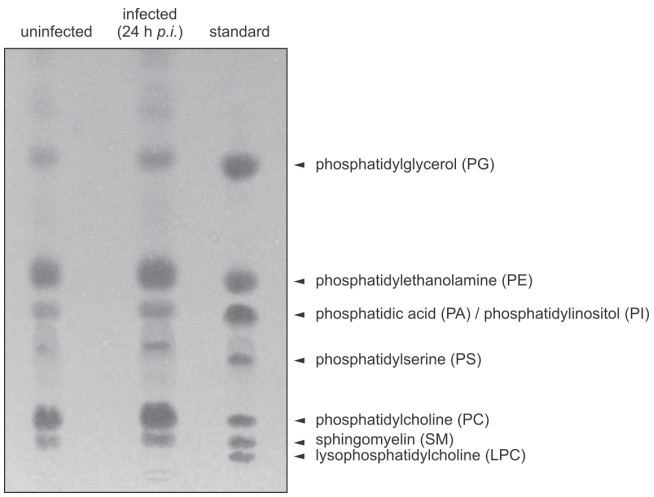

Figure 3-31. TLC of lipid extracts from uninfected and infected HeLa cells. Lipid extracts of uninfected and infected HeLa cells was subjected to normal phase TLC, providing a separation of different lipid classes. A standard solution comprising major lipid classes was additionally subjected to the TLC plate, allowing for correct identification of the detected spots in the lipid extracts.

Both approaches – the direct and TLC coupled measurement of lipids – were combined to obtain a comprehensive overview of changes in lipid composition upon infection with *C. trachomatis*. A complete list of detected and assigned peaks is given in Table 3-4.

Table 3-4. Peak assignment of MALDI-TOF mass spectrometry analysis. Assignments of ion signals detected in the MALDI-TOF mass spectra of lipid extracts from uninfected and infected HeLa cells. Unassigned mass peaks are marked in red. Results are from two independent biological experiments.

Mass (m/z) (Da)	Assignment	Condition (uninfected / infected)	MALDI-TOF ion mode (positive / negative)
369.4	Cholesterol + H^+ / - H_2O	Uninfected / infected	Positive
706.0	DHSM (16:0) + H^+	Uninfected / infected	Positive
728.0	DHSM (16:0) + Na^+	Uninfected / infected	Positive
703.6	SM (16:0) + H^+	Uninfected / infected	Positive
725.6	SM (16:0) + Na^+	Uninfected / infected	Positive
813.6	SM (24:1) + H^+	Infected	Positive
835.6	SM (24:1) + Na^+	Infected	Positive

706.9	PC (14:0/16:0) + H^+	Uninfected / infected	Positive
728.6	PC (14:0/16:0) + Na^+	Uninfected / infected	Positive
732.6	PC (16:0/16:1) + H^+	Uninfected / infected	Positive
734.6	PC (16:0/16:0) + H^+	Uninfected / infected	Positive
754.6	PC (16:0/16:1) + Na^+	Uninfected / infected	Positive
756.6	PC (16:0/16:0) + Na^+	Uninfected / infected	Positive
760.6	PC (16:0/18:1) + H^+	Uninfected / infected	Positive
782.6	PC (16:0/18:1) + Na^+	Uninfected / infected	Positive
808.6	PC (18:0/18:2) + Na^+	Uninfected / infected	Positive
740.5	Unassigned	Infected	Positive
742.5	Unassigned	Infected	Positive
794.7	Unassigned	Infected	Positive
816.7	Unassigned	Infected	Positive
454.1	LPC (14:0) + H^+	Infected	Positive
476.1	LPC (14:0) + Na^+	Infected	Positive
740.6	PE (16:0/18:1) + Na^+	Uninfected / infected	Positive
746.6	PE (18:0/18:1) + H^+	Uninfected / infected	Positive
762.6	PE (16:0/18:1) +2 Na^+	Uninfected / infected	Positive
768.6	PE (18:0/18:1) + Na^+	Uninfected / infected	Positive
790.6	PE (18:0/20:4) + Na^+	Uninfected / infected	Positive
813.1	PE (18:0/20:4) +2 Na^+	Uninfected / infected	Positive
700.6	Unassigned	Infected	Positive
722.6	Unassigned	Infected	Positive
771.6	PG (16:0/18:1) + H^+	Uninfected / infected	Positive
793.6	PG (16:0/18:1) + Na^+	Uninfected / infected	Positive
703.6	Unassigned	Infected	Positive
725.6	Unassigned	Infected	Positive
731.6	Unassigned	Infected	Positive
753.6	Unassigned	Infected	Positive
859.6	PI (16:0/18:1) + H^+	Uninfected / infected	Positive
881.7	PI (16:0/18:1) + Na^+	Uninfected / infected	Positive
909.6	PI (18:0/20:4) + H^+	Uninfected / infected	Positive
931.6	PI (18:0/20:4) + Na^+	Uninfected / infected	Positive
784.6	PS (16:0/18:1) + H^+	Uninfected / infected	Positive
812.6	PS (18:0/18:1) + H^+	Uninfected / infected	Positive
834.9	PS (18:0/18:1) + Na^+	Uninfected / infected	Positive
716.5	PE (16:0/18:1)	Uninfected / infected	Negative

742.5	PE (18:0/18:2)	Uninfected / infected	Negative
744.5	PE (18:0/18:1)	Uninfected / infected	Negative
766.5	PE (18:0/20:4)	Uninfected / infected	Negative
662.5	PE (14:0/16:0)	Infected	Negative
690.5	PE (16:0/16:0)	Infected	Negative
747.5	PG (16:0/18:1)	Uninfected / infected	Negative
773.5	PG (18:0/18:2)	Uninfected / infected	Negative
693.5	PG (14:0/16:0)	Infected	Negative
721.6	PG (16:0/16:0)	Infected	Negative
833.6	PI (16:0/18:2)	Uninfected / infected	Negative
835.6	PI (16:0/18:1)	Uninfected / infected	Negative
861.6	PI (18:0/18:2)	Uninfected / infected	Negative
863.6	PI (18:0/18:1)	Uninfected / infected	Negative
885.6	PI (18:0/20:4)	Uninfected / infected	Negative
887.6	PI (18:0/20:3)	Uninfected / infected	Negative
807.6	PI (16:0/16:1)	Infected	Negative
760.6	PS (16:0/18:1)	Uninfected / infected	Negative
788.6	PS (18:0/18:1)	Uninfected / infected	Negative
1394.0	CL (14:0/16:0/18:2/18:2)	Uninfected / infected	Negative
1422.0	CL (16:0/16:0/18:2/18:2)	Uninfected / infected	Negative
1448.0	CL (16:0/18:1/18:2/18:2)	Uninfected / infected	Negative
1450.0	CL (16:0/18:1/18:1/18:2)	Uninfected / infected	Negative
1474.1	CL (18:1/18:1/18:2/18:2)	Uninfected / infected	Negative
1476.0	CL (18:1/18:1/18:1/18:2)	Uninfected / infected	Negative
1373.9	CL (16:0/16:0/16:0/16:0)	Infected	Negative

Based on both MALDI-TOF mass spectrometry approaches, the direct and the TLC coupled measurement of lipids, all major naturally occuring lipid classes were detected, including cholesterol, SM, dihydrosphingomyelin (DHSM), PC, PE, PG, PI, PS, and CL. In infected cells, PE, PG, PI, and CL species with shorter fatty acid chains were predominantly present compared to uninfected cells (Table 3-4). The lyso-form of PC (LPC) was exclusively found in infected cells. Furthermore, several species of PG were only found in lipid extracts from infected cells. Interestingly, additional peaks at m/z = 700.6, m/z = 703.6, m/z = 722.6, m/z = 725.6, m/z = 731.6, m/z = 740.5, m/z = 742.5, m/z = 753.6, m/z = 794.7, and m/z = 816.7 were observed in infected cells (Table 3-4, red labeling), showing a distinct 14 Da difference compared to their corresponding lipid species, namely PE (16:0/16:0) + H^+, PG (14:0/16:0) + H^+, PE (16:0/16:0) + Na^+, PG (14:0/16:0) + Na^+, PG (16:0/16:0) +

H^+, PC (16:0/16:1) + Na^+, PC (16:0/16:0) + Na^+, PG (16:0/16:0) + Na^+, PC (18:0/20:4) + H^+, and PC (18:0/20:4) + Na^+, respectively. These peaks could not be assigned to any lipid species typically occurring in eukaryotic cells.

3.3.2 Temporal changes in lipid composition during the chlamydial infection cycle

Analysis of lipids at a single time point in the developmental cycle of *C. trachomatis* (24 h *p.i.*) can not sufficiently reveal temporal variations of the lipid composition and does not cover changes occuring at later stages. Therefore, time course experiments were performed to cover the complete chlamydial developmental cycle. Lipid extracts from four different time points of infection and two uninfected samples were analyzed (Figure 3-32).

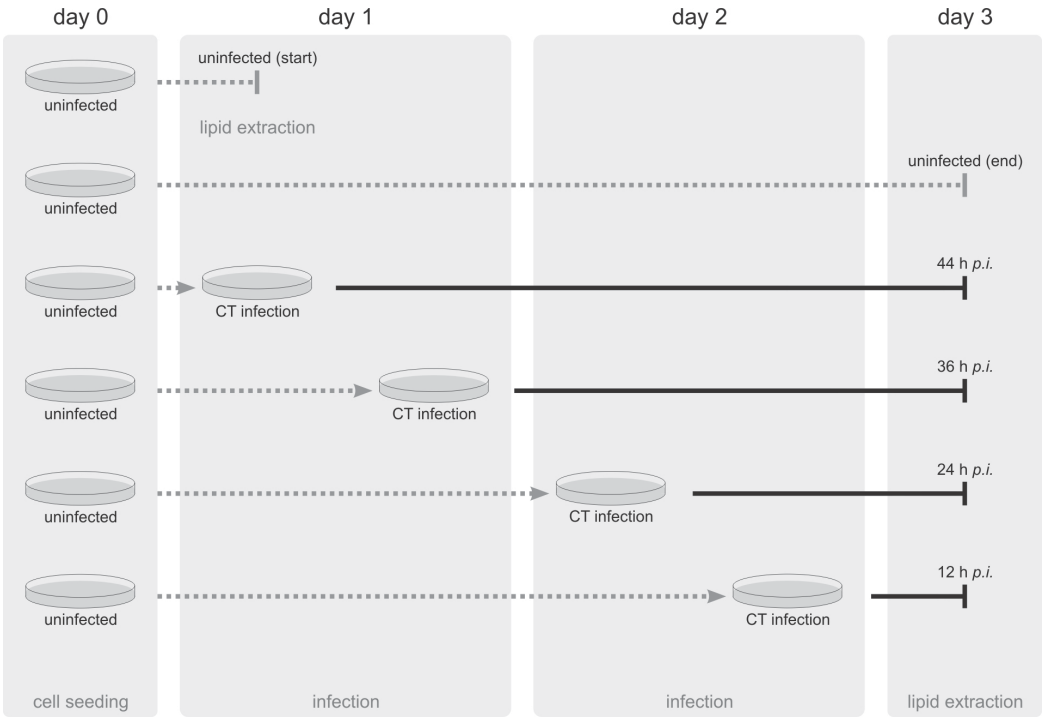

Figure 3-32. Workflow scheme of time course lipid analysis. Lipids were extracted from uninfected and infected HeLa cells (*C. trachomatis* L2, MOI 2.5) according to Folch *et al.*, 1957 and subsequently analyzed by MALDI-TOF mass spectrometry. Cells were infected for 12 h, 24 h, 36 h, and 44 h to cover the complete chlamydial developmental cycle. Lipids from uninfected cells (start) and uninfected cells (end) reflect the lipid composition at the beginning and at the end of the experiment, respectively.

Cells were infected at different time points; lipids were extracted at the same time point (Figure 3-32). To differentiate between cell type specific and cell type independent effects on the lipid composition, two different cell lines, HeLa cells and HEp-2 cells, were used for the time course

experiments (Figure 3-33 A). Extracted lipids amounts were normalized based on cell numbers, which were microscopically determined prior to MALDI-TOF mass spectrometry measurement (Figure 3-33 B).

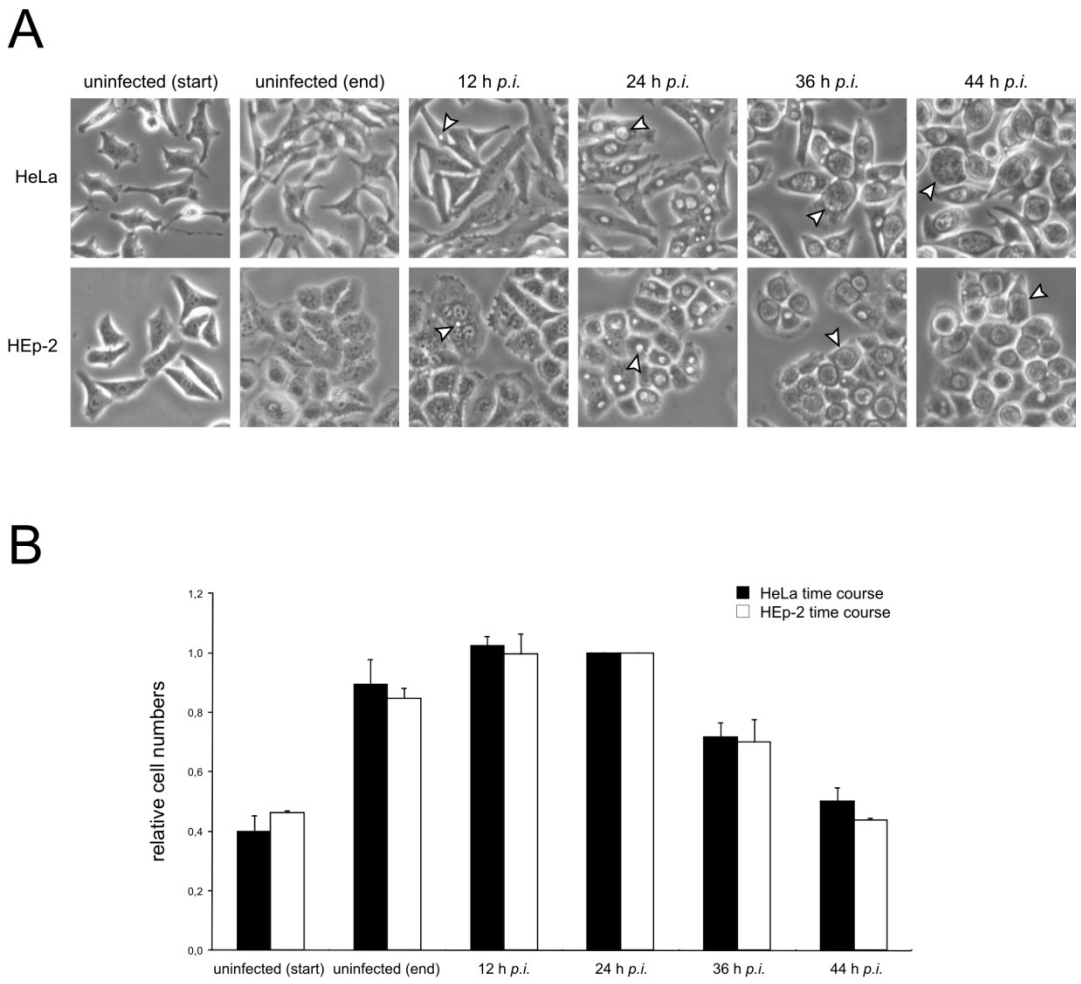

Figure 3-33. Cell numbers during infection time course. (A) Microscopy pictures of cells infected with *C. trachomatis*. HeLa cells and HEp-2 cells were infected for 12 h, 24 h, 36 h, and 44 h. White arrows mark inclusions. (B) Quantification of cell numbers from Figure 3-33 A. Cell numbers were normalized to the 24 h time point. Results are from two independent biological experiments.

Negative ion mode MALDI-TOF measurement of all time points revealed major changes in PI and CL lipid composition during the chlamydial developmental cycle in HeLa cells. Focussing on lipids with lower masses (m/z < 900), PI species with comparably long fatty acid residues (PI (18:0/20:4), PI (18:0/20:3)) decreased during the progression of the cycle, while PI species with shorter fatty acid residues (PI (16:0/16:1), PI (16:0/18:2), PI (16:0/18:1), PI (18:0/18:2), PI (18:0/186:1)) increased over time (Figure 3-34 A). These changes are also reflected in the quantification of Figure 3-34 A (Figure 3-34 B).

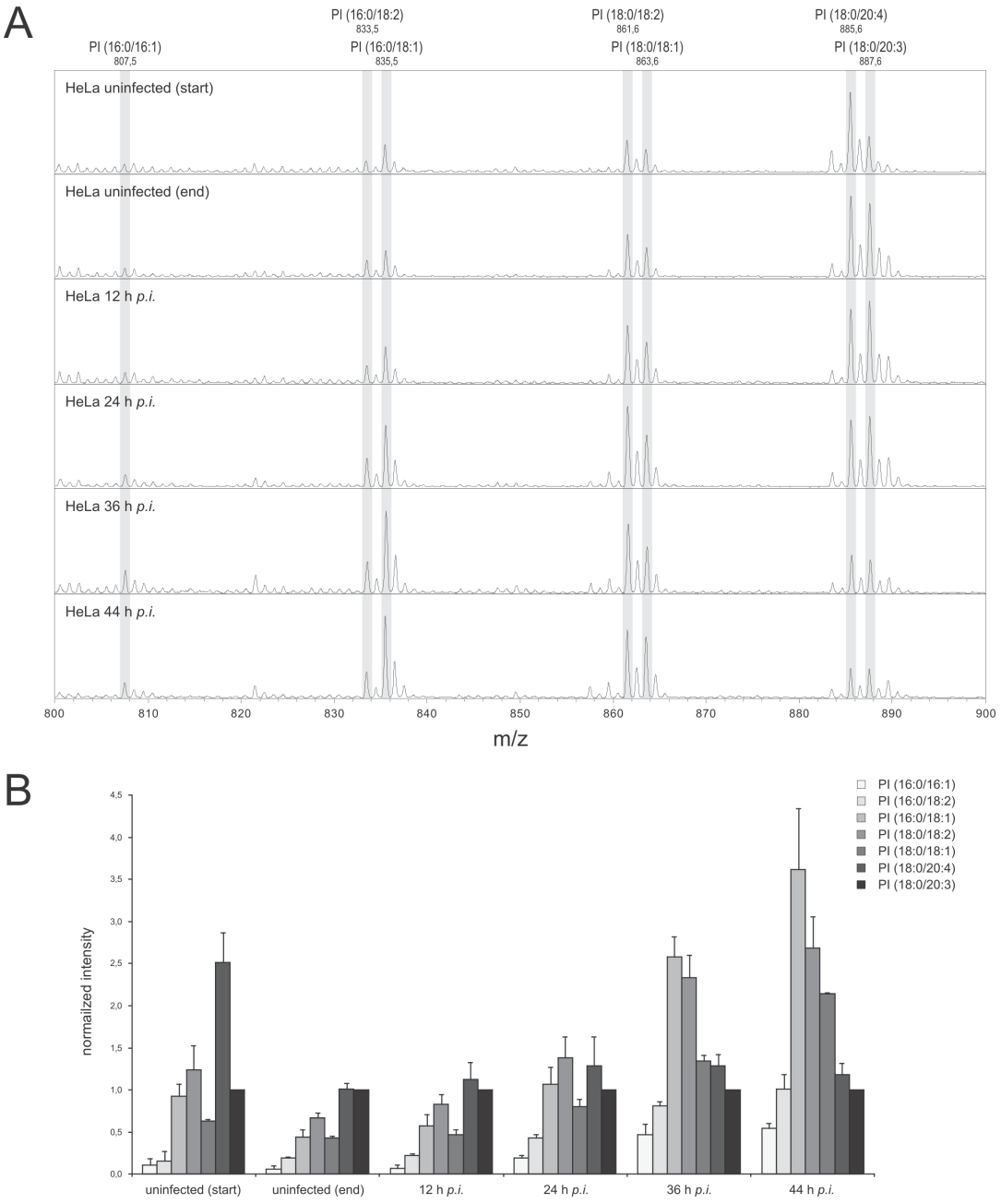

Figure 3-34. Lipid profile of infection time course in HeLa cells (intermediate masses). (A) Negative ion mode mass spectra of lipid extracts from *C. trachomatis* infection time course in HeLa cells. HeLa cells were infected for 12 h, 24 h, 36 h, and 44 h. PI species with long fatty acid residues decrease over time, while PI species with short fatty acid residues increase. Figure shows representative mass spectra of two independent biological experiments. (B) Bar diagram quantifying changes in PI composition during infection of HeLa cells with *C. trachomatis* (Figure 3-34 A). Values are normalized to PI (18:0/20:3). Results are from two independent biological experiments. Error bars indicate SE.

Negative ion mode MALDI-TOF measurement of HEp-2 cells infected with *C. trachomatis* resulted in the detection of the same lipid species with lower masses (m/z < 900) as in infected HeLa cells. Furthermore, the same tendency of changes in the lipid profile was observed (Figure 3-35).

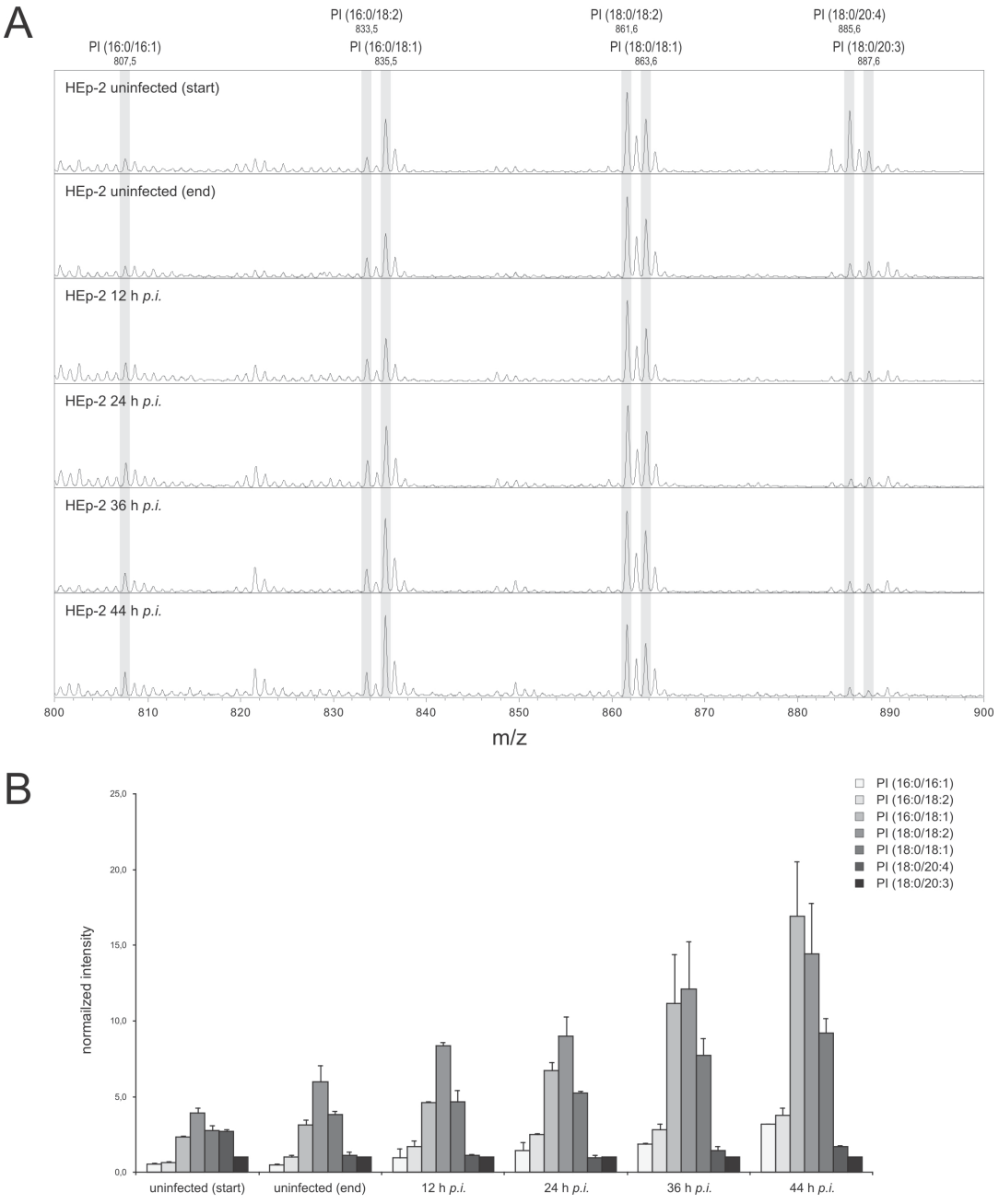

Figure 3-35. Lipid profile of infection time course in HEp-2 cells (intermediate masses). (A) Negative ion mode mass spectra of lipid extracts from *C. trachomatis* infection time course in HEp-2 cells. HEp-2 cells were infected for 12 h, 24 h, 36 h, and 44 h. PI species with long fatty acid residues decrease over time, while PI species with short fatty acid residues increase. Figure shows representative mass spectra of two independent biological experiments. (B) Bar diagram quantifying changes in PI composition during infection of HEp-2 cells with *C. trachomatis* (Figure 3-35 A). Values are normalized to PI (18:0/20:3). Results are from two independent biological experiments. Error bars indicate SE.

Among the lipids with higher masses (m/z > 1300), CL levels were found to be affected during progression of the infection in HeLa cells. While a core set of CL species (CL (2x16:0/2x18:2), CL (16:0/18:1/2x18:2), CL (16:0/2x18:1/18:2), CL (2x18:1/2x18:2), CL (3x18:1/18:2)) remained

unchanged during infection, CL species with shorter fatty acid residues (CL (4x16:0), CL (14:0/16:0/2x18:2)) increased over time (Figure 3-36). Furthermore, additional unassigned peaks (m/z = 1331.9, m/z = 1345.9, m/z = 1359.9) increased during the infectious cycle. Interestingly, these peaks differ from the mass of CL (4x16:0) by a multitude of 14 Da (Figure 3-36 A).

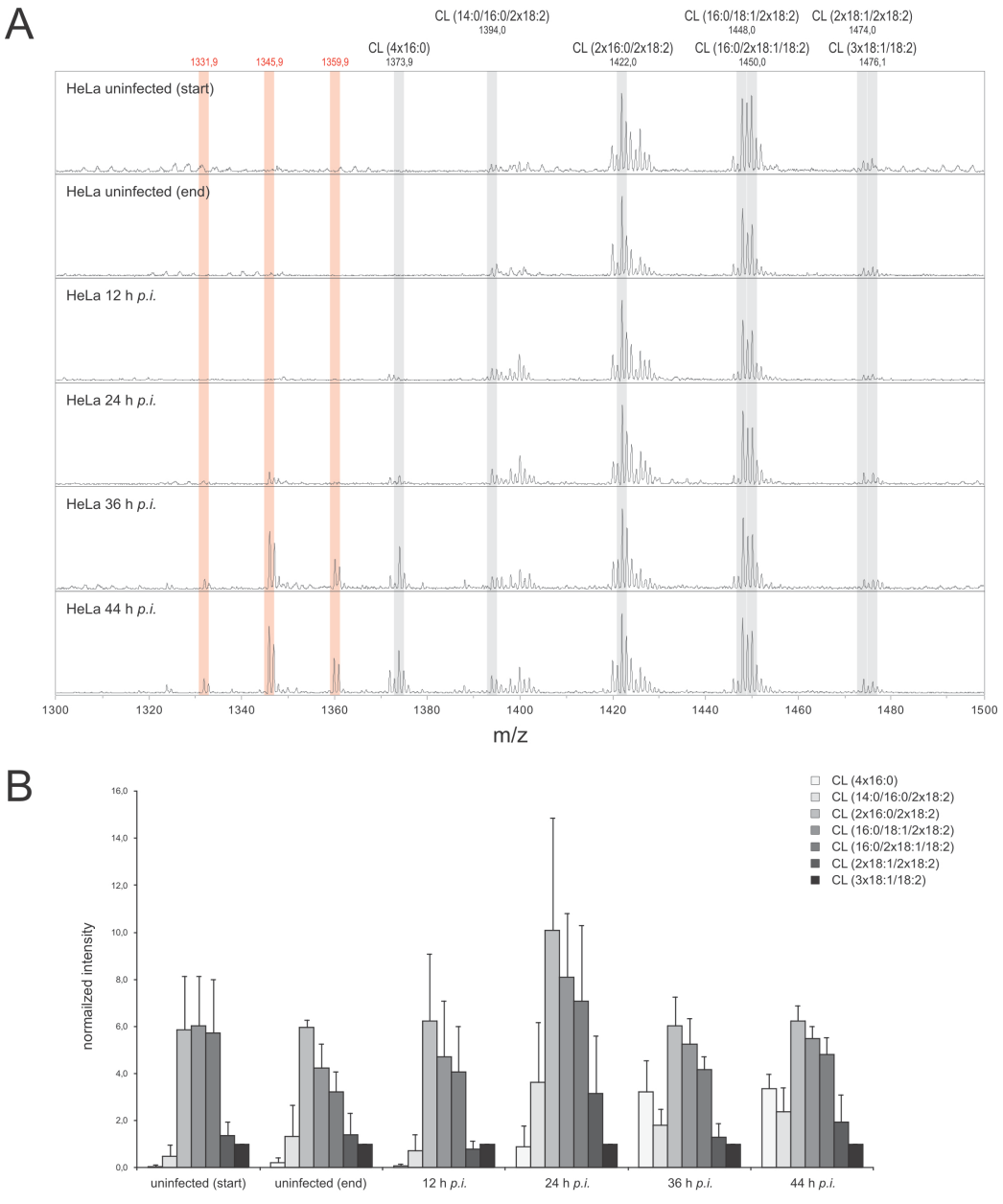

Figure 3-36. Lipid profile of infection time course in HeLa cells (high masses). (A) Negative ion mode mass spectra of lipid extracts from *C. trachomatis* infection time course in HeLa cells. HeLa cells were infected for 12 h, 24 h, 36 h, and 44 h. CL species with short fatty acid residues increase over time. Red marks indicate unassigned mass peaks increasing during the developmental cycle. Figure shows representative mass spectra of two independent biological experiments. (B) Bar diagram quantifying changes in CL composition during infection of HeLa cells with *C. trachomatis* (Figure 3-36 A). Values are normalized to CL (3x18:1/18:2). Results are from two independent biological experiments. Error bars indicate SE.

Similar changes were detected during *C. trachomatis* infection of HEp-2 cells. CL species with shorter fatty acid residues (CL (4x16:0), CL (14:0/16:0/2x18:2)) were found to increase during the infection cycle (Figure 3-37). Again, peaks at m/z = 1331.9, m/z = 1345.9, and m/z = 1359.9 were found to increase during the infectious cycle (Figure 3-37 A).

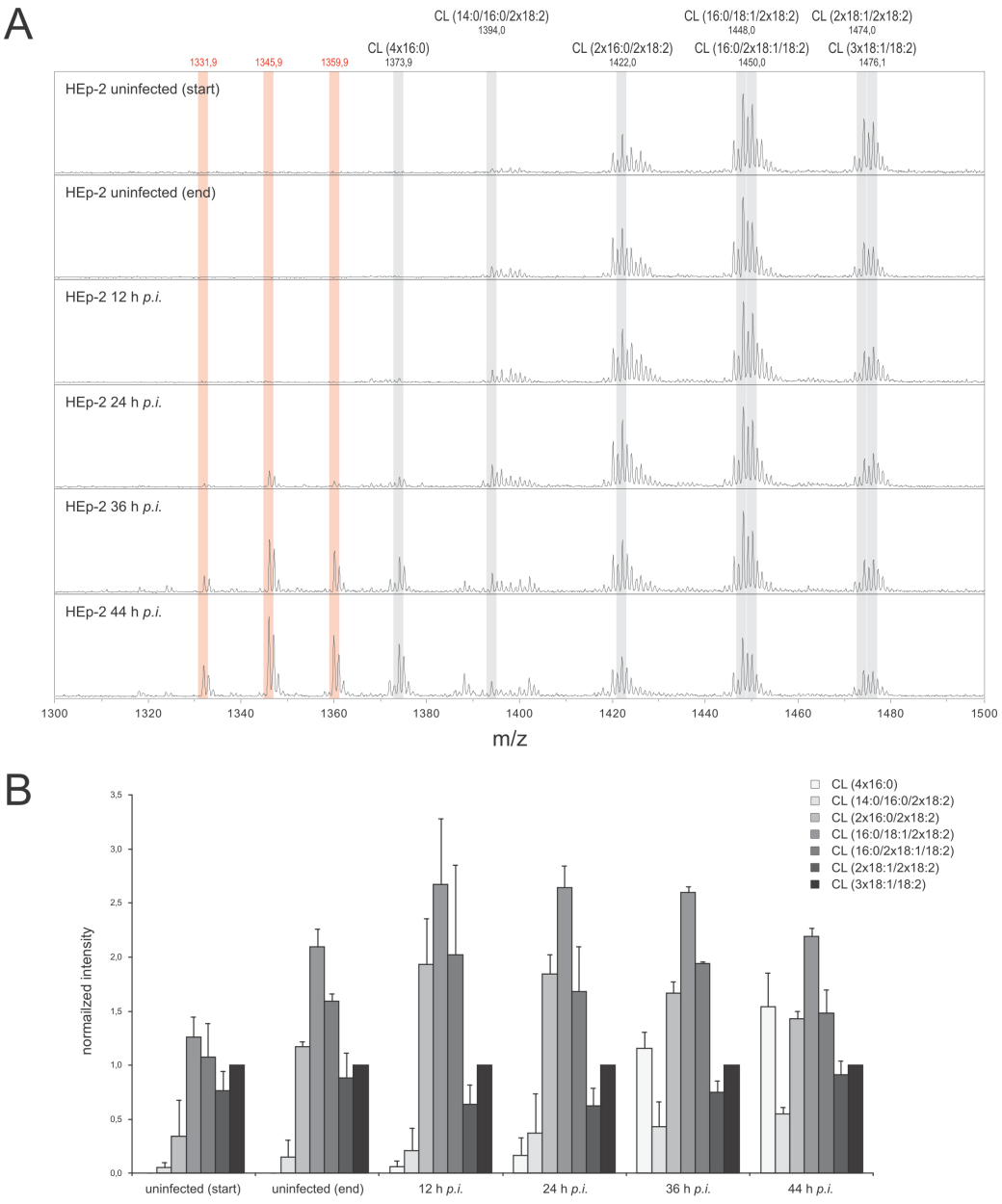

Figure 3-37. Lipid profile of infection time course in HEp-2 cells (high masses). (A) Negative ion mode mass spectra of lipid extracts from *C. trachomatis* infection time course in HEp-2 cells. HEp-2 cells were infected for 12 h, 24 h, 36 h, and 44 h. CL species with short fatty acid residues increase over time. Red marks indicate unassigned mass peaks increasing during the developmental cycle. Figure shows representative mass spectra of two independent biological experiments. (B) Bar diagram quantifying changes in CL composition during infection of HEp-2 cells with *C. trachomatis* (Figure 3-37 A). Values are normalized to CL (3x18:1/18:2). Results are from two independent biological experiments. Error bars indicate SE.

Among lipid species with m/z < 800, PE species (PE (14:0/16:0), PE (2x16:0), PE (16:0/18:1), PE (18:0/18:2), PE (18:0/18:1), PE (18:0/20:4)), and PG species (PG (14:0/16:0), PG (2x16:0), PG (16:0/18:1), PE (18:0/18:2)) were detected, while short fatty acid lipids (PE (14:0/16:0), PE (2x16:0), PG (14:0/16:0), PG (2x16:0)) were found mainly at later infection time points (Figure 3-38). Interestingly, peaks at m/z = 676.5, m/z = 702.5, and m/z = 707.5 were observed, with a distinct 14 Da difference compared to PE (2x16:0), PE (16:0/18:1), and PG (2x16:0), respectively.

Figure 3-38. Lipid profile of infection time course in HeLa and HEp-2 cells (low masses) (part I). Negative ion mode mass spectra of lipid extracts from *C. trachomatis* infection time course in HeLa and HEp-2 cells. Cells were infected for 12 h, 24 h, 36 h, and 44 h. Red marks indicate unassigned mass peaks increasing during the developmental cycle. Figure shows representative mass spectra of two independent biological experiments.

Positive ion mode MALDI-TOF spectra of all time points of the developmental cycle revealed SM (16:0) and several PC species with nearly no changes during progression of the infection (Figure 3-39). Remarkably, additional peaks at m/z = 740.5, m/z = 742.5, and m/z = 768.6 were detected, with a distinct 14 Da difference compared to PC (16:0/16:1) + Na^+, PC (16:0/16:0) + Na^+, and PC (16:0/18:1) + Na^+, respectively.

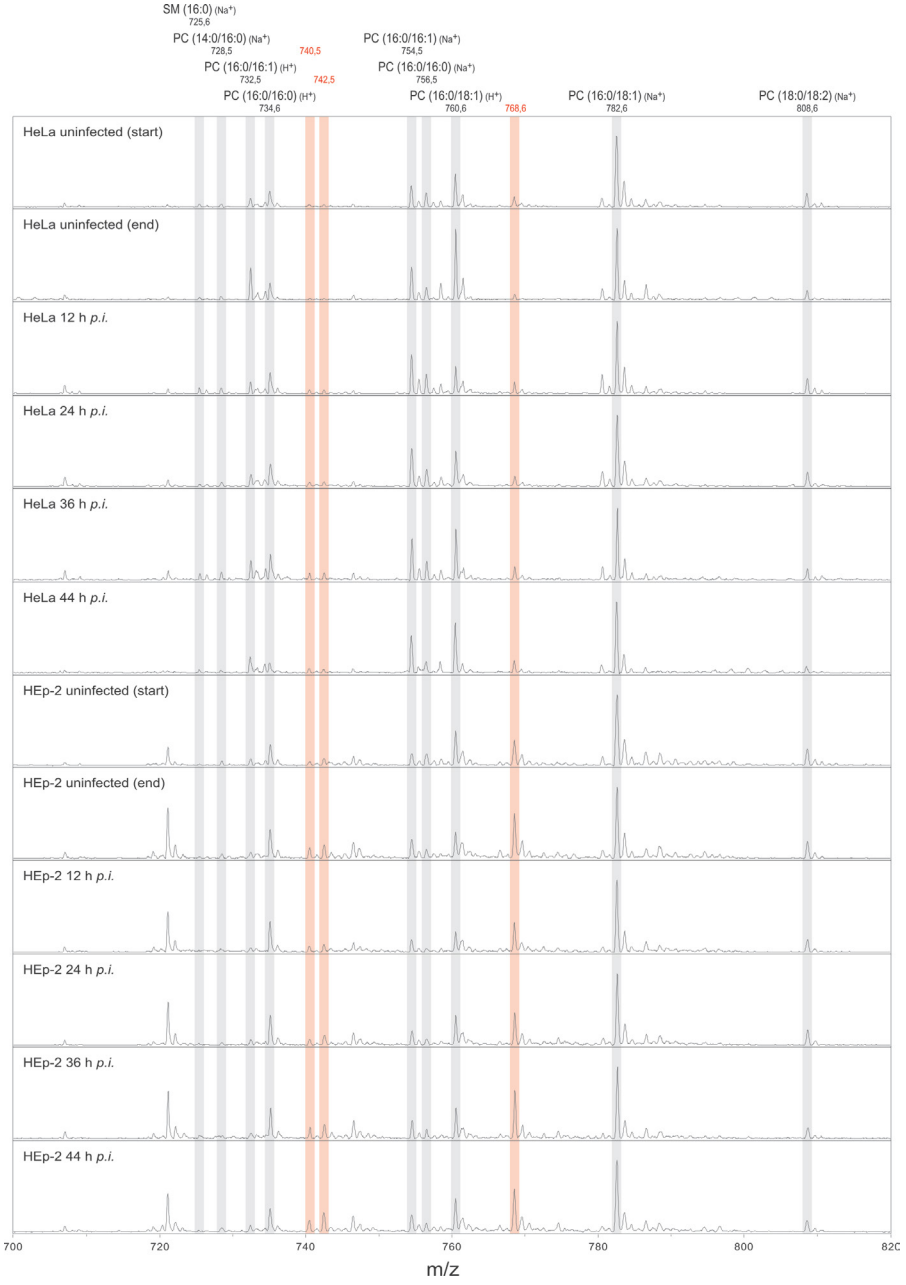

Figure 3-39. Lipid profile of infection time course in HeLa and HEp-2 cells (low masses) (part II). Positive ion mode mass spectra of lipid extracts from *C. trachomatis* infection time course in HeLa and HEp-2 cells. Cells were infected for 12 h, 24 h, 36 h, and 44 h. Red marks indicate unassigned mass peaks increasing during the developmental cycle. Figure shows representative mass spectra of two independent biological experiments.

Taken together, these data show that *C. trachomatis* changes the overall lipid composition of infected cells. During the infectious cycle, PI species with long fatty acid residues decreased, while short chain PI and CL species increased. Interestingly, LPC species are only detected in infected cells. Furthermore, peaks with a characteristic 14 Da shift compared to their related lipids were observed exclusively in infected cells.

3.3.3 Impact of cPLA2 and CRLS1 on chlamydial growth and progeny formation

To further elucidate the relevance of the detected changes in lipid composition for the successful progression of *C. trachomatis* infection, two host cell enzymes implicated in processing and biosynthesis of phospholipids were studied. cPLA2 is involved in modifying glycerophospholipids, preparing them for the translocation to the chlamydial inclusion. cPLA2 is activated during *C. trachomatis* infection (Su *et al.*, 2004; Vignola *et al.*, 2010). Active cPLA2 can hydrolyze glycerophospholipids, cleaving the fatty acid residue at the *sn*-2 position of the glycerol backbone. The remaining lysophospholipid is then translocated to the chlamydial inclusion and taken up by the bacteria. Subsequently, a *Chlamydia*-derived branched chain fatty acid is added to the *sn*-2 position (Wylie *et al.*, 1997; Su *et al.*, 2004). These branched chain fatty acids are found in prokaryotic, but not in eukaryotic cells. Due to this branch within the fatty acid, a mass difference of 14 Da (CH_2 group) is observed in comparison to the corresponding straight chain fatty acid (Kaneda, 1991).

CRLS1 catalyzes the formation of CL from phosphatidylglycerol and CDP-diacylglycerol (Figure 3-40). The enzyme is localized to the inner membrane of mitochondria and is expressed in HeLa cells (Chen *et al.*, 2006; Lu *et al.*, 2006), while no homolog can be found in *C. trachomatis*.

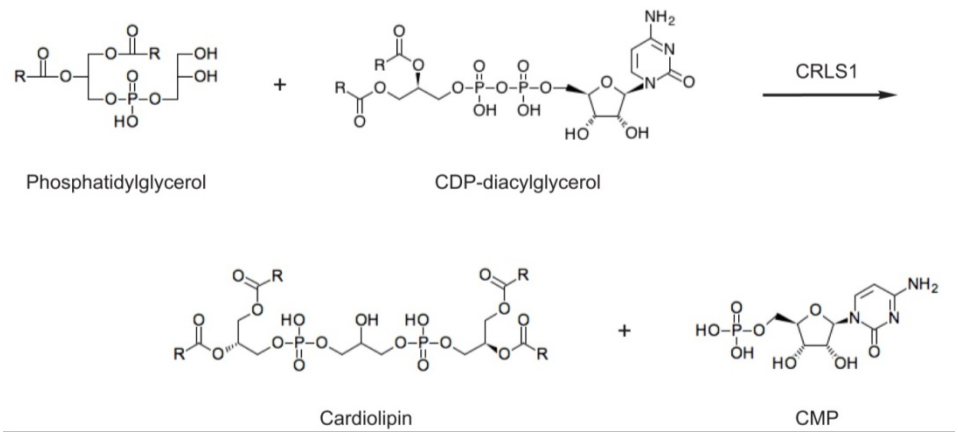

Figure 3-40. Enzymatic reaction of CRLS1. CRLS1 catalyzes the formation of CL from phosphatidylglycerol and CDP-diacylglycerol. CRLS1 is present in human cells, but not in *C. trachomatis*.

To investigate the influence of cPLA2 and CRLS1 on the lipid composition of host cells during infection, both the development of *C. trachomatis* in cPLA2 and CRLS1 knockdown cells and the formation of infectious progeny were analyzed. For this purpose, cells were transfected with the respective siRNA and infected with *C. trachomatis*. After 48 h, cells were lysed to release infectious particles and untreated cells were reinfected with infectious particles to monitor progeny formation (infectivity) (Figure 3-41).

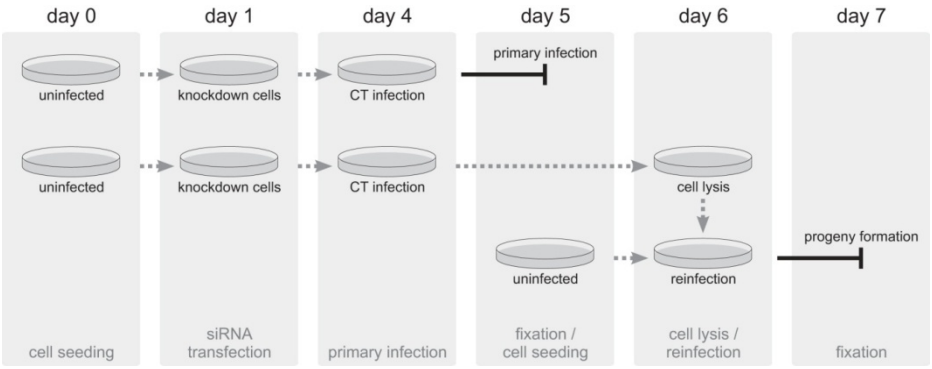

Figure 3-41. Workflow scheme of infectivity assay. Cells were transfected with respective siRNA at day 1 and left for 72 h to achieve a maximum knockdown of cPLA2 or CRLS1. At day 4, cells were infected with *C. trachomatis* for 24 h, fixed, and stained for inclusions and nuclei. Additionally, cells were infected for 48 h, lysed, and titrated on untreated cells to monitor progeny formation (infectivity) after another 24 h.

Knockdown efficiency for cPLA2 was measured by Western blot analysis, CRLS1 knockdown was monitored by qRT-PCR (Figure 3-42). Neither cPLA2 knockdown nor CRLS1 knockdown did affect cell viability (data not shown). Furthermore, *C. trachomatis* infection (24 h *p.i.*) did not change mRNA levels of cPLA2 and CRLS1 as detected by DNA microarray analysis (data not shown).

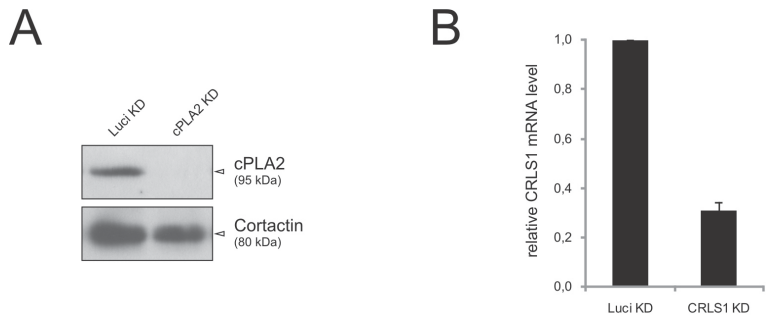

Figure 3-42. Confirmation of cPLA2 and CRLS1 knockdown. (A) Western blot showing nearly complete knockdown of cPLA2 after siRNA-mediated gene silencing of luciferase (Luci) or cPLA2. Cortactin represents loading control. (B) Bar diagram showing knockdown of CRLS1 after siRNA-mediated gene silencing of luciferase (Luci) or CRLS1. Knockdown was detected by qRT-PCR and normalized to GAPDH.

Fixed cells were stained for *C. trachomatis* OMP1, analyzed by automated microscopy, and a relative value for inclusions per nuclei was calculated. Knockdown of cPLA2 or CRLS1 did not affect primary infection (Figure 3-43 A). In contrast, formation of infectious particles was significantly decreased by cPLA2 and CRLS1 knockdown to approximately 60 % (Figure 3-43, A and B).

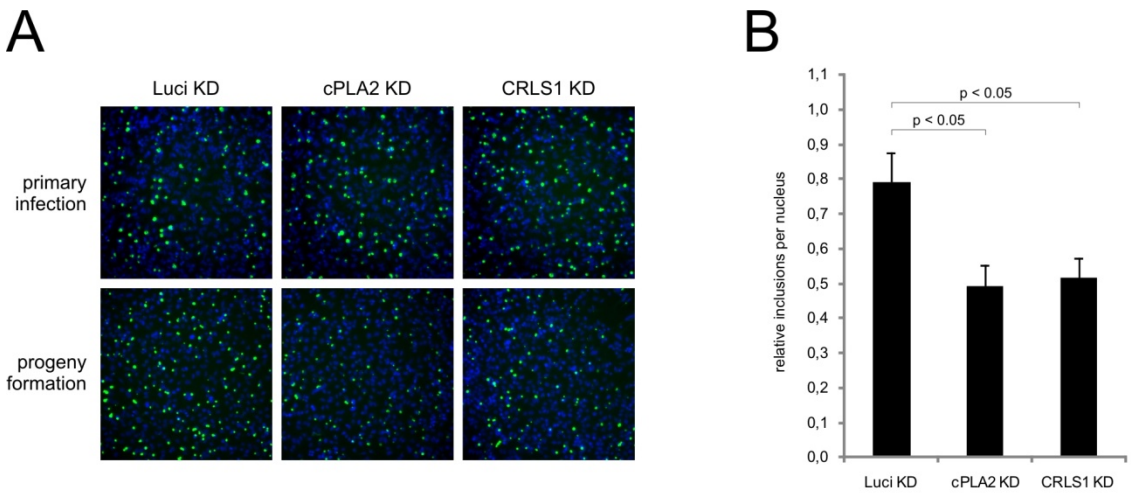

Figure 3-43. Infectivity assay after cPLA2 or CRLS1 knockdown. (A) Immunofluorescence staining of *C. trachomatis* OMP1 (green) and nuclei (blue). (B) Quantification of inclusions per nucleus during secondary infection (progeny formation). Neither cPLA2 nor CRLS1 knockdown reduced primary infection. However, formation of infectious particles was significantly decreased by cPLA2 and CRLS1 knockdown.

Taken together, these results demonstrate that knockdown of cPLA2 and CRLS1 leads to a reduced reinfection rate. Although *C. trachomatis* invasion and establishment of infection is not influenced by knockdown of cPLA2 and CRLS1, both enzymes play a crucial role in the process of infectious particle formation.

3.3.4 Discussion

In this approach, MALDI-TOF mass spectrometry analysis of lipids was performed to globally study changes in the lipid composition of C*. trachomatis* infected host cells. This revealed a prominent shift of the PI and CL composition towards lipid species with short fatty acids during the progression of the infectious cycle. Moreover, peaks with a distinct mass difference of 14 Da in comparison to the respective PI, PE, PG, and CL lipid species were detected in infected cells, suggesting the presence of lipids with *Chlamydia*-derived branched chain fatty acids and, thus, the involvement of remodeling enzymes in this process. Hence, both CRLS1 and cPLA2 were shown to be involved in successful replication of *Chlamydia*, since knockdown of these enzymes resulted in a decreased formation of infectious particles. Collectively, these results demonstrate a crucial role of CL during *Chlamydia* infection, highlight the impact of cPLA2 in lipid remodeling, and illustrate the importance of host cell trafficking pathways for the successful replication of *Chlamydia*.

CL is a major membrane protein found exclusively in mitochondria and plays an important role for mitochondrial structure and function (Hatch, 1998; Nie *et al.*, 2010). It is connected with mitochondrial energy production (Eble *et al.*, 1990; Hatch, 1998; Gomez and Robinson, 1999) and apoptosis (Lutter *et al.*, 2000). CL deficiency is associated with X-linked cardioskeletal myopathy and neutropenia (Barth syndrome), caused by mutations in tafazzin, a transacylase involved in fatty acid remodeling of CL (Bione *et al.*, 1996; Houtkooper *et al.*, 2009). Albeit its functional and clinical importance, it has been reported that CL deficiency due to CRLS1 knockdown does not impact cell viability, mitochondrial membrane potential, numbers of mitochondria, or ATP levels (Choi *et al.*, 2007; Huang *et al.*, 2008). However, knockdown of CRLS1 resulted in significantly decreased CL levels and an altered ultrastructure of mitochondria with disorganized cristae (Choi *et al.*, 2007; Huang *et al.*, 2008). Interestingly, CRLS1 knockdown cells exhibited a decreased susceptibility to apoptotic stimuli like actinomycin D or rotenone (Huang *et al.*, 2008). Here, the reduction of chlamydial progeny formation after CRLS1 knockdown shows for the first time the importance of CRLS1 activity and, thus CL, for chlamydial growth. This observation might be explained by a critical structural and functional role of CL for the late developmental stages of *C. trachomatis*, as the observed alterations in CL lipid composition are mainly detected beginning at 24 h *p.i.* Despite this, it is tempting to suggest a connection of *C. trachomatis*-induced alteration of CL composition and *Chlamydia*-mediated inhibition of apoptosis. Thus, stimulating mitochondrial metabolism, modifying the molecular fatty acid composition of CL, and re-routing CL species to the chlamydial inclusion could be an mechanism of actively decreasing the susceptibility of the host cell to apoptosis.

Using a mutant CHO cell line unable to synthesize CTP, which is generally necessary for glycerophospholipid synthesis, it has been shown that *C. trachomatis* does not depend on the *de novo* host cell glycerophospholipid synthesis (Wylie *et al.*, 1997; Hatch and McClarty, 1998a). Due to a mutation in its CTP synthetase, this cell line is dependent on exogenous cytidine or lipids in the cell culture medium. Contrary to this, the results presented here indicate for the first time a dependency of *Chlamydia* on host cell CL synthesis, as knockdown of CRLS1, the enzyme catalyzing the final step of CL synthesis, led to a reduction of infectious particles. This discrepancy might be explained by residual glycerophospholipid pools in the CTP synthase deficient cell line after being cultured under restrictive conditions, sufficiently promoting intracellular growth of *C. trachomatis*. In contrast, CRLS1 knockdown cells used in the work presented here only show remaining CL levels insufficient for chlamydial development. It will be interesting to analyze CRLS1 knockdown cells for their lipid composition and to test for the relevance of other glycerophospholipid synthesis pathways to chlamydial growth via siRNA-mediated gene silencing.

Remodeling of CL during *C. trachomatis* infection has been investigated before, showing the alteration of the molecular fatty acid composition of CL (Hatch and McClarty, 1998b). McClarty and colleagues analyzed the uptake and incorporation of radioactively labeled myrisate, palmitate, or oleate into *de novo* synthesized mitochondrial lipids (PG, CL) upon infection, suggesting a link to elevated mitochondrial metabolism (Hatch and McClarty, 1998b). The results presented here extend these observations, demonstrating both the chlamydial influence on the overall CL composition and the remodeling of the molecular CL fatty acid composition with *Chlamydia*-derived fatty acids. Since the latter requires the transport of CL to the chlamydial inclusion, a close association of mitochondria and the inclusion is of importance. This association has been shown for *C. psittaci* by electron microscopy (Matsumoto, 1981; Matsumoto *et al.*, 1991).

The host cell enzyme cPLA2 gets activated upon *C. trachomatis* infection and is involved in the deacylation of glycerophospholipids at the *sn*-2 position (Su *et al.*, 2004). Pharmacological inhibition of cPLA2 reduces glycerophospholipid uptake and bacterial replication (Su *et al.*, 2004; Vignola *et al.*, 2010). Here, the knockdown of cPLA2 leads to a significant reduction in infectious particle formation, indicating an central role of cPLA2 in the processing of glycerophospholipids for the uptake by *Chlamydia* (Wylie *et al.*, 1997). Valdivia and colleagues were unable to detect a decreased progeny formation of *C. trachomatis* after cPLA2 knockdown (Vignola *et al.*, 2010). However, this observation could be due to a low knockdown efficiency (< 10 % residual cPLA2 levels), while the efficiency of cPLA2 knockdown in the study presented here is considerably higher (< 1 % residual cPLA2 levels).

Another explanation for the inhibitory phenotype of cPLA2 knockdown could be the role of lysophospholipids in modulating membrane curvature and membrane tubules formation, thereby assisting membrane transport (Brown *et al.*, 2003, San Pietro *et al.*, 2009). These transport events have been shown to be necessary for *C. trachomatis* replication (Carabeo *et al.*, 2003; Robertson *et al.*, 2009). Furthermore, the production of lysophospholipids by cPLA2 is a prerequisite for the generation of glycerophospholipids with *Chlamydia*-derived branched chain fatty acids (Su *et al.*, 2004; Vignola *et al.*, 2010) (Figure 3-44).

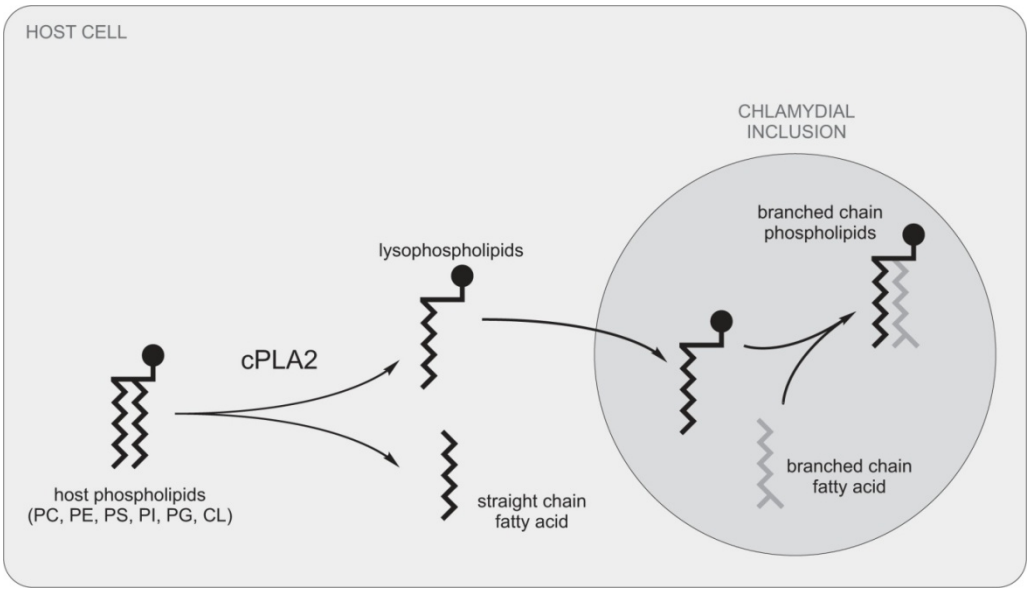

Figure 3-44. Model of CL biosynthesis and phospholipid acquisition by *Chlamydia*. During *C. trachomatis* infection, host phospholipids are hydrolyzed at the *sn*-2 position by activated cPLA2, resulting in lysophospholipids and straight chain fatty acids. The lysophospholipids are then transported to the chlamydial inclusion and taken up by the bacteria. Subsequently, lysophospholipids are modified by the addition of a prokaryotic branched chain fatty acid to the *sn*-2 position.

To synthesize branched chain fatty acids, *Chlamydia* and other prokaryotes use isoleucine as precursor of the α-keto acid primer during fatty acid biosynthesis (Kaneda, 1991; Wylie *et al.*, 1997). A branch within the fatty acid results in a mass difference of 14 Da – equal to the mass of a CH_2 group – in comparison to the corresponding straight chain fatty acid (Kaneda, 1991), for example between CL (4x16:0) and CL (15:0/3x16:0). In this study, both the intermediate product of the modification process, the lysophospholipid (LPC) and the final product of the remodeling process, the branched chain lipid, have been detected in infected cells. These branched chain fatty acids could be detected in PC, PE, PG, and CL species. Branched chain fatty acids in *C. trachomatis* infected cells have been described previously (Wylie *et al.*, 1997). Nonetheless, this study is the first to show remodeling of CL with branched chain fatty acids.

cPLA2 has been demonstrated to process CL despite its rather uncommon structure compared to other glycerophospholipids (Schlame and Rüstow, 1990; Schlame, 2008). However, cPLA2 is not the only host cell enzyme involved in modifying glycerophospholipids. The group of PLA2 enzymes consists of 20 enzymes classified in mammals (Ghosh *et al.*, 2006). Moreover, enzymes belonging to the group of phospholipase A1 (PLA1) can deacylate glycerophospholipids at the *sn*-1 position and are also present in mammalian cells (Ghosh *et al.*, 2006). Additionally, tafazzin, a CL-specific transacylase, might also be involved in the process of CL modification during infection (Bione *et al.*, 1996; Houtkooper *et al.*, 2009). It will be interesting to investigate the influence of these lipid-modifying enzymes on the molecular lipid composition and, subsequently, on the successful replication of *C. trachomatis*.

Another product of cPLA2 activity is arachidonic acid, which serves as a precursor of eicosanoid-derived metabolites. Cellular lipoxygenases and cyclooxygenases catalyze the formation of leukotrienes and prostanoids, respectively. It has been shown that *C. trachomatis* infection induces the expression of cyclooxygenase 2 (COX2) in epithelial cells (Fukuda *et al.*, 2005) (see also Table 6-2) and promotes production and release of prostaglandin E_2, which in turn stimulates IL8 release in epithelial cells (Krausse-Opatz *et al.*, 2004; Fukuda *et al.*, 2005). Furthermore, COX2 inhibition was demonstrated to reduce *C. pneumoniae* growth (Rupp *et al.*, 2004; Yan *et al.*, 2008). These results underline the importance of cPLA2 function during *Chlamydia* infection and create an additional explanation for the inhibitory effect of cPLA2 knockdown on chlamydial infection observed in the work presented here.

Previous studies have analyzed lipid changes during *C. trachomatis* infection by means of TLC, indicating both trafficking and modification of lipids by *Chlamydia* (Wylie *et al.*, 1997; Hatch and McClarty, 1998a). Lipid composition of infected cells was either described by composition of fatty acids or composition of lipid classes. In contrast, the study presented here shows a comprehensive and detailed description of the lipid composition in infected cells, specifically detecting single lipid species. McClarty and colleagues have described the increase of short chain and branched chain fatty acids over time and a decrease of other straight chain fatty acids, suggesting the modification of host lipids by *Chlamydia* (Wylie *et al.*, 1997). Here, detection of LPC contributes to this finding, as LPC constitutes an intermediate step of the modification process. Furthermore, a shift towards lipids with short and branched chain fatty acids upon infection implicates an increased fluidity of membranes (Hazel and Williams, 1990). This modulation of bacterial or inclusion membrane stability might be favored by *Chlamydia* towards the end of the developmental cycle. However, further

studies have to be performed to distinguish between lipid changes of the host cell and in the bacteria.

For the detection of lipids by mass spectrometry, other soft-ionization techniques like electrospray ionization (ESI) have been used more frequently compared with MALDI-TOF mass spectrometry (Pulfer and Murphy, 2003; Schiller *et al.*, 2004). The major advantage of ESI mass spectrometry is the possibility of coupling the prior separation of lipid classes directly with their detection, namely the combination of HPLC and ESI mass spectrometry online (Pulfer and Murphy, 2003). Further, MALDI-TOF mass spectrometry bears the risk of detecting interferences from ions derived from the matrix (Pulfer and Murphy, 2003). However, MALDI-TOF mass spectrometry has also several advantages: the method is fast and convenient, requires only low amounts of lipid extract, and has both a high reproducibility and sensitivity (Schiller *et al.*, 2004). Moreover, the approach used in the study presented here combines TLC with MALDI-TOF mass spectrometry offline, thereby matching the advantages of HPLC/ESI online methods.

In summary, these data show an example of how *Chlamydia* subverts host cellular trafficking pathways to ensure its intracellular replication. Further work will focus on the specific mechanisms of lipid trafficking to the chlamydial inclusion in general and on the processes involved in CL transport and remodeling in more detail.

CONCLUSIONS AND OUTLOOK

4 Conclusions and outlook

Following the investigation of *Chlamydia*'s repertoire to exploit the host cell, several additional questions remain to be answered.

Tarp has been shown to interact with a multitude of cellular SH2 and SH3 domains. Further studies will have to focus on validating these additional interactions, especially ABL2 and NCK2, and dissecting their spatiotemporal profile during the progression of the developmental cycle. This could be performed by blue native gel electrophoresis, a common approach for the identification and analysis of multiprotein complexes (Swamy *et al.*, 2006). Also, the detailed phosphorylation status of Tarp's phospho-sites at different time points of invasion might be investigated by mass spectrometry. Moreover, solving the three-dimensional structure of Tarp would greatly add to the understanding of how Tarp interacts with host cell proteins, especially via SH2 and SH3 interactions.

The outcome of Tarp-mediated signaling induced by other interaction partners than SHC1 is best explored by analyzing the transcriptional impact of these interactors using DNA microarray analysis, as described in this study. The development of a heterologous Tarp expression system could be a major advantage in this regard – the infection-independent setting of such a system would facilitate the detailed investigation of Tarp interactions by both siRNA-mediated knockdown of interaction partners and mutational analysis of the Tarp sequence and its interaction interfaces. This would also allow studying the role of RASA1, CRKL, and LCK for SHC1-independent MEK/ERK activation. Moreover, it will be interesting to dissect the role of all SHC1 isoforms in early *Chlamydia*-induced cell survival by isoform-specific knockdown and to further investigate the MEK/ERK-independent branch of SHC1 signaling.

Future investigation the *Chlamydia*'s impact on the host cell lipid composition includes the lipid analysis after knockdown of cPLA2 or CRLS1. Also, ultrastructural analysis of infected cPLA2 and CRLS1 knockdown cells, e.g., by electron microscopy, could give additional insight into the association of mitochondria and the chlamydial inclusion. Using fluorescently labeled lipids and lipid tracers, trafficking of lipids during infection could be investigated. Moreover, the purification of bacteria from infected host cells at various time points of infection would allow to distinguish between lipid changes of the host cell and the bacteria. This study showed the relevance of enzymes involved in biosynthesis and modification of lipids. It will be interesting to further study the impact of other lipid synthesis pathways, phospholipid-modifying enzymes, and lipid transporters on the replication of *C. trachomatis* via siRNA-mediated gene silencing.

REFERENCES

5 References

Abdelrahman, Y.M., and R.J. Belland. 2005. The chlamydial developmental cycle. *FEMS Microbiol Rev*. 29:949-959.

Al-Younes, H.M., T. Rudel, V. Brinkmann, A.J. Szczepek, and T.F. Meyer. 2001. Low iron availability modulates the course of *Chlamydia pneumoniae* infection. *Cell Microbiol*. 3:427-437.

Antoku, S., K. Saksela, G.M. Rivera, and B.J. Mayer. 2008. A crucial role in cell spreading for the interaction of Abl PxxP motifs with Crk and Nck adaptors. *J Cell Sci*. 121:3071-3082.

Arora, S., Y. Wang, Z. Jia, S. Vardar-Sengul, A. Munawar, K.S. Doctor, M. Birrer, M. McClelland, E. Adamson, and D. Mercola. 2008. Egr1 regulates the coordinated expression of numerous EGF receptor target genes as identified by ChIP-on-chip. *Genome Biol*. 9:R166.

Asahi, M., T. Azuma, S. Ito, Y. Ito, H. Suto, Y. Nagai, M. Tsubokawa, Y. Tohyama, S. Maeda, M. Omata, T. Suzuki, and C. Sasakawa. 2000. *Helicobacter pylori* CagA protein can be tyrosine phosphorylated in gastric epithelial cells. *J Exp Med*. 191:593-602.

Ashburner, M., C.A. Ball, J.A. Blake, D. Botstein, H. Butler, J.M. Cherry, A.P. Davis, K. Dolinski, S.S. Dwight, J.T. Eppig, M.A. Harris, D.P. Hill, L. Issel-Tarver, A. Kasarskis, S. Lewis, J.C. Matese, J.E. Richardson, M. Ringwald, G.M. Rubin, and G. Sherlock. 2000. Gene ontology: tool for the unification of biology. The Gene Ontology Consortium. *Nature Genetics*. 25:25-29.

Backert, S., S.M. Feller, and S. Wessler. 2008. Emerging roles of Abl family tyrosine kinases in microbial pathogenesis. *Trends Biochem Sci*. 33:80-90.

Barila, D., R. Mangano, S. Gonfloni, J. Kretzschmar, M. Moro, D. Bohmann, and G. Superti-Furga. 2000. A nuclear tyrosine phosphorylation circuit: c-Jun as an activator and substrate of c-Abl and JNK. *Embo J*. 19:273-281.

Barila, D., and G. Superti-Furga. 1998. An intramolecular SH3-domain interaction regulates c-Abl activity. *Nature Genetics*. 18:280-282.

Beatty, W.L. 2006. Trafficking from CD63-positive late endocytic multivesicular bodies is essential for intracellular development of *Chlamydia trachomatis*. *J Cell Sci*. 119:350-359.

Beatty, W.L. 2007. Lysosome repair enables host cell survival and bacterial persistence following *Chlamydia trachomatis* infection. *Cell Microbiol*. 9:2141-2152.

Beatty, W.L. 2008. Late endocytic multivesicular bodies intersect the chlamydial inclusion in the absence of CD63. *Infect Immun*. 76:2872-2881.

Beatty, W.L., G.I. Byrne, and R.P. Morrison. 1993. Morphologic and antigenic characterization of interferon gamma-mediated persistent *Chlamydia trachomatis* infection in vitro. *Proc Natl Acad Sci U S A*. 90:3998-4002.

Belland, R., D.M. Ojcius, and G.I. Byrne. 2004. Chlamydia. *Nat Rev Microbiol*. 2:530-531.

Betts-Hampikian, H.J., and K.A. Fields. 2010. The Chlamydial Type III Secretion Mechanism: Revealing Cracks in a Tough Nut. *Front Microbiol*. 1:114.

Bione, S., P. D'Adamo, E. Maestrini, A.K. Gedeon, P.A. Bolhuis, and D. Toniolo. 1996. A novel X-linked gene, G4.5. is responsible for Barth syndrome. *Nature Genetics*. 12:385-389.

Bivona, T.G., S. Quatela, and M.R. Philips. 2006. Analysis of Ras activation in living cells with GFP-RBD. *Methods Enzymol*. 407:128-143.

Blasi, F., P. Tarsia, and S. Aliberti. 2009. *Chlamydophila pneumoniae*. *Clin Microbiol Infect*. 15:29-35.

Bouillet, P., J.F. Purton, D.I. Godfrey, L.C. Zhang, L. Coultas, H. Puthalakath, M. Pellegrini, S. Cory, J.M. Adams, and A. Strasser. 2002. BH3-only Bcl-2 family member Bim is required for apoptosis of autoreactive thymocytes. *Nature*. 415:922-926.

Brown, W.J., K. Chambers, and A. Doody. 2003. Phospholipase A2 (PLA2) enzymes in membrane trafficking: mediators of membrane shape and function. *Traffic*. 4:214-221.

Brunham, R.C., and J. Rey-Ladino. 2005. Immunology of Chlamydia infection: implications for a *Chlamydia trachomatis* vaccine. *Nat Rev Immunol*. 5:149-161.

Buchholz, K.R., and R.S. Stephens. 2008. The cytosolic pattern recognition receptor NOD1 induces inflammatory interleukin-8 during *Chlamydia trachomatis* infection. *Infect Immun*. 76:3150-3155.

Bush, R.M., and K.D. Everett. 2001. Molecular evolution of the *Chlamydiaceae*. *Int J Syst Evol Microbiol*. 51:203-220.

Byrne, G.I., and D.M. Ojcius. 2004. *Chlamydia* and apoptosis: life and death decisions of an intracellular pathogen. *Nat Rev Microbiol*. 2:802-808.

Campbell, L.A., and C.C. Kuo. 2004. *Chlamydia pneumoniae* - an infectious risk factor for atherosclerosis? *Nat Rev Microbiol*. 2:23-32.

Carabeo, R.A., D.J. Mead, and T. Hackstadt. 2003. Golgi-dependent transport of cholesterol to the *Chlamydia trachomatis* inclusion. *Proc Natl Acad Sci U S A*. 100:6771-6776.

Cell Signaling Technology. 2010. Product Pathways - MAPK Signaling. Accessed on June 14, 2011. Available from http://www.cellsignal.com/reference/pathway/pdfs/MAPK_ERK_Growth.pdf

Centers for Disease Control and Prevention. 2010. Chlamydial Infections - Sexually Transmitted Diseases Treatment Guidelines. Accessed on June 14, 2011. Available from http://www.cdc.gov/std/treatment/2010/chlamydial-infections.htm

Chen, D., X.Y. Zhang, and Y. Shi. 2006. Identification and functional characterization of hCLS1, a human cardiolipin synthase localized in mitochondria. *Biochem J*. 398:169-176.

Chen, X.M., P.L. Splinter, P.S. Tietz, B.Q. Huang, D.D. Billadeau, and N.F. LaRusso. 2004. Phosphatidylinositol 3-kinase and frabin mediate *Cryptosporidium parvum* cellular invasion via activation of Cdc42. *J Biol Chem*. 279:31671-31678.

Chivers, C.E., E. Crozat, C. Chu, V.T. Moy, D.J. Sherratt, and M. Howarth. 2010. A streptavidin variant with slower biotin dissociation and increased mechanostability. *Nat Methods*. 7:391-393.

Choi, S.Y., F. Gonzalvez, G.M. Jenkins, C. Slomianny, D. Chretien, D. Arnoult, P.X. Petit, and M.A. Frohman. 2007. Cardiolipin deficiency releases cytochrome c from the inner mitochondrial membrane and accelerates stimuli-elicited apoptosis. *Cell Death Differ*. 14:597-606.

Christie, P.J., K. Atmakuri, V. Krishnamoorthy, S. Jakubowski, and E. Cascales. 2005. Biogenesis, architecture, and function of bacterial type IV secretion systems. *Annu Rev Microbiol*. 59:451-485.

Churin, Y., L. Al-Ghoul, O. Kepp, T.F. Meyer, W. Birchmeier, and M. Naumann. 2003. *Helicobacter pylori* CagA protein targets the c-Met receptor and enhances the motogenic response. *J Cell Biol*. 161:249-255.

Clifton, D.R., C.A. Dooley, S.S. Grieshaber, R.A. Carabeo, K.A. Fields, and T. Hackstadt. 2005. Tyrosine phosphorylation of the chlamydial effector protein Tarp is species specific and not required for recruitment of actin. *Infect Immun*. 73:3860-3868.

Clifton, D.R., K.A. Fields, S.S. Grieshaber, C.A. Dooley, E.R. Fischer, D.J. Mead, R.A. Carabeo, and T. Hackstadt. 2004. A chlamydial type III translocated protein is tyrosine-phosphorylated at the site of entry and associated with recruitment of actin. *Proc Natl Acad Sci U S A*. 101:10166-10171.

Cocchiaro, J.L., and R.H. Valdivia. 2009. New insights into *Chlamydia* intracellular survival mechanisms. *Cell Microbiol*. 11:1571-1578.

Collette, Y., S. Arold, C. Picard, K. Janvier, S. Benichou, R. Benarous, D. Olive, and C. Dumas. 2000. HIV-2 and SIV nef proteins target different Src family SH3 domains than does HIV-1 Nef because of a triple amino acid substitution. *J Biol Chem*. 275:4171-4176.

Dautry-Varsat, A., A. Subtil, and T. Hackstadt. 2005. Recent insights into the mechanisms of *Chlamydia* entry. *Cell Microbiol*. 7:1714-1722.

de la Maza, L.M., M.J. Plunkett, E.J. Carlson, E.M. Peterson, and C.W. Czarniecki. 1987. Ultrastructural analysis of the anti-chlamydial activity of recombinant murine interferon-gamma. *Exp Mol Pathol*. 47:13-25.

Delevoye, C., M. Nilges, P. Dehoux, F. Paumet, S. Perrinet, A. Dautry-Varsat, and A. Subtil. 2008. SNARE protein mimicry by an intracellular bacterium. *PLoS Pathogens*. 4:e1000022.

Dhanasekaran, N., and E. Premkumar Reddy. 1998. Signaling by dual specificity kinases. *Oncogene*. 17:1447-1455.

Eble, K.S., W.B. Coleman, R.R. Hantgan, and C.C. Cunningham. 1990. Tightly associated cardiolipin in the bovine heart mitochondrial ATP synthase as analyzed by 31P nuclear magnetic resonance spectroscopy. *J Biol Chem*. 265:19434-19440.

Elwell, C.A., A. Ceesay, J.H. Kim, D. Kalman, and J.N. Engel. 2008. RNA interference screen identifies Abl kinase and PDGFR signaling in *Chlamydia trachomatis* entry. *PLoS Pathogens*. 4:e1000021.

Everett, K.D., R.M. Bush, and A.A. Andersen. 1999. Emended description of the order *Chlamydiales*, proposal of *Parachlamydiaceae* fam. nov. and *Simkaniaceae* fam. nov., each containing one monotypic genus, revised taxonomy of the family *Chlamydiaceae*, including a new genus and five new species, and standards for the identification of organisms. *Int J Syst Bacteriol*. 49 Pt 2:415-440.

Fagiani, E., G. Giardina, L. Luzi, M. Cesaroni, M. Quarto, M. Capra, G. Germano, M. Bono, M. Capillo, P. Pelicci, and L. Lanfrancone. 2007. RaLP, a new member of the Src homology and collagen family, regulates cell migration and tumor growth of metastatic melanomas. *Cancer Res*. 67:3064-3073.

Faherty, C.S., and A.T. Maurelli. 2008. Staying alive: bacterial inhibition of apoptosis during infection. *Trends Microbiol*. 16:173-180.

Fan, T., H. Lu, H. Hu, L. Shi, G.A. McClarty, D.M. Nance, A.H. Greenberg, and G. Zhong. 1998. Inhibition of apoptosis in *Chlamydia*-infected cells: blockade of mitochondrial cytochrome c release and caspase activation. *J Exp Med*. 187:487-496.

Faro, S. 1985. *Chlamydia trachomatis* infection in women. *J Reprod Med*. 30:273-278.

Ferraro, E., D. Peluso, A. Via, G. Ausiello, and M. Helmer-Citterich. 2007. SH3-Hunter: discovery of SH3 domain interaction sites in proteins. *Nucleic Acids Res*. 35:W451-454.

Fink, S.L., and B.T. Cookson. 2005. Apoptosis, pyroptosis, and necrosis: mechanistic description of dead and dying eukaryotic cells. *Infect Immun*. 73:1907-1916.

Fischer, S.F., J. Vier, S. Kirschnek, A. Klos, S. Hess, S. Ying, and G. Hacker. 2004. *Chlamydia* inhibit host cell apoptosis by degradation of proapoptotic BH3-only proteins. *J Exp Med*. 200:905-916.

Folch, J., M. Lees, and G.H. Sloane Stanley. 1957. A simple method for the isolation and purification of total lipides from animal tissues. *J Biol Chem*. 226:497-509.

Franz, W.M., P. Berger, and J.Y. Wang. 1989. Deletion of an N-terminal regulatory domain of the c-abl tyrosine kinase activates its oncogenic potential. *Embo J*. 8:137-147.

Fukuda, E.Y., S.P. Lad, D.P. Mikolon, M. Iacobelli-Martinez, and E. Li. 2005. Activation of lipid metabolism contributes to interleukin-8 production during *Chlamydia trachomatis* infection of cervical epithelial cells. *Infect Immun*. 73:4017-4024.

Gambhir, M., M.G. Basanez, F. Turner, J. Kumaresan, and N.C. Grassly. 2007. Trachoma: transmission, infection, and control. *Lancet Infect Dis*. 7:420-427.

Ghosh, M., D.E. Tucker, S.A. Burchett, and C.C. Leslie. 2006. Properties of the Group IV phospholipase A2 family. *Prog Lipid Res*. 45:487-510.

Ghosh, P. 2004. Process of protein transport by the type III secretion system. *Microbiol Mol Biol Rev*. 68:771-795.

Girish, V., and A. Vijayalakshmi. 2004. Affordable image analysis using NIH Image/ImageJ. *Indian J Cancer*. 41:47.

Gomez, B., Jr., and N.C. Robinson. 1999. Phospholipase digestion of bound cardiolipin reversibly inactivates bovine cytochrome bc1. *Biochemistry*. 38:9031-9038.

Goraca, A. 2002. New views on the role of endothelin (minireview). *Endocr Regul*. 36:161-167.

Gordus, A., and G. MacBeath. 2006. Circumventing the problems caused by protein diversity in microarrays: implications for protein interaction networks. *J Am Chem Soc*. 128:13668-13669.

Grayston, J.T., and S. Wang. 1975. New knowledge of chlamydiae and the diseases they cause. *J Infect Dis*. 132:87-105.

Gregorc, U., S. Ivanova, M. Thomas, E. Guccione, B. Glaunsinger, R. Javier, V. Turk, L. Banks, and B. Turk. 2007. Cleavage of MAGI-1, a tight junction PDZ protein, by caspases is an important step for cell-cell detachment in apoptosis. *Apoptosis*. 12:343-354.

Grieshaber, S.S., N.A. Grieshaber, and T. Hackstadt. 2003. *Chlamydia trachomatis* uses host cell dynein to traffic to the microtubule-organizing center in a p50 dynamitin-independent process. *J Cell Sci*. 116:3793-3802.

Guo, W., and F.G. Giancotti. 2004. Integrin signalling during tumour progression. *Nat Rev Mol Cell Biol*. 5:816-826.

Gurumurthy, R.K., A.P. Maurer, N. Machuy, S. Hess, K.P. Pleissner, J. Schuchhardt, T. Rudel, and T.F. Meyer. 2010. A loss-of-function screen reveals Ras- and Raf-independent MEK-ERK signaling during *Chlamydia trachomatis* infection. *Sci Signal*. 3:ra21.

Hackstadt, T., D.D. Rockey, R.A. Heinzen, and M.A. Scidmore. 1996. *Chlamydia trachomatis* interrupts an exocytic pathway to acquire endogenously synthesized sphingomyelin in transit from the Golgi apparatus to the plasma membrane. *Embo J*. 15:964-977.

Hackstadt, T., M.A. Scidmore, and D.D. Rockey. 1995. Lipid metabolism in *Chlamydia trachomatis*-infected cells: directed trafficking of Golgi-derived sphingolipids to the chlamydial inclusion. *Proc Natl Acad Sci U S A*. 92:4877-4881.

Hackstadt, T., M.A. Scidmore-Carlson, E.I. Shaw, and E.R. Fischer. 1999. The *Chlamydia trachomatis* IncA protein is required for homotypic vesicle fusion. *Cell Microbiol*. 1:119-130.

Haggerty, C.L., S.L. Gottlieb, B.D. Taylor, N. Low, F. Xu, and R.B. Ness. 2010. Risk of sequelae after *Chlamydia trachomatis* genital infection in women. *J Infect Dis*. 201 Suppl 2:S134-155.

Hantschel, O., B. Nagar, S. Guettler, J. Kretzschmar, K. Dorey, J. Kuriyan, and G. Superti-Furga. 2003. A myristoyl/phosphotyrosine switch regulates c-Abl. *Cell*. 112:845-857.

Hatakeyama, M. 2008. SagA of CagA in *Helicobacter pylori* pathogenesis. *Curr Opin Microbiol*. 11:30-37.

Hatch, G.M. 1998. Cardiolipin: biosynthesis, remodeling and trafficking in the heart and mammalian cells (Review). *Int J Mol Med*. 1:33-41.

Hatch, G.M., and G. McClarty. 1998a. Phospholipid composition of purified *Chlamydia trachomatis* mimics that of the eucaryotic host cell. *Infect Immun*. 66:3727-3735.

Hatch, G.M., and G. McClarty. 1998b. Cardiolipin remodeling in eukaryotic cells infected with *Chlamydia trachomatis* is linked to elevated mitochondrial metabolism. *Biochem Biophys Res Commun*. 243:356-360.

Hazel, J.R., and E.E. Williams. 1990. The role of alterations in membrane lipid composition in enabling physiological adaptation of organisms to their physical environment. *Prog Lipid Res*. 29:167-227.

Hengartner, M.O. 2000. The biochemistry of apoptosis. *Nature*. 407:770-776.

Heuer, D., C. Kneip, A.P. Maurer, and T.F. Meyer. 2007. Tackling the intractable - approaching the genetics of *Chlamydiales*. *Int J Med Microbiol*. 297:569-576.

Heuer, D., A. Rejman Lipinski, N. Machuy, A. Karlas, A. Wehrens, F. Siedler, V. Brinkmann, and T.F. Meyer. 2009. *Chlamydia* causes fragmentation of the Golgi compartment to ensure reproduction. *Nature*. 457:731-735.

Higashi, H., R. Tsutsumi, A. Fujita, S. Yamazaki, M. Asaka, T. Azuma, and M. Hatakeyama. 2002. Biological activity of the *Helicobacter pylori* virulence factor CagA is determined by variation in the tyrosine phosphorylation sites. *Proc Natl Acad Sci U S A*. 99:14428-14433.

Hill, M.M., C. Adrain, P.J. Duriez, E.M. Creagh, and S.J. Martin. 2004. Analysis of the composition, assembly kinetics and activity of native Apaf-1 apoptosomes. *Embo J*. 23:2134-2145.

Houtkooper, R.H., M. Turkenburg, B.T. Poll-The, D. Karall, C. Perez-Cerda, A. Morrone, S. Malvagia, R.J. Wanders, W. Kulik, and F.M. Vaz. 2009. The enigmatic role of tafazzin in cardiolipin metabolism. *Biochim Biophys Acta*. 1788:2003-2014.

Huang, Z., J. Jiang, V.A. Tyurin, Q. Zhao, A. Mnuskin, J. Ren, N.A. Belikova, W. Feng, I.V. Kurnikov, and V.E. Kagan. 2008. Cardiolipin deficiency leads to decreased cardiolipin peroxidation and increased resistance of cells to apoptosis. *Free Radic Biol Med*. 44:1935-1944.

Hueck, C.J. 1998. Type III protein secretion systems in bacterial pathogens of animals and plants. *Microbiol Mol Biol Rev*. 62:379-433.

Hybiske, K., and R.S. Stephens. 2007. Mechanisms of host cell exit by the intracellular bacterium *Chlamydia*. *Proc Natl Acad Sci U S A*. 104:11430-11435.

Jaattela, M. 2002. Programmed cell death: many ways for cells to die decently. *Ann Med*. 34:480-488.

Jackson, P., and D. Baltimore. 1989. N-terminal mutations activate the leukemogenic potential of the myristoylated form of c-abl. *Embo J*. 8:449-456.

Jewett, T.J., C.A. Dooley, D.J. Mead, and T. Hackstadt. 2008. *Chlamydia trachomatis* tarp is phosphorylated by src family tyrosine kinases. *Biochem Biophys Res Commun*. 371:339-344.

Jewett, T.J., E.R. Fischer, D.J. Mead, and T. Hackstadt. 2006. Chlamydial TARP is a bacterial nucleator of actin. *Proc Natl Acad Sci U S A*. 103:15599-15604.

Jewett, T.J., N.J. Miller, C.A. Dooley, and T. Hackstadt. 2010. The conserved Tarp actin binding domain is important for chlamydial invasion. *PLoS Pathogens*. 6:e1000997.

Jones, N., and D.J. Dumont. 2000. Tek/Tie2 signaling: new and old partners. *Cancer Metastasis Rev*. 19:13-17.

Jones, R.B., A. Gordus, J.A. Krall, and G. MacBeath. 2006. A quantitative protein interaction network for the ErbB receptors using protein microarrays. *Nature*. 439:168-174.

Juban, G., G. Giraud, B. Guyot, S. Belin, J.J. Diaz, J. Starck, C. Guillouf, F. Moreau-Gachelin, and F. Morle. 2009. Spi-1 and Fli-1 directly activate common target genes involved in ribosome biogenesis in Friend erythroleukemic cells. *Mol Cell Biol*. 29:2852-2864.

Kaneda, T. 1991. Iso- and anteiso-fatty acids in bacteria: biosynthesis, function, and taxonomic significance. *Microbiol Rev*. 55:288-302.

Kanehisa, M., S. Goto, M. Furumichi, M. Tanabe, and M. Hirakawa. 2010. KEGG for representation and analysis of molecular networks involving diseases and drugs. *Nucleic Acids Res*. 38:D355-360.

Karayiannis, P., and D. Hobson. 1981. Amino acid requirements of a *Chlamydia trachomatis* genital strain in McCoy cell cultures. *J Clin Microbiol*. 13:427-432.

Kari, L., M.M. Goheen, L.B. Randall, L.D. Taylor, J.H. Carlson, W.M. Whitmire, D. Virok, K. Rajaram, V. Endresz, G. McClarty, D.E. Nelson, and H.D. Caldwell. 2011. Generation of targeted *Chlamydia trachomatis* null mutants. *Proc Natl Acad Sci U S A*. 108:7189-7193.

Keates, S., A.C. Keates, M. Warny, R.M. Peek, Jr., P.G. Murray, and C.P. Kelly. 1999. Differential activation of mitogen-activated protein kinases in AGS gastric epithelial cells by cag+ and cag- *Helicobacter pylori*. *J Immunol*. 163:5552-5559.

Kenny, B., R. DeVinney, M. Stein, D.J. Reinscheid, E.A. Frey, and B.B. Finlay. 1997. Enteropathogenic *E. coli* (EPEC) transfers its receptor for intimate adherence into mammalian cells. *Cell*. 91:511-520.

Kerr, J.F., A.H. Wyllie, and A.R. Currie. 1972. Apoptosis: a basic biological phenomenon with wide-ranging implications in tissue kinetics. *Br J Cancer*. 26:239-257.

Krausse-Opatz, B., C. Schmidt, U. Fendrich, A. Bialowons, V. Kaever, H. Zeidler, J. Kuipers, and L. Kohler. 2004. Production of prostaglandin E2 in monocytes stimulated in vitro by *Chlamydia trachomatis*, *Chlamydophila pneumoniae*, and *Mycoplasma fermentans*. *Microbial Pathogenesis*. 37:155-161.

Kumar, Y., J. Cocchiaro, and R.H. Valdivia. 2006. The obligate intracellular pathogen *Chlamydia trachomatis* targets host lipid droplets. *Curr Biol*. 16:1646-1651.

Kuo, C.C., L. Jackson, L.A. Campbell, and J.T. Grayston. 1995. *Chlamydia pneumoniae* (TWAR). *Clin Microbiol Rev*. 8:451-461.

Lane, B.J., C. Mutchler, S. Al Khodor, S.S. Grieshaber, and R.A. Carabeo. 2008. Chlamydial entry involves TARP binding of guanine nucleotide exchange factors. *PLoS Pathogens*. 4:e1000014.

Larkin, M.A., G. Blackshields, N.P. Brown, R. Chenna, P.A. McGettigan, H. McWilliam, F. Valentin, I.M. Wallace, A. Wilm, R. Lopez, J.D. Thompson, T.J. Gibson, and D.G. Higgins. 2007. Clustal W and Clustal X version 2.0. *Bioinformatics*. 23:2947-2948.

Lerner, E.C., and T.E. Smithgall. 2002. SH3-dependent stimulation of Src-family kinase autophosphorylation without tail release from the SH2 domain in vivo. *Nat Struct Biol*. 9:365-369.

Lewis, J.M., and M.A. Schwartz. 1998. Integrins regulate the association and phosphorylation of paxillin by c-Abl. *J Biol Chem*. 273:14225-14230.

Li, S.S. 2005. Specificity and versatility of SH3 and other proline-recognition domains: structural basis and implications for cellular signal transduction. *Biochem J*. 390:641-653.

Locksley, R.M., N. Killeen, and M.J. Lenardo. 2001. The TNF and TNF receptor superfamilies: integrating mammalian biology. *Cell*. 104:487-501.

Lu, B., F.Y. Xu, Y.J. Jiang, P.C. Choy, G.M. Hatch, C. Grunfeld, and K.R. Feingold. 2006. Cloning and characterization of a cDNA encoding human cardiolipin synthase (hCLS1). *J Lipid Res*. 47:1140-1145.

Lutter, M., M. Fang, X. Luo, M. Nishijima, X. Xie, and X. Wang. 2000. Cardiolipin provides specificity for targeting of tBid to mitochondria. *Nat Cell Biol*. 2:754-761.

Luzi, L., S. Confalonieri, P.P. Di Fiore, and P.G. Pelicci. 2000. Evolution of Shc functions from nematode to human. *Curr Opin Genet Dev*. 10:668-674.

Mabey, D., and R.W. Peeling. 2002. Lymphogranuloma venereum. *Sex Transm Infect*. 78:90-92.

MacBeath, G., and S.L. Schreiber. 2000. Printing proteins as microarrays for high-throughput function determination. *Science*. 289:1760-1763.

Mao, X., and X. Chen. 2005. Crystallization and X-ray crystallographic analysis of human STAT1. *Acta Crystallogr Sect F Struct Biol Cryst Commun*. 61:666-668.

Mathews, S.A., K.M. Volp, and P. Timms. 1999. Development of a quantitative gene expression assay for *Chlamydia trachomatis* identified temporal expression of sigma factors. *FEBS Lett*. 458:354-358.

Matsumoto, A. 1981. Isolation and electron microscopic observations of intracytoplasmic inclusions containing *Chlamydia psittaci*. *J Bacteriol*. 145:605-612.

Matsumoto, A., H. Bessho, K. Uehira, and T. Suda. 1991. Morphological studies of the association of mitochondria with chlamydial inclusions and the fusion of chlamydial inclusions. *J Electron Microsc (Tokyo)*. 40:356-363.

Mayer, B.J. 2001. SH3 domains: complexity in moderation. *J Cell Sci*. 114:1253-1263.

McClarty, G., H. Fan, and A.A. Andersen. 1993. Diversity in nucleotide acquisition by antigenically similar *Chlamydia psittaci* of avian origin. *FEMS Microbiol Lett*. 108:325-331.

McCubrey, J.A., L.S. Steelman, W.H. Chappell, S.L. Abrams, E.W. Wong, F. Chang, B. Lehmann, D.M. Terrian, M. Milella, A. Tafuri, F. Stivala, M. Libra, J. Basecke, C. Evangelisti, A.M. Martelli, and R.A. Franklin. 2007. Roles of the Raf/MEK/ERK pathway in cell growth, malignant transformation and drug resistance. *Biochim Biophys Acta*. 1773:1263-1284.

McDowall, M., N.M. Edwards, C.A. Jahoda, and P.I. Hynd. 2008. The role of activins and follistatins in skin and hair follicle development and function. *Cytokine Growth Factor Rev*. 19:415-426.

Mehlitz, A., S. Banhart, S. Hess, M. Selbach, and T.F. Meyer. 2008. Complex kinase requirements for *Chlamydia trachomatis* Tarp phosphorylation. *FEMS Microbiol Lett*. 289:233-240.

Meng, W., S. Sawasdikosol, S.J. Burakoff, and M.J. Eck. 1999. Structure of the amino-terminal domain of Cbl complexed to its binding site on ZAP-70 kinase. *Nature*. 398:84-90.

Mimuro, H., T. Suzuki, J. Tanaka, M. Asahi, R. Haas, and C. Sasakawa. 2002. Grb2 is a key mediator of *Helicobacter pylori* CagA protein activities. *Mol Cell*. 10:745-755.

Moarefi, I., M. LaFevre-Bernt, F. Sicheri, M. Huse, C.H. Lee, J. Kuriyan, and W.T. Miller. 1997. Activation of the Src-family tyrosine kinase Hck by SH3 domain displacement. *Nature*. 385:650-653.

Moore, E.R., E.R. Fischer, D.J. Mead, and T. Hackstadt. 2008. The chlamydial inclusion preferentially intercepts basolaterally directed sphingomyelin-containing exocytic vacuoles. *Traffic*. 9:2130-2140.

Munoz, E., D. Xu, M. Kemp, F. Zhang, J. Liu, and R.J. Linhardt. 2006. Affinity, kinetic, and structural study of the interaction of 3-O-sulfotransferase isoform 1 with heparan sulfate. *Biochemistry*. 45:5122-5128.

Nagar, B., O. Hantschel, M.A. Young, K. Scheffzek, D. Veach, W. Bornmann, B. Clarkson, G. Superti-Furga, and J. Kuriyan. 2003. Structural basis for the autoinhibition of c-Abl tyrosine kinase. *Cell*. 112:859-871.

Neef, R., M.A. Kuske, E. Prols, and J.P. Johnson. 2002. Identification of the human PHLDA1/TDAG51 gene: down-regulation in metastatic melanoma contributes to apoptosis resistance and growth deregulation. *Cancer Res*. 62:5920-5929.

Nie, J., X. Hao, D. Chen, X. Han, Z. Chang, and Y. Shi. 2010. A novel function of the human CLS1 in phosphatidylglycerol synthesis and remodeling. *Biochim Biophys Acta*. 1801:438-445.

Oh, E.S., and J.R. Couchman. 2004. Syndecans-2 and -4; close cousins, but not identical twins. *Mol Cells*. 17:181-187.

Ojcius, D.M., R. Hellio, and A. Dautry-Varsat. 1997. Distribution of endosomal, lysosomal, and major histocompatability complex markers in a monocytic cell line infected with *Chlamydia psittaci*. *Infect Immun*. 65:2437-2442.

Paland, N., L. Bohme, R.K. Gurumurthy, A. Maurer, A.J. Szczepek, and T. Rudel. 2008. Reduced display of tumor necrosis factor receptor I at the host cell surface supports infection with *Chlamydia trachomatis*. *J Biol Chem*. 283:6438-6448.

Paumet, F., J. Wesolowski, A. Garcia-Diaz, C. Delevoye, N. Aulner, H.A. Shuman, A. Subtil, and J.E. Rothman. 2009. Intracellular bacteria encode inhibitory SNARE-like proteins. *PLoS One*. 4:e7375.

Peeling, R.W., and R.C. Brunham. 1996. Chlamydiae as pathogens: new species and new issues. *Emerg Infect Dis*. 2:307-319.

Pelicci, G., L. Lanfrancone, F. Grignani, J. McGlade, F. Cavallo, G. Forni, I. Nicoletti, T. Pawson, and P.G. Pelicci. 1992. A novel transforming protein (SHC) with an SH2 domain is implicated in mitogenic signal transduction. *Cell*. 70:93-104.

Perfettini, J.L., M. Gissot, P. Souque, and D.M. Ojcius. 2002. Modulation of apoptosis during infection with *Chlamydia*. *Methods Enzymol*. 358:334-344.

Poppe, M., S.M. Feller, G. Romer, and S. Wessler. 2007. Phosphorylation of *Helicobacter pylori* CagA by c-Abl leads to cell motility. *Oncogene*. 26:3462-3472.

Pulfer, M., and R.C. Murphy. 2003. Electrospray mass spectrometry of phospholipids. *Mass Spectrom Rev*. 22:332-364.

Rajalingam, K., M. Sharma, C. Lohmann, M. Oswald, O. Thieck, C.J. Froelich, and T. Rudel. 2008. Mcl-1 is a key regulator of apoptosis resistance in *Chlamydia trachomatis*-infected cells. *PLoS One*. 3:e3102.

Ravichandran, K.S. 2001. Signaling via Shc family adapter proteins. *Oncogene*. 20:6322-6330.

Reed, J.C. 2000. Mechanisms of apoptosis. *Am J Pathol*. 157:1415-1430.

Rejman Lipinski, A., J. Heymann, C. Meissner, A. Karlas, V. Brinkmann, T.F. Meyer, and D. Heuer. 2009. Rab6 and Rab11 regulate *Chlamydia trachomatis* development and golgin-84-dependent Golgi fragmentation. *PLoS Pathogens*. 5:e1000615.

Reutershan, J., and K. Ley. 2004. Bench-to-bedside review: acute respiratory distress syndrome - how neutrophils migrate into the lung. *Critical care*. 8:453-461.

Robertson, D.K., L. Gu, R.K. Rowe, and W.L. Beatty. 2009. Inclusion biogenesis and reactivation of persistent *Chlamydia trachomatis* requires host cell sphingolipid biosynthesis. *PLoS Pathogens*. 5:e1000664.

Rockey, D.D., D. Grosenbach, D.E. Hruby, M.G. Peacock, R.A. Heinzen, and T. Hackstadt. 1997. *Chlamydia psittaci* IncA is phosphorylated by the host cell and is exposed on the cytoplasmic face of the developing inclusion. *Mol Microbiol*. 24:217-228.

Rozen, S., and H. Skaletsky. 2000. Primer3 on the WWW for general users and for biologist programmers. *Methods Mol Biol*. 132:365-386.

Rupp, J., M. Berger, N. Reiling, J. Gieffers, C. Lindschau, H. Haller, K. Dalhoff, and M. Maass. 2004. Cox-2 inhibition abrogates *Chlamydia pneumoniae*-induced PGE2 and MMP-1 expression. *Biochem Biophys Res Commun*. 320:738-744.

Rushworth, L.K., A.D. Hindley, E. O'Neill, and W. Kolch. 2006. Regulation and role of Raf-1/B-Raf heterodimerization. *Mol Cell Biol*. 26:2262-2272.

Saka, H.A., and R.H. Valdivia. 2010. Acquisition of nutrients by *Chlamydiae*: unique challenges of living in an intracellular compartment. *Curr Opin Microbiol*. 13:4-10.

Saksela, K., G. Cheng, and D. Baltimore. 1995. Proline-rich (PxxP) motifs in HIV-1 Nef bind to SH3 domains of a subset of Src kinases and are required for the enhanced growth of Nef+ viruses but not for down-regulation of CD4. *Embo J*. 14:484-491.

Sambrook, J., and D.W. Russel. 2001. Molecular Cloning: A Laboratory Manual. CSHL Press, New York, NY.

San Pietro, E., M. Capestrano, E.V. Polishchuk, A. DiPentima, A. Trucco, P. Zizza, S. Mariggio, T. Pulvirenti, M. Sallese, S. Tete, A.A. Mironov, C.C. Leslie, D. Corda, A. Luini, and R.S. Polishchuk. 2009. Group IV phospholipase A(2)alpha controls the formation of inter-cisternal continuities involved in intra-Golgi transport. *PLoS Biol*. 7:e1000194.

Sanner, M.F. 1999. Python: a programming language for software integration and development. *J Mol Graph Model*. 17:57-61.

Scaffidi, C., I. Schmitz, J. Zha, S.J. Korsmeyer, P.H. Krammer, and M.E. Peter. 1999. Differential modulation of apoptosis sensitivity in CD95 type I and type II cells. *J Biol Chem*. 274:22532-22538.

Schachter, J. 1999. Infection and disease epidemiology. *In Chlamydia*: intracellular biology, pathogenesis, and immunity. R.S. Stephens, editor. ASM Press, Washington, DC. 139-169.

Schachter, J., and H.D. Caldwell. 1980. Chlamydiae. *Annu Rev Microbiol*. 34:285-309.

Schachter, J., and A.O. Osoba. 1983. Lymphogranuloma venereum. *Br Med Bull*. 39:151-154.

Schiller, J., R. Suss, J. Arnhold, B. Fuchs, J. Lessig, M. Muller, M. Petkovic, H. Spalteholz, O. Zschornig, and K. Arnold. 2004. Matrix-assisted laser desorption and ionization time-of-flight (MALDI-TOF) mass spectrometry in lipid and phospholipid research. *Prog Lipid Res*. 43:449-488.

Schlame, M. 2008. Cardiolipin synthesis for the assembly of bacterial and mitochondrial membranes. *J Lipid Res*. 49:1607-1620.

Schlame, M., and B. Rustow. 1990. Lysocardiolipin formation and reacylation in isolated rat liver mitochondria. *Biochem J*. 272:589-595.

Schlessinger, J., and M.A. Lemmon. 2003. SH2 and PTB domains in tyrosine kinase signaling. *Sci STKE*. 2003:re12.

Schubbert, S., K. Shannon, and G. Bollag. 2007. Hyperactive Ras in developmental disorders and cancer. *Nat Rev Cancer*. 7:295-308.

Scidmore, M.A. 2011. Recent advances in *Chlamydia* subversion of host cytoskeletal and membrane trafficking pathways. *Microbes Infect*. 13:527-535.

Scidmore, M.A., E.R. Fischer, and T. Hackstadt. 2003. Restricted fusion of *Chlamydia trachomatis* vesicles with endocytic compartments during the initial stages of infection. *Infect Immun*. 71:973-984.

Scidmore, M.A., and T. Hackstadt. 2001. Mammalian 14-3-3beta associates with the *Chlamydia trachomatis* inclusion membrane via its interaction with IncG. *Mol Microbiol*. 39:1638-1650.

Selbach, M., F.E. Paul, S. Brandt, P. Guye, O. Daumke, S. Backert, C. Dehio, and M. Mann. 2009. Host cell interactome of tyrosine-phosphorylated bacterial proteins. *Cell Host Microbe*. 5:397-403.

Shannon, P., A. Markiel, O. Ozier, N.S. Baliga, J.T. Wang, D. Ramage, N. Amin, B. Schwikowski, and T. Ideker. 2003. Cytoscape: a software environment for integrated models of biomolecular interaction networks. *Genome Research*. 13:2498-2504.

Shima, K., G. Kuhlenbaumer, and J. Rupp. 2010. *Chlamydia pneumoniae* infection and Alzheimer's disease: a connection to remember? *Med Microbiol Immunol*. 199:283-289.

Smith, K.M., R. Yacobi, and R.A. Van Etten. 2003. Autoinhibition of Bcr-Abl through its SH3 domain. *Mol Cell*. 12:27-37.

Stephens, R.S. 1999. Genomic autobiographies of chlamydiae. *In Chlamydia*: intracellular biology, pathogenesis, and immunity. R.S. Stephens, editor. ASM Press, Washington, DC. 9-27.

Stephens, R.S., G. Myers, M. Eppinger, and P.M. Bavoil. 2009. Divergence without difference: phylogenetics and taxonomy of *Chlamydia* resolved. *FEMS Immunol Med Microbiol*. 55:115-119.

Su, H., G. McClarty, F. Dong, G.M. Hatch, Z.K. Pan, and G. Zhong. 2004. Activation of Raf/MEK/ERK/cPLA2 signaling pathway is essential for chlamydial acquisition of host glycerophospholipids. *J Biol Chem*. 279:9409-9416.

Subtil, A., C. Parsot, and A. Dautry-Varsat. 2001. Secretion of predicted Inc proteins of *Chlamydia pneumoniae* by a heterologous type III machinery. *Mol Microbiol*. 39:792-800.

Sudol, M. 1998. From Src Homology domains to other signaling modules: proposal of the 'protein recognition code'. *Oncogene*. 17:1469-1474.

Suzuki, M., H. Mimuro, T. Suzuki, M. Park, T. Yamamoto, and C. Sasakawa. 2005. Interaction of CagA with Crk plays an important role in *Helicobacter pylori*-induced loss of gastric epithelial cell adhesion. *J Exp Med*. 202:1235-1247.

Swamy, M., G.M. Siegers, S. Minguet, B. Wollscheid, and W.W. Schamel. 2006. Blue native polyacrylamide gel electrophoresis (BN-PAGE) for the identification and analysis of multiprotein complexes. *Sci STKE*. 2006:pl4.

Swimm, A., B. Bommarius, Y. Li, D. Cheng, P. Reeves, M. Sherman, D. Veach, W. Bornmann, and D. Kalman. 2004. Enteropathogenic *Escherichia coli* use redundant tyrosine kinases to form actin pedestals. *Mol Biol Cell*. 15:3520-3529.

Tammer, I., S. Brandt, R. Hartig, W. Konig, and S. Backert. 2007. Activation of Abl by *Helicobacter pylori*: a novel kinase for CagA and crucial mediator of host cell scattering. *Gastroenterology*. 132:1309-1319.

Tampakaki, A.P., V.E. Fadouloglou, A.D. Gazi, N.J. Panopoulos, and M. Kokkinidis. 2004. Conserved features of type III secretion. *Cell Microbiol*. 6:805-816.

Tapinos, N., and A. Rambukkana. 2005. Insights into regulation of human Schwann cell proliferation by Erk1/2 via a MEK-independent and p56Lck-dependent pathway from leprosy bacilli. *Proc Natl Acad Sci U S A*. 102:9188-9193.

Thomas, J.O., and A.A. Travers. 2001. HMG1 and 2, and related 'architectural' DNA-binding proteins. *Trends Biochem Sci*. 26:167-174.

Trentmann, O., M. Horn, A.C. van Scheltinga, H.E. Neuhaus, and I. Haferkamp. 2007. Enlightening energy parasitism by analysis of an ATP/ADP transporter from chlamydiae. *PLoS Biol*. 5:e231.

Tse, S.M., D. Mason, R.J. Botelho, B. Chiu, M. Reyland, K. Hanada, R.D. Inman, and S. Grinstein. 2005. Accumulation of diacylglycerol in the *Chlamydia* inclusion vacuole: possible role in the inhibition of host cell apoptosis. *J Biol Chem*. 280:25210-25215.

Valdivia, R.H. 2008. *Chlamydia* effector proteins and new insights into chlamydial cellular microbiology. *Curr Opin Microbiol*. 11:53-59.

van der Geer, P., S. Wiley, G.D. Gish, and T. Pawson. 1996. The Shc adaptor protein is highly phosphorylated at conserved, twin tyrosine residues (Y239/240) that mediate protein-protein interactions. *Curr Biol*. 6:1435-1444.

Vignola, M.J., D.F. Kashatus, G.A. Taylor, C.M. Counter, and R.H. Valdivia. 2010. cPLA2 regulates the expression of type I interferons and intracellular immunity to *Chlamydia trachomatis*. *J Biol Chem*. 285:21625-21635.

Wei, M.C., W.X. Zong, E.H. Cheng, T. Lindsten, V. Panoutsakopoulou, A.J. Ross, K.A. Roth, G.R. MacGregor, C.B. Thompson, and S.J. Korsmeyer. 2001. Proapoptotic BAX and BAK: a requisite gateway to mitochondrial dysfunction and death. *Science*. 292:727-730.

Willis, S.N., and J.M. Adams. 2005. Life in the balance: how BH3-only proteins induce apoptosis. *Curr Opin Cell Biol*. 17:617-625.

Wreghitt, T. 1993. Chlamydial infection of the respiratory tract. *Commun Dis Rep CDR Rev*. 3:R119-124.

Wright, H.R., A. Turner, and H.R. Taylor. 2008. Trachoma. *Lancet*. 371:1945-1954.

Wylie, J.L., G.M. Hatch, and G. McClarty. 1997. Host cell phospholipids are trafficked to and then modified by *Chlamydia trachomatis*. *J Bacteriol*. 179:7233-7242.

Yan, Y., S. Silvennoinen-Kassinen, L. Tormakangas, M. Leinonen, and P. Saikku. 2008. Selective cyclooxygenase inhibitors prevent the growth of *Chlamydia pneumoniae* in HL cells. *Int J Antimicrob Agents*. 32:78-83.

Zhao, J., K.A. Kim, and A. Abo. 2009. Tipping the balance: modulating the Wnt pathway for tissue repair. *Trends Biotechnol*. 27:131-136.

APPENDIX

6 Appendix

6.1 Supplemental material

Table 6-1. Dissociation constants of Tarp SH2 interactions. Peptides were synthesized as nonphosphorylated, singly, or doubly phosphorylated variants. Amino acid sequence of peptides is given in the footnotes. Phosphorylation is indicated by an X. Dissociation constants K_D (nM) of peptide/domain interactions are shown in the table. Each peptide was incubated twice with an array (K_D1, K_D2). Only domains giving an interaction value in both experiments were included in the interaction map, as a mean of the two values. Blank cells indicate that the K_D was below the 2 µM threshold.

		Peptide 1[a]		Peptide 2[b]		Peptide 3[c]		Peptide 4[d]		Peptide 5[e]		Peptide 6[f]		Peptide 7[g]		Peptide 8[h]	
Number	**Name**	**K_D1 (nM)**	**K_D2 (nM)**	**K_D1 (nM)**	**K_D2 (nM)**	**K_D1 (nM)**	**K_D2 (nM)**	**K_D1 (nM)**	**K_D2 (nM)**	**K_D1 (nM)**	**K_D2 (nM)**	**K_D1 (nM)**	**K_D2 (nM)**	**K_D1 (nM)**	**K_D2 (nM)**	**K_D1 (nM)**	**K_D2 (nM)**
SH2#1	PIK3R1-N							1563	360	310					745		
SH2#2	PIK3R1-C									922				542			
SH2#3	PIK3R1-NC						59		988	1264	532				990		
SH2#97	PIK3R3-N		1827			715	847		798	867	409		913		1225		
SH2#106	PIK3R3-NC	1919				206	804	1054	1048	417	459	765		860	1424		
SH2#99	PIK3R2-N					394	494	428	495	247	202			886	841		
SH2#107	PIK3R2-NC		19					647	1089								
SH2#102	ABL2	82	627	624	521	5	48	12	22	14	16	126	115	8	6	873	777
SH2#46	ABL1	1724	657			796	531		1055	758	330	1586	1917		295		
SH2#10	FGR					327	409	622	333	360	292	1049		930	663		
SH2#15	SRC														713		
SH2#120	SYK-NC	1541				152	304	175	235	297	225	1996		672	597		
SH2#19	LYN							1402									
SH2#69	FER						354				847				524		
SH2#88	HCK					903	778	1101	1675	183	245			917	893		
SH2#109	LCK									1623	1523				1847		
SH2#95	FES					1429											
SH2#37	YES1		1954			1800	518	787	524	567	570				21		
SH2#5	PLCG1-C														1872		
SH2#115	PLCG2-C										1548						
SH2#116	PLCG2-NC						942	1748	458				269				
SH2#11	GRB2					815	179	12		1125	357						
SH2#63	GRB7								1946								
SH2#94	GRB10							1284						433			

SH2#13	CRK		206			1029		1487		1569	1262					
SH2#45	CRKL	1037	454			364	505	1119	1853		105				1707	
SH2#14	NCK1					494				1893					954	
SH2#26	NCK2		1819			344	219	110		159	282			365	156	
SH2#9	PTPN11-NC							1867								
SH2#72	APS								1945							
SH2#84	SH3BP2					4		907	1949	988	926					
SH2#61	LNK		969			1835		1127		1653	1524					
SH2#112	SH2B		843													
SH2#51	SHC1	163	117	1396	1708	8	35		518	216	115		1672	21	39	
SH2#65	SHC3	880	652				163	1234	1675	466	935				286	
SH2#91	JAK3									1804	1485					
SH2#39	BRDG1														1655	
SH2#49	RIN1		1437													
SH2#50	SH2D3A									1140						
SH2#113	RASA1-N	1029	1669			71	73	77	56	30	88	933	626	77	133	
SH2#114	RASA1-NC					1766										
SH2#110	SH2D2A									1253						
SH2#111	SH2D3C				1242					1223		622			2	
SH2#20	VAV1								1600	1416	1632					
SH2#28	VAV2					167		84	505	32	28		1417	141	212	
SH2#67	PTPN6-C										1069		1397			
SH2#96	CTEN					323		1997		523	1053					
SH2#59	E138606			1954	1913							1246	1373			
SH2#83	E105251										1397					
SH2#125	SHB			1426		1052		789	954			943				
SH2#25	TNS					1793										
SH2#66	TENC1	697				476	915			675	1029					
SH2#21	TENS1										1799					
SH2#A	CBL					1824						1688				
STAT2	STAT2										949					
PTB#22	DOK4					1538						1386				
PTB#24	IRS1									809	953					
PTB#32	GULP1					1887										
PTB#44	DOK5L									519						

[a] Peptide 1, amino acid sequence EPIRTTENIXESIGGSRT, *C. trachomatis* serovar D

[b] Peptide 2, amino acid sequence EPIRTTENIYESIGGSRT, *C. trachomatis* serovar D

[c] Peptide 3, amino acid sequence EPISTTENIXENIYESID, *C. trachomatis* serovar L2

[d] Peptide 4, amino acid sequence EPISTTENIYENIXESID, *C. trachomatis* serovar L2

[e] Peptide 5, amino acid sequence EPISTTENIXENIXESID, *C. trachomatis* serovar L2

[f] Peptide 6, amino acid sequence EPISTTENIYENIYESID, *C. trachomatis* serovar L2

[g] Peptide 7, amino acid sequence EPISTTENIXESIDDSST, *C. trachomatis* serovar L2

[h] Peptide 8, amino acid sequence EPISTTENIYESIDDSST, *C. trachomatis* serovar L2

X = phosphotyrosine

Table 6-2. Infection-dependently regulated genes. List of genes regulated in an infection-dependent manner. Genes are sorted according to their fold regulation. A 1.6-fold expression cutoff was taken as selection criterion.

Gene identifier	Gene name	Full name	Fold change	p-value
NM_004267	CHST2	CHST2,C6ST	4.16	3.95E-13
NM_001657	AREG	AREG,amphiregulin (schwannoma-derived growth factor)	3.79	0.00E+00
NM_012242	DKK1	DKK1,SK,DKK-1	3.53	0.00E+00
NM_001946	DUSP6	DUSP6,dual specificity phosphatase 6	3.11	1.16E-13
THC1837102	THC1837102	THC1837102	2.78	1.20E-04
NM_004419	DUSP5	DUSP5,dual specificity phosphatase 5	2.75	6.15E-36
XM_379108	LOC400969	LOC400969	2.74	6.33E-21
M57765	IL11	IL11,AGIF,IL-11	2.72	0.00E+00
BC037430	PHLDA1	PHLDA1,PHRIP,TDAG51,DT1P1B11,MGC131738	2.71	0.00E+00
THC1870278	THC1870278	THC1870278	2.59	3.71E-08
BC018929	PHLDA1	PHLDA1,PHRIP,TDAG51,DT1P1B11,MGC131738	2.42	0.00E+00
U17077	MALL	MALL,BENE,MGC4419	2.37	1.44E-12
NM_001432	EREG	EREG,ER	2.33	3.48E-11
NM_013409	FST	FST,FS	2.32	1.38E-33
NM_005114	HS3ST1	HS3ST1,heparan sulfate (glucosamine) 3-O-sulfotransferase 1	2.29	2.75E-19
NM_001993	F3	F3,coagulation factor III (thromboplastin, tissue factor)	2.27	0.00E+00
NM_007350	PHLDA1	PHLDA1,PHRIP,TDAG51,DT1P1B11,MGC131738	2.26	7.99E-40
NM_005686	SOX13	SOX13,ICA12,Sox-13,MGC117216,SRY-box 13	2.25	3.42E-25
NM_003633	ENC1	ENC1,NRPB,CCL28,ENC-1,PIG10,TP53I10,FLJ39259	2.24	1.33E-14
AF220656	PHLDA1	PHLDA1,pleckstrin homology-like domain, family A, member 1	2.23	6.38E-10
NM_005490	SH2D3A	SH2D3A,NSP1	2.22	8.74E-03
NM_032270	LRRC8C	LRRC8C,AD158,FAD158,MGC138551,DKFZp586J1119	2.20	5.49E-40
NM_139314	ANGPTL4	ANGPTL4,NL2,ARP4,FIAF,PGAR,HFARP,pp1158,ANGPTL2	2.13	1.14E-02
XM_370948	SBK1	SBK1	2.11	5.75E-03
BC042545	RAB22A	RAB22A,MGC16770	2.06	3.38E-06
AY049781	ENC1	ENC1,NRPB,CCL28,ENC-1,PIG10,TP53I10,FLJ39259	2.05	3.56E-19
A_32_P4882	A_32_P4882	A_32_P4882	2.04	2.09E-16

NM_013940	OR10H1	OR10H1	2.03	3.33E-11
NM_006504	PTPRE	PTPRE,protein tyrosine phosphatase, receptor type, E	2.03	1.22E-26
NM_000584	IL8	IL8,interleukin 8	2.03	3.00E-05
AK074235	B3GNT5	B3GNT5,B3GN-T5,beta3Gn-T5	1.99	9.98E-32
BX325074	VASP	VASP	1.99	3.00E-05
NM_018948	ERRFI1	ERRFI1,MIG6,RALT,MIG-6,GENE-33	1.98	2.81E-41
NM_000080	CHRNE	CHRNE,ACHRE,CMS1D,CMS1E,CMS2A,FCCMS,SCCMS	1.97	3.46E-03
NM_023016	C2orf26	C2orf26	1.97	3.36E-18
NM_001671	ASGR1	ASGR1,asialoglycoprotein receptor 1	1.93	1.22E-02
D86519	NPY6R	NPY6R,neuropeptide Y receptor Y6 (pseudogene)	1.93	4.84E-02
NM_005952	MT1X	MT1X,MT1,MT-1l	1.90	4.43E-31
NM_139172	MDAC1	MDAC1	1.89	5.59E-20
NM_003266	TLR4	TLR4,TOLL,CD284,hToll	1.89	7.80E-04
ENST00000322282	ENST00000322282	ENST00000322282	1.89	4.77E-19
AK123439	AK123439	AK123439	1.89	1.11E-02
NM_130901	OTUD7A	OTUD7A,OTUD7,C15orf16,CEZANNE2	1.89	8.90E-03
THC1862126	THC1862126	THC1862126	1.89	1.32E-02
THC1847096	THC1847096	THC1847096	1.87	1.94E-17
NM_004431	EPHA2	EPHA2,EphA2	1.86	4.89E-21
THC1935995	THC1935995	THC1935995	1.85	6.15E-03
AK024943	USH1C	USH1C,PDZ73,AIE-75,DFNB18,PDZ-45,PDZ-73,NY-CO-37,NY-CO-38,ush1cpst,PDZ-73/NY-CO-38	1.83	3.67E-02
NM_003631	PARG	PARG,poly (ADP-ribose) glycohydrolase	1.83	2.94E-03
A_24_P797366	A_24_P797366	A_24_P797366	1.83	7.11E-06
BC035496	CITED4	CITED4	1.83	2.74E-08
NM_002923	RGS2	RGS2,regulator of G-protein signalling 2, 24 kDa	1.82	1.05E-07
NM_002017	FLI1	FLI1,Friend leukemia virus integration 1	1.81	7.00E-05
THC1993781	THC1993781	THC1993781	1.80	1.89E-02
BC016648	FOSL1	FOSL1,FRA1,fra-1	1.79	8.12E-25
NM_144652	LETM2	LETM2,FLJ25409	1.79	8.14E-09
NM_000170	GLDC	GLDC,glycine dehydrogenase (decarboxylating, glycine decarboxylase, glycine cleavage system protein P)	1.79	4.00E-04
NM_152594	SPRED1	SPRED1,FLJ33903	1.79	4.90E-04
THC1833111	THC1833111	THC1833111	1.77	7.28E-08
BC063316	FBXL17	FBXL17,Fbl17,Fbx13,FBXO13,DKFZp434C1715	1.76	5.34E-09
AL136788	C3orf31	C3orf31,MGC16471,DKFZp434E0519	1.76	7.10E-06
A_23_P208579	A_23_P208579	A_23_P208579	1.76	1.63E-03
NM_001945	DTR	DTR,diphtheria toxin receptor (heparin-binding epidermal growth factor-like growth factor)	1.76	4.53E-13

NM_000963	PTGS2	PTGS2,prostaglandin-endoperoxide synthase 2 (prostaglandin G/H synthase and cyclooxygenase)	1.76	6.27E-19
AF333388	LOC645745	LOC645745	1.75	2.11E-06
A_32_P101073	A_32_P101073	A_32_P101073	1.75	2.84E-08
NM_014992	DAAM1	DAAM1,KIAA0666	1.75	2.32E-42
AK002195	ARHGAP18	ARHGAP18,MacGAP,FLJ25728,MGC126757,MGC138145,bA307O14.2	1.75	8.90E-10
NM_002185	IL7R	IL7R,interleukin 7 receptor	1.74	8.17E-20
THC1892644	THC1892644	THC1892644	1.73	3.76E-15
NM_024827	HDAC11	HDAC11,histone deacetylase 11	1.73	1.69E-02
NM_174945	ZNF575	ZNF575,FLJ32567	1.72	4.32E-07
NM_145110	MAP2K3	MAP2K3,MEK3,MKK3,MAPKK3,PRKMK3	1.72	1.26E-12
AK056774	H19	H19,ASM,BWS,ASM1,MGC4485,PRO2605,D11S813E,predicted protein of HQ2605	1.72	1.50E-02
NM_144777	SCEL	SCEL,FLJ21667,MGC22531	1.71	6.75E-13
AB058715	CDH23	CDH23,USH1D,DFNB12,FLJ00233,FLJ36499,KIAA1774,KIAA1812,MGC102761,DKFZp434P2350	1.71	4.89E-02
A_32_P104469	A_32_P104469	A_32_P104469	1.71	5.09E-08
BC015940	NT5E	NT5E,NT,eN,NT5,NTE,eNT,CD73,E5NT	1.70	5.14E-24
NM_006465	ARID3B	ARID3B,BDP,DRIL2	1.70	4.40E-16
NM_004864	PLAB	PLAB,prostate differentiation factor	1.69	1.08E-12
NM_032933	C18orf45	C18orf45,FLJ44259,MGC11386,MGC138577	1.68	2.30E-04
NM_032181	FLJ13391	FLJ13391,hypothetical protein FLJ13391	1.68	2.28E-15
NM_003311	PHLDA2	PHLDA2,IPL,BRW1C,BWR1C,HLDA2,TSSC3	1.68	1.42E-15
NM_001511	CXCL1	CXCL1,chemokine (C-X-C motif) ligand 1 (melanoma growth stimulating activity, alpha)	1.67	5.88E-24
NM_002480	PPP1R12A	PPP1R12A,protein phosphatase 1, regulatory (inhibitor) subunit 12A	1.67	1.39E-06
X97261	MT1L	MT1L,MT1,MTF,MT1R,metallothionein 1R	1.67	5.88E-25
THC1950983	THC1950983	THC1950983	1.66	4.00E-05
NM_016643	LOC51333	LOC51333	1.66	4.66E-03
AF406557	PTPRE	PTPRE,PTPE,HPTPE,DKFZp313F1310,R-PTP-EPSILON	1.66	1.97E-18
NM_001394	DUSP4	DUSP4,TYP,HVH2,MKP2,MKP-2	1.66	1.03E-09
NM_005950	MT1G	MT1G,MT1,MT1K,MGC12386	1.66	4.65E-34
AL832345	PRKCE	PRKCE,PKCE,MGC125656,MGC125657,nPKC-epsilon	1.66	1.16E-12
NM_018413	CHST11	CHST11,C4ST,C4ST1,C4ST-1,HSA269537	1.66	1.14E-20
BC017197	MCL1	MCL1,myeloid cell leukemia sequence 1 (BCL2-related)	1.65	1.57E-08
NM_203349	SHC4	SHC4,RaLP,MGC34023	1.65	4.50E-02
BC033310	GDA	GDA,CYPIN,GUANASE,MGC9982,NEDASIN,KIAA1258	1.65	2.82E-11
AK058031	TGM2	TGM2,TG2,TGC	1.65	1.08E-11
NM_020803	KLHL8	KLHL8,FLJ46304,KIAA1378	1.65	2.07E-03
A_32_P192044	A_32_P192044	A_32_P192044	1.65	9.65E-03

AY358798	PHGDHL1	PHGDHL1,FLJ26351,FLJ30001,FLJ30548,FLJ42413,MGC90487	1.65	3.52E-02
NM_002999	SDC4	SDC4,syndecan 4 (amphiglycan, ryudocan)	1.64	1.57E-14
AK093501	RC3H1	RC3H1,RNF198,KIAA2025,RP5-1198E17.5	1.64	1.79E-06
NM_005946	MT1A	MT1A,MT1,MTC,MT1S,MGC32848	1.63	3.80E-08
ENST00000316643	ENST00000316643	ENST00000316643	1.63	4.02E-03
NM_015472	WWTR1	WWTR1,TAZ,DKFZP586I1419	1.63	1.57E-06
THC1946380	THC1946380	THC1946380	1.62	5.00E-05
A_24_P187626	A_24_P187626	A_24_P187626	1.62	1.95E-17
BC007034	MT2A	MT2A,MT2	1.62	7.25E-19
NM_005556	KRT7	KRT7,keratin 7	1.62	2.66E-08
NM_174953	ATP2A3	ATP2A3,SERCA3	1.62	1.07E-06
NM_001986	ETV4	ETV4,E1AF,PEA3,E1A-F,PEAS3	1.61	1.06E-03
NM_000490	AVP	AVP,arginine vasopressin (neurophysin II, antidiuretic hormone, diabetes insipidus, neurohypophyseal)	1.61	8.08E-03
NM_033306	CASP4	CASP4,caspase 4, apoptosis-related cysteine protease	1.61	8.08E-15
NM_005285	NPBWR1	NPBWR1,GPR7,MGC129755	1.61	1.40E-04
NM_153344	C6orf141	C6orf141,MGC46457	1.61	2.04E-15
BC007242	ETV4	ETV4,E1AF,PEA3,E1A-F,PEAS3	1.61	1.40E-02
NM_003028	SHB	SHB,RP11-3J10.8	1.61	2.42E-12
NM_032407	PCDHGC5	PCDHGC5,MGC138286,MGC138288,PCDH-GAMMA-C5	1.60	9.57E-06
BC024020	TMEM49	TMEM49,VMP1,DKFZP566I133	1.60	5.31E-03
BM701491	LOC145853	LOC145853	1.60	2.86E-02
NM_014331	SLC7A11	SLC7A11,xCT,CCBR1	1.60	1.41E-02
NM_005953	MT2A	MT2A,MT2	1.60	2.99E-37
AJ243670	UBAP2L	UBAP2L,NICE-4,FLJ42300,KIAA0144	1.60	4.35E-06
NM_053056	CCND1	CCND1,cyclin D1 (PRAD1: parathyroid adenomatosis 1)	1.60	1.84E-11
THC2004644	THC2004644	THC2004644	-1.60	1.80E-04
AW901958	PRKCB1	PRKCB1,PKCB,PRKCB,PRKCB2,MGC41878,PKC-beta	-1.61	1.01E-03
A_32_P231250	A_32_P231250	A_32_P231250	-1.61	2.45E-02
AK123333	AK123333	AK123333	-1.61	4.51E-06
THC1910570	THC1910570	THC1910570	-1.61	8.01E-06
AF086541	LOC92196	LOC92196	-1.61	9.43E-03
AK097640	TPRX1	TPRX1,TPRX,FLJ40321	-1.62	1.08E-03
THC2000697	THC2000697	THC2000697	-1.62	3.00E-04
NM_020970	KIAA1641	KIAA1641,FLJ21281	-1.62	1.20E-04
BF592593	GRIN2D	GRIN2D,EB11,NMDAR2D	-1.62	2.00E-05
A_32_P233049	A_32_P233049	A_32_P233049	-1.62	3.90E-02

NM_007034	DNAJB4	DNAJB4,DnaJ (Hsp40) homolog, subfamily B, member 4	-1.62	4.39E-17
AK024270	KLHL24	KLHL24,DRE1,FLJ25796	-1.62	1.30E-04
BC013024	LOC154822	LOC154822	-1.62	8.10E-14
A_24_P230100	A_24_P230100	A_24_P230100	-1.62	4.82E-06
BI517435	BI517435	BI517435	-1.63	6.58E-03
NM_058168	GDEP	GDEP	-1.63	1.72E-02
AF086297	NBR2	NBR2,MGC104305,DKFZp686F081	-1.64	3.55E-08
NM_153008	FLJ30277	FLJ30277,FLJ30278	-1.64	1.71E-02
NM_016188	ACTL6B	ACTL6B,ACTL6,BAF53B	-1.64	2.50E-04
A_32_P133464	A_32_P133464	A_32_P133464	-1.64	3.60E-15
A_24_P178475	A_24_P178475	A_24_P178475	-1.64	2.03E-06
AK056190	DFNB31	DFNB31,WHRN,CIP98,KIAA1526,RP11-9M16.1,DKFZP434N014	-1.64	2.08E-07
BF897263	BF897263	BF897263	-1.65	1.10E-04
AL833897	AL833897	AL833897	-1.65	8.03E-07
AK058070	MDH1B	MDH1B,FLJ25341,RP11-95H11	-1.66	2.93E-03
NM_153768	CABYR	CABYR,CBP86,FSP-2,MGC9117	-1.67	7.06E-03
AB037793	USP35	USP35	-1.67	3.08E-21
NM_024584	FLJ13646	FLJ13646	-1.67	1.21E-07
NM_004821	HAND1	HAND1,Hxt,eHand,Thing1	-1.67	4.10E-02
AL137350	FAM44A	FAM44A,FLJ33215,KIAA1327	-1.68	2.10E-04
THC1848900	THC1848900	THC1848900	-1.68	7.80E-04
NM_033427	CTTNBP2	CTTNBP2,Orf4,C7orf8,CORTBP2,FLJ34229,KIAA1758,MGC104579	-1.68	4.63E-06
AK124638	PLCXD3	PLCXD3	-1.69	1.23E-17
A_24_P110521	A_24_P110521	A_24_P110521	-1.69	5.00E-05
A_32_P215003	A_32_P215003	A_32_P215003	-1.70	3.76E-03
BE904671	EPHA5	EPHA5,CEK7,EHK1,HEK7,TYRO4	-1.71	6.77E-16
ENST00000334819	ENST00000334819	ENST00000334819	-1.71	4.25E-06
AK074353	HBP1	HBP1,FLJ16340	-1.71	2.05E-19
THC1933749	THC1933749	THC1933749	-1.71	8.03E-03
NM_006813	PROL2	PROL2,proline rich 2	-1.72	3.90E-04
NM_002133	HMOX1	HMOX1,heme oxygenase (decycling) 1	-1.72	6.51E-10
BU729607	HMGB2	HMGB2,HMG2	-1.73	1.64E-03
NM_005279	GPR1	GPR1	-1.73	3.00E-05
AF080397	FZR1	FZR1,FZR,CDH1,FZR2,HCDH,HCDH1,CDC20C,KIAA1242	-1.73	3.04E-10
A_32_P117453	A_32_P117453	A_32_P117453	-1.73	2.00E-05
ENST00000328259	ENST00000328259	ENST00000328259	-1.75	2.83E-06

NM_152405	JMY	JMY,FLJ37870	-1.76	3.47E-07
M76744	CEACAM1	CEACAM1,BGP,BGP1,BGPI	-1.77	4.49E-08
THC1859333	THC1859333	THC1859333	-1.77	1.00E-04
A_32_P110042	A_32_P110042	A_32_P110042	-1.77	6.00E-05
THC1827959	THC1827959	THC1827959	-1.78	3.04E-03
NM_006238	PPARD	PPARD,FAAR,NUC1,NUCI,NR1C2,NUCII,PPARB,MGC3931,PPAR-beta	-1.78	1.17E-03
A_32_P61538	A_32_P61538	A_32_P61538	-1.79	2.90E-04
BC040628	GTF2A1	GTF2A1,TF2A1,TFIIA,MGC129969,MGC129970	-1.82	9.50E-04
A_32_P213543	A_32_P213543	A_32_P213543	-1.83	1.41E-02
A_32_P97536	A_32_P97536	A_32_P97536	-1.84	4.74E-08
A_23_P108534	A_23_P108534	A_23_P108534	-1.85	2.62E-03
NM_024859	FLJ21687	FLJ21687,JM10,MGC138889	-1.87	7.03E-03
M96843	ID2B	ID2B	-1.88	2.15E-10
THC1826185	THC1826185	THC1826185	-1.88	6.30E-04
NM_153032	FLJ32065	FLJ32065,MGC90301	-1.89	1.79E-07
NM_000459	TEK	TEK,TEK tyrosine kinase, endothelial (venous malformations, multiple cutaneous and mucosal)	-1.90	3.00E-05
NM_014848	SV2B	SV2B,synaptic vesicle glycoprotein 2B	-1.91	3.57E-37
A_32_P73707	A_32_P73707	A_32_P73707	-1.91	9.40E-04
NM_182522	FAM19A4	FAM19A4,TAFA4,TAFA-4,FLJ25161	-1.91	2.44E-02
AF251079	DACT1	DACT1,DPR1,FRODO,HDPR1,DAPPER,THYEX3,DAPPER1	-1.92	3.00E-05
NM_001710	BF	BF,B-factor, properdin	-1.96	1.43E-17
AK091057	LOC285535	LOC285535	-1.96	1.17E-06
NM_001964	EGR1	EGR1,early growth response 1	-1.97	2.13E-07
AB002297	DOCK3	DOCK3,PBP,MOCA,KIAA0299	-1.98	1.12E-03
BX091616	BX091616	BX091616	-2.00	1.82E-03
NM_139241	FGD4	FGD4,FRABP,FRABIN,ZFYVE6,MGC57222,DKFZp313E1818	-2.00	1.59E-08
AK057247	NEK10	NEK10,FLJ32685	-2.00	2.22E-15
AK123235	CCDC108	CCDC108,MGC35338,DKFZp434O0527	-2.02	2.47E-11
ENST00000309333	ENST00000309333	ENST00000309333	-2.02	1.03E-06
AF152502	PCDHB9	PCDHB9,PCDH3H,MGC119555,MGC119556,PCDH-BETA9	-2.05	1.43E-07
AK023134	ECAT8	ECAT8,FLJ13072	-2.07	2.45E-08
NM_006308	HSPB3	HSPB3,heat shock 27 kDa protein 3	-2.07	0.00E+00
AF086511	AF086511	AF086511	-2.28	1.79E-10
NM_033503	BMF	BMF,FLJ00065	-2.44	2.01E-09
NM_001956	EDN2	EDN2,endothelin 2	-2.94	0.00E+00

Table 6-3. SHC1-dependently regulated genes. List of genes regulated in an SHC1-dependent manner. Genes are sorted according to their fold regulation. A 1.6-fold expression cutoff was taken as selection criterion.

Gene identifier	Gene name	Full name	Fold change	p-value
NM_033503	BMF	BMF,FLJ00065	3.15	6.73E-14
NM_031418	C11orf25	C11orf25,chromosome 11 open reading frame 25	2.74	7.00E-05
NM_006919	SERPINB3	SERPINB3,serine (or cysteine) proteinase inhibitor, clade B (ovalbumin), member 3	2.63	3.21E-13
NM_005994	TBX2	TBX2,T-box 2	2.51	0.00E+00
NM_153032	FLJ32065	FLJ32065,MGC90301	2.41	2.94E-16
NM_025212	CXXC4	CXXC4,IDAX	2.37	2.79E-03
THC1819187	THC1819187	THC1819187	2.34	2.30E-04
NM_001964	EGR1	EGR1,early growth response 1	2.32	7.84E-42
NM_021995	UTS2	UTS2,UII,U-II,UCN2,PRO1068	2.28	1.20E-04
NM_002974	SERPINB4	SERPINB4,PI11,SCCA1,SCCA2,LEUPIN,SCCA-2	2.28	2.17E-22
BU729607	HMGB2	HMGB2,HMG2	2.21	5.58E-08
NM_000550	TYRP1	TYRP1,tyrosinase-related protein 1	2.18	3.60E-04
NM_139284	LGI4	LGI4,LGIL3	2.16	7.70E-11
BX094364	BX094364	BX094364	2.07	5.37E-03
ENST00000333984	ENST00000333984	ENST00000333984	2.03	1.00E-05
AF220656	PHLDA1	PHLDA1,pleckstrin homology-like domain, family A, member 1	2.02	1.79E-10
BC018929	PHLDA1	PHLDA1,PHRIP,TDAG51,DT1P1B11,MGC131738	2.00	1.57E-23
A_23_P211468	A_23_P211468	A_23_P211468	2.00	3.00E-05
AK023629	AK023629	AK023629	1.98	1.78E-08
NM_013409	FST	FST,FS	1.98	1.04E-09
AK001987	FLJ11125	FLJ11125	1.98	9.49E-08
AB007870	NUPL1	NUPL1,PRO2463,KIAA0410	1.98	5.13E-11
NM_002546	TNFRSF11B	TNFRSF11B,tumor necrosis factor receptor superfamily, member 11b (osteoprotegerin)	1.97	1.66E-20
A_32_P180538	A_32_P180538	A_32_P180538	1.95	7.67E-03
NM_000029	AGT	AGT,angiotensinogen (serine (or cysteine) proteinase inhibitor, clade A (alpha-1 antiproteinase, antitrypsin), member 8)	1.92	9.91E-21
NM_012258	HEY1	HEY1,CHF2,OAF1,HERP2,HESR1,HRT-1,MGC1274	1.92	4.25E-41
NM_203349	SHC4	SHC4,RaLP,MGC34023	1.91	1.22E-17
NM_000104	CYP1B1	CYP1B1,cytochrome P450, family 1, subfamily B, polypeptide 1	1.90	6.00E-05
NM_016040	TMED5	TMED5,CGI-100,RP5-976O13.2	1.88	0.00E+00
THC1910374	THC1910374	THC1910374	1.88	4.67E-19
NM_003897	IER3	IER3,DIF2,IEX1,PRG1,DIF-2,GLY96,IEX-1,IEX-1L	1.87	7.31E-09
NM_000459	TEK	TEK,TEK tyrosine kinase, endothelial (venous malformations, multiple cutaneous and mucosal)	1.87	9.24E-07

NM_001242	TNFRSF7	TNFRSF7,tumor necrosis factor receptor superfamily, member 7	1.85	2.40E-04
AB028957	SATB2	SATB2,FLJ21474,FLJ32076,KIAA1034,MGC119474,MGC119477	1.84	5.50E-07
NM_024680	E2F8	E2F8,FLJ23311	1.84	2.99E-13
THC1877698	THC1877698	THC1877698	1.84	1.44E-13
BC023566	RASEF	RASEF,RAB45,FLJ31614	1.83	2.00E-05
NM_006216	SERPINE2	SERPINE2,GDN,PI7,PN1,PNI	1.82	2.05E-20
NM_002314	LIMK1	LIMK1,LIM domain kinase 1	1.82	0.00E+00
NM_012080	FAM16AX	FAM16AX,family with sequence similarity 16, member A, X-linked	1.81	6.37E-36
THC2005782	THC2005782	THC2005782	1.81	3.48E-08
AK024362	LOC147650	LOC147650,MGC125919,MGC125920	1.81	0.00E+00
ENST00000332248	ENST00000332248	ENST00000332248	1.79	2.26E-02
NM_145056	MGC15476	MGC15476	1.79	6.00E-05
NM_001047	SRD5A1	SRD5A1,steroid-5-alpha-reductase, alpha polypeptide 1 (3-oxo-5 alpha-steroid delta 4-dehydrogenase alpha 1)	1.78	2.76E-24
NM_017933	FLJ20701	FLJ20701,HMFN2073	1.78	3.95E-28
AL832448	SLC2A14	SLC2A14,GLUT14	1.77	1.23E-02
NM_004350	RUNX3	RUNX3,AML2,CBFA3,PEBP2aC,FLJ34510	1.77	4.72E-13
NM_015115	DCUN1D4	DCUN1D4,KIAA0276	1.77	5.94E-17
NM_006469	IVNS1ABP	IVNS1ABP,ND1,NS-1,NS1BP,FLARA3,NS1-BP,HSPC068,FLJ10069,FLJ10411,FLJ10962,FLJ35593,KIAA0850, DKFZp686K06216	1.77	7.50E-22
A_32_P129689	A_32_P129689	A_32_P129689	1.77	4.00E-05
NM_005114	HS3ST1	HS3ST1,heparan sulfate (glucosamine) 3-O-sulfotransferase 1	1.75	1.77E-28
NM_005931	MICB	MICB,MHC class I polypeptide-related sequence B	1.75	7.73E-08
NM_001511	CXCL1	CXCL1,chemokine (C-X-C motif) ligand 1 (melanoma growth stimulating activity, alpha)	1.75	1.18E-09
A_24_P384029	A_24_P384029	A_24_P384029	1.75	6.72E-23
BC005178	HES1	HES1,HHL,HRY,HES-1,FLJ20408	1.75	1.68E-09
A_32_P146169	A_32_P146169	A_32_P146169	1.75	2.15E-02
NM_007329	DMBT1	DMBT1,GP340,muclin	1.74	3.16E-07
THC1881984	THC1881984	THC1881984	1.73	5.52E-12
A_32_P27991	A_32_P27991	A_32_P27991	1.73	3.20E-03
AL832945	LOC284262	LOC284262	1.72	5.59E-09
BC018658	REEP3	REEP3,C10orf74	1.72	0.00E+00
AF085962	AF085962	AF085962	1.72	2.50E-03
A_24_P1873	A_24_P1873	A_24_P1873	1.71	1.85E-02
BC044246	KIAA1913	KIAA1913,TTMC	1.71	2.08E-06
AB037855	KIAA1434	KIAA1434,FLJ11085,MGC26147,RP5-1022P6.2	1.71	1.00E-05
NM_080593	HIST1H2BK	HIST1H2BK,H2B/S,H2BFT,H2BFAiii,MGC131989	1.70	6.21E-11

BC039118	STX6	STX6	1.70	6.62E-13
NM_002280	KRTHA5	KRTHA5,HA5,Ha-5,hHa5	1.70	2.10E-04
AK095176	C10orf39	C10orf39,FLJ37857	1.70	1.87E-22
BC007329	TLE6	TLE6,GRG6,FLJ14009,MGC14966	1.70	1.42E-03
A_32_P85360	A_32_P85360	A_32_P85360	1.70	1.39E-02
NM_018653	GPRC5C	GPRC5C,RAIG3,RAIG-3,MGC131820	1.69	1.80E-04
AL359062	COL8A1	COL8A1,MGC9568	1.69	3.41E-16
AK093577	MKL2	MKL2,MRTF-B,NPD001,FLJ31823,DKFZp686J1745	1.69	1.88E-16
NM_032995	ARHGEF4	ARHGEF4,ASEF,GEF4,STM6	1.68	3.23E-11
NM_000067	CA2	CA2,CAII,Car2,CA II,CA-II	1.68	1.88E-06
NM_152336	FLJ32310	FLJ32310	1.68	1.50E-04
THC1982550	THC1982550	THC1982550	1.68	3.00E-05
A_32_P71768	A_32_P71768	A_32_P71768	1.68	1.00E-05
A_32_P75141	A_32_P75141	A_32_P75141	1.68	1.85E-27
NM_003483	HMGA2	HMGA2,BABL,LIPO,HMGIC,HMGI-C	1.68	5.86E-03
A_32_P225328	A_32_P225328	A_32_P225328	1.68	4.65E-15
NM_021205	RHOU	RHOU,ARHU,WRCH1,hG28K,CDC42L1,FLJ10616,DJ646B12.2,fJ646B12.2	1.68	9.65E-09
NM_004460	FAP	FAP,fibroblast activation protein, alpha	1.68	3.59E-37
U83115	AIM1	AIM1,absent in melanoma 1	1.67	3.89E-08
NM_006202	PDE4A	PDE4A,phosphodiesterase 4A, cAMP-specific (phosphodiesterase E2 dunce homolog, Drosophila)	1.67	7.14E-13
AV756170	RPS11	RPS11	1.67	3.95E-03
AK055368	ETV1	ETV1,ER81,MGC104699,MGC120533,MGC120534,DKFZp781L0674	1.67	7.28E-03
NM_012285	KCNH4	KCNH4,potassium voltage-gated channel, subfamily H (eag-related), member 4	1.67	2.70E-03
BC037430	PHLDA1	PHLDA1,PHRIP,TDAG51,DT1P1B11,MGC131738	1.67	6.92E-14
NM_002026	FN1	FN1,fibronectin 1	1.67	8.86E-21
A_24_P490704	A_24_P490704	A_24_P490704	1.66	1.83E-06
NM_006186	NR4A2	NR4A2,nuclear receptor subfamily 4, group A, member 2	1.66	4.57E-06
NM_016122	NY-REN-58	NY-REN-58,NY-REN-58 antigen	1.66	3.54E-13
THC1949165	THC1949165	THC1949165	1.66	3.03E-10
THC1816039	THC1816039	THC1816039	1.65	3.00E-05
AK094718	FLJ22536	FLJ22536,FLJ12803	1.65	1.01E-25
NM_005269	GLI	GLI,glioma-associated oncogene homolog (zinc finger protein)	1.65	2.08E-02
A_32_P36412	A_32_P36412	A_32_P36412	1.64	9.33E-06
NM_003020	SGNE1	SGNE1,secretory granule, neuroendocrine protein 1 (7B2 protein)	1.64	3.00E-05
NM_001146	ANGPT1	ANGPT1,AGP1,AGPT,ANG1	1.64	3.15E-14
THC1868308	THC1868308	THC1868308	1.64	1.76E-11

NM_144707	PROM2	PROM2,PROM-2,MGC138714	1.63	6.35E-03
A_32_P155588	A_32_P155588	A_32_P155588	1.63	3.66E-02
AK094629	AK094629	AK094629	1.63	5.80E-04
NM_020432	PHTF2	PHTF2,FLJ33324,MGC86999,DKFZP564F013	1.63	1.19E-11
NM_175061	JAZF1	JAZF1,TIP27,DKFZp761K2222	1.63	2.27E-06
NM_024760	TLE6	TLE6,GRG6,FLJ14009,MGC14966	1.63	1.58E-06
AF273047	GOLGA4	GOLGA4,GCP2,GOLG,p230,MU-RMS-40.18	1.63	6.98E-06
NM_005252	FOS	FOS,v-fos FBJ murine osteosarcoma viral oncogene homolog	1.63	3.00E-05
NM_004117	FKBP5	FKBP5,FK506 binding protein 5	1.62	3.38E-03
NM_015192	PLCB1	PLCB1,PLC-I,PI-PLC,PLC-154,FLJ45792	1.62	2.55E-12
NM_006380	APPBP2	APPBP2,amyloid beta precursor protein (cytoplasmic tail) binding protein 2	1.62	2.15E-08
NM_014454	PA26	PA26,p53 regulated PA26 nuclear protein	1.62	2.03E-34
THC1808272	THC1808272	THC1808272	1.62	3.94E-15
AF220047	C3orf10	C3orf10,MDS027,hHBrk1,HSPC300	1.62	1.87E-02
AK093435	FLJ36116	FLJ36116	1.61	4.05E-03
THC1924019	THC1924019	THC1924019	1.61	6.47E-09
BU729734	MATR3	MATR3,MGC9105,KIAA0723,DKFZp686K0542,DKFZp686K23100	1.61	1.00E-04
BM664049	NCF1	NCF1,NCF1A,NOXO2,p47phox,SH3PXD1A	1.61	5.20E-04
THC1849267	THC1849267	THC1849267	1.61	4.50E-06
NM_020200	PRTFDC1	PRTFDC1,HHGP,FLJ11888	1.61	5.47E-16
NM_003272	GPR137B	GPR137B,TM7SF1	1.61	2.60E-04
BC016285	PRKACB	PRKACB,PKACB,MGC9320,MGC41879,DKFZp781I2452	1.61	1.10E-02
BC007436	FAM44B	FAM44B	1.60	1.23E-06
AB007950	TMCC2	TMCC2,HUCEP11,FLJ38497,KIAA0481	1.60	3.37E-10
NM_080741	NEU4	NEU4,MGC18222,MGC102757	1.60	3.34E-07
NM_005388	PDCL	PDCL,phosducin-like	-1.60	2.46E-06
NM_138432	SDSL	SDSL,SDS-RS1	-1.60	1.25E-12
NM_000224	KRT18	KRT18,keratin 18	-1.60	4.56E-14
NM_018999	KIAA1128	KIAA1128,Gcap14,FLJ14262,FLJ25809,bA486O22.1	-1.60	6.61E-31
AK024475	PLEKHG4	PLEKHG4,DKFZP434I216,puratrophin1	-1.60	1.59E-07
NM_022445	TPK1	TPK1,PP20,HTPK1	-1.60	3.73E-02
BG178211	BG178211	BG178211	-1.61	2.39E-09
NM_001769	CD9	CD9,CD9 antigen (p24)	-1.61	1.93E-13
NM_024859	FLJ21687	FLJ21687,JM10,MGC138889	-1.61	2.55E-03
NM_144722	FLJ23577	FLJ23577,FLJ23164,FLJ25395,KIAA1770,MGC102842	-1.61	5.42E-11
NM_144603	NOXO1	NOXO1,P41NOX,P41NOXA,P41NOXB,P41NOXC,SH3PXD5,MGC20258	-1.61	2.48E-08

NM_018964	SLC37A1	SLC37A1,G3PP,FLJ22340	-1.61	1.86E-15
ENST00000328614	ENST00000328614	ENST00000328614	-1.61	1.00E-05
NM_022469	GREM2	GREM2,PRDC,DAND3,CKTSF1B2	-1.62	1.68E-02
NM_017590	ZC3H7B	ZC3H7B,RoXaN,FLJ13787,KIAA1031,DKFZp434K0920	-1.62	3.50E-04
NM_181526	MYL9	MYL9,LC20,MLC2,MRLC1,MYRL2,MGC3505	-1.62	1.66E-08
NM_003725	RODH	RODH,3-hydroxysteroid epimerase	-1.62	3.04E-08
THC1893261	THC1893261	THC1893261	-1.62	1.54E-02
NM_025149	FLJ20920	FLJ20920	-1.62	6.08E-06
A_24_P686014	A_24_P686014	A_24_P686014	-1.62	7.00E-06
NM_002646	PIK3C2B	PIK3C2B,phosphoinositide-3-kinase, class 2, beta polypeptide	-1.62	1.00E-05
ENST00000329590	ENST00000329590	ENST00000329590	-1.62	1.70E-04
NM_013404	MSLN	MSLN,mesothelin	-1.62	5.00E-05
NM_000475	NR0B1	NR0B1,AHC,AHX,DSS,GTD,HHG,AHCH,DAX1,DAX-1,NROB1	-1.62	6.00E-05
NM_000228	LAMB3	LAMB3,laminin, beta 3	-1.62	4.84E-16
AL713754	DKFZp667M2411	DKFZp667M2411	-1.62	1.78E-18
NM_005100	AKAP12	AKAP12,A kinase (PRKA) anchor protein (gravin) 12	-1.62	1.24E-06
ENST00000327707	ENST00000327707	ENST00000327707	-1.62	6.12E-18
A_24_P229911	A_24_P229911	A_24_P229911	-1.62	1.21E-12
BC030956	GNGT1	GNGT1,GNG1	-1.62	6.00E-05
A_24_P471242	A_24_P471242	A_24_P471242	-1.62	1.13E-13
NM_004096	EIF4EBP2	EIF4EBP2,4EBP2	-1.62	1.01E-03
NM_000248	MITF	MITF,microphthalmia-associated transcription factor	-1.63	7.46E-18
AK095472	TMEM64	TMEM64,DKFZp762C1112	-1.63	1.01E-15
A_23_P254384	A_23_P254384	A_23_P254384	-1.63	1.44E-16
AB033040	RNF150	RNF150,MGC125502	-1.63	6.80E-08
AK095098	COL25A1	COL25A1,CLAC	-1.63	3.44E-06
NM_014051	TMEM14A	TMEM14A,PTD011,C6orf73	-1.63	2.05E-19
ENST00000332794	ENST00000332794	ENST00000332794	-1.63	8.81E-06
NM_018242	FLJ10847	FLJ10847,MATE1,MATE2,MGC64822	-1.63	1.05E-11
NM_000447	PSEN2	PSEN2,presenilin 2 (Alzheimer disease 4)	-1.63	5.86E-09
NM_003368	USP1	USP1,ubiquitin specific protease 1	-1.63	4.24E-13
A_24_P247233	A_24_P247233	A_24_P247233	-1.63	2.87E-09
THC1843344	THC1843344	THC1843344	-1.63	2.00E-05
THC1991717	THC1991717	THC1991717	-1.63	3.05E-06
A_24_P230466	A_24_P230466	A_24_P230466	-1.63	2.95E-12
NM_006827	TMP21	TMP21,transmembrane trafficking protein	-1.63	0.00E+00

NM_007271	STK38	STK38,serine/threonine kinase 38	-1.64	0.00E+00
THC1924184	THC1924184	THC1924184	-1.64	9.25E-03
NM_003356	UCP3	UCP3,uncoupling protein 3 (mitochondrial, proton carrier)	-1.64	1.44E-03
NM_004473	FOXE1	FOXE1,TTF2,FOXE2,HFKH4,HFKL5,TITF2,TTF-2,FKHL15	-1.64	7.97E-09
AK091178	LOC285401	LOC285401	-1.64	3.57E-10
NM_003979	GPRC5A	GPRC5A,RAI3,RAIG1,GPCR5A	-1.64	3.25E-30
NM_006992	LRRC23	LRRC23,B7,LRPB7,B7 isoform	-1.64	1.04E-09
AB007952	FBXO28	FBXO28,Fbx28,FLJ10766,KIAA0483	-1.64	4.70E-04
S73202	argininosuccinate synthetase	argininosuccinate synthetase	-1.64	8.90E-22
A_24_P418687	A_24_P418687	A_24_P418687	-1.64	2.63E-06
AL832465	NPNT	NPNT,POEM,EGFL6L	-1.65	4.10E-06
A_24_P792988	A_24_P792988	A_24_P792988	-1.65	3.95E-23
A_24_P230486	A_24_P230486	A_24_P230486	-1.65	1.26E-07
NM_007075	WDR45	WDR45,JM5,WDRX1,WIPI4,WIPI-4	-1.65	5.21E-17
A_24_P264644	A_24_P264644	A_24_P264644	-1.65	1.37E-12
NM_014521	SH3BP4	SH3BP4,TTP,BOG25	-1.65	1.23E-10
A_24_P118391	A_24_P118391	A_24_P118391	-1.65	0.00E+00
AJ001827	UBPH	UBPH,FLJ38870	-1.65	2.00E-05
A_32_P211494	A_32_P211494	A_32_P211494	-1.65	6.30E-04
NM_020987	ANK3	ANK3,ankyrin 3, node of Ranvier (ankyrin G)	-1.65	2.10E-04
AB014511	ATP9A	ATP9A,ATPIIA,KIAA0611	-1.66	1.26E-09
NM_023076	FLJ23360	FLJ23360,hypothetical protein FLJ23360	-1.66	1.14E-08
NM_002999	SDC4	SDC4,syndecan 4 (amphiglycan, ryudocan)	-1.66	2.64E-10
A_24_P213336	A_24_P213336	A_24_P213336	-1.66	1.27E-25
NM_005542	INSIG1	INSIG1,CL-6,MGC1405	-1.66	8.63E-28
BC045163	BC045163	BC045163	-1.66	6.00E-05
ENST00000332105	ENST00000332105	ENST00000332105	-1.66	1.52E-11
THC1983708	THC1983708	THC1983708	-1.66	5.97E-13
NM_144492	CLDN14	CLDN14,DFNB29	-1.66	3.00E-02
NM_024110	CARD14	CARD14,BIMP2,CARMA2	-1.66	1.45E-03
THC1881484	THC1881484	THC1881484	-1.66	1.78E-06
ENST00000332292	ENST00000332292	ENST00000332292	-1.66	4.36E-06
NM_016230	CYB5R4	CYB5R4,NCB5OR,dJ676J13.1,RP4-676J13.1	-1.66	9.00E-05
NM_153291	FAM10A5	FAM10A5	-1.67	8.04E-20
A_24_P358857	A_24_P358857	A_24_P358857	-1.67	4.07E-10
NM_013411	AK2	AK2,ADK2	-1.67	1.68E-12

NM_001159	AOX1	AOX1,AO,AOH1	-1.67	5.84E-03
A_32_P157671	A_32_P157671	A_32_P157671	-1.67	1.61E-17
NM_016533	NINJ2	NINJ2	-1.67	3.54E-08
A_24_P281605	A_24_P281605	A_24_P281605	-1.67	3.43E-14
THC1953252	THC1953252	THC1953252	-1.67	2.60E-04
A_24_P812018	A_24_P812018	A_24_P812018	-1.67	2.46E-30
A_24_P255954	A_24_P255954	A_24_P255954	-1.67	2.25E-20
A_24_P186746	A_24_P186746	A_24_P186746	-1.67	2.97E-26
THC1901913	THC1901913	THC1901913	-1.67	5.80E-04
NM_152748	KIAA1324L	KIAA1324L,FLJ31340	-1.67	2.04E-09
A_24_P127362	A_24_P127362	A_24_P127362	-1.67	5.33E-09
NM_144765	EVA1	EVA1,EVA,MPZL2	-1.67	1.26E-06
NM_017540	GALNT10	GALNT10,FLJ00205,FLJ11715,GalNAcT10,DKFZp586H0623,pp-GalNAc-T10	-1.68	7.98E-09
NM_020179	C11orf75	C11orf75,FN5	-1.68	2.57E-06
NM_018194	FLJ10724	FLJ10724,melanoma antigen recognized by T cells 2	-1.68	3.00E-05
A_24_P332595	A_24_P332595	A_24_P332595	-1.68	9.98E-13
NM_007283	MGLL	MGLL,MGL,HU-K5	-1.68	9.94E-21
NM_001753	CAV1	CAV1,caveolin 1, caveolae protein, 22 kDa	-1.68	1.27E-06
NM_173624	FLJ40504	FLJ40504,MGC138231,MGC138233	-1.68	4.83E-08
NM_172229	KREMEN2	KREMEN2,KRM2,MGC10791,MGC16709	-1.68	7.79E-12
NM_006366	CAP2	CAP2,adenylyl cyclase-associated protein 2	-1.68	5.18E-09
NM_001831	CLU	CLU,clusterin (complement lysis inhibitor, SP-40,40, sulfated glycoprotein 2, testosterone-repressed prostate message 2, apolipoprotein J)	-1.68	1.99E-32
ENST00000330515	ENST00000330515	ENST00000330515	-1.68	7.23E-03
A_24_P153003	A_24_P153003	A_24_P153003	-1.68	1.91E-11
NM_015996	SIDT2	SIDT2,CGI-40,FLJ90656,DKFZp686L17253	-1.68	5.53E-08
AL833897	AL833897	AL833897	-1.68	9.47E-03
BC046196	TGOLN2	TGOLN2,TGN38,TGN46,TGN48,TGN51,TTGN2,MGC14722	-1.69	5.37E-06
ENST00000316797	ENST00000316797	ENST00000316797	-1.69	6.08E-16
NM_018421	TBC1D2	TBC1D2,TBC1 domain family, member 2	-1.69	1.55E-33
AF277193	LSM12	LSM12,FLJ30656,MGC104211	-1.69	2.32E-39
AB007935	IGSF3	IGSF3,immunoglobulin superfamily, member 3	-1.69	9.59E-20
AK074645	APOL6	APOL6,APOL-VI,FLJ90164,MGC57495,DKFZp667M075	-1.69	2.00E-05
A_24_P281443	A_24_P281443	A_24_P281443	-1.69	1.40E-08
NM_018393	TCP11L1	TCP11L1,FLJ11336,FLJ11386,dJ85M6.3	-1.69	6.98E-17
ENST00000330088	ENST00000330088	ENST00000330088	-1.69	0.00E+00
A_24_P187355	A_24_P187355	A_24_P187355	-1.70	1.32E-11

ENST00000330461	ENST00000330461	ENST00000330461	-1.70	4.77E-15
A_24_P409420	A_24_P409420	A_24_P409420	-1.70	5.03E-17
NM_032208	ANTXR1	ANTXR1,ATR,TEM8,FLJ10601,FLJ11298,FLJ21776	-1.70	3.08E-07
NM_174887	IFT20	IFT20	-1.70	5.58E-20
NM_002284	KRTHB6	KRTHB6,HB6,Hb1,MNX,hHb6,KRTHB1	-1.70	1.16E-02
A_24_P401124	A_24_P401124	A_24_P401124	-1.70	2.40E-23
U28918	ST13	ST13,HIP,HOP,P48,AAG2,SNC6,HSPABP,FAM10A1,HSPABP1,PRO0786,FLJ27260,MGC129952	-1.70	8.33E-13
A_24_P247454	A_24_P247454	A_24_P247454	-1.70	1.44E-08
NM_182487	OLFML2A	OLFML2A,FLJ00237,PRO34319	-1.70	4.49E-07
A_24_P247303	A_24_P247303	A_24_P247303	-1.70	2.43E-21
A_24_P161733	A_24_P161733	A_24_P161733	-1.70	3.18E-07
ENST00000331037	ENST00000331037	ENST00000331037	-1.70	2.93E-17
ENST00000302335	ENST00000302335	ENST00000302335	-1.70	2.97E-12
A_24_P418216	A_24_P418216	A_24_P418216	-1.70	1.41E-17
ENST00000330116	ENST00000330116	ENST00000330116	-1.70	3.88E-19
BC033310	GDA	GDA,CYPIN,GUANASE,MGC9982,NEDASIN,KIAA1258	-1.70	2.73E-03
NM_001312	CRIP2	CRIP2,CRIP,CRP2,ESP1	-1.70	7.00E-05
NM_018375	SLC39A9	SLC39A9,FLJ11274,MGC74989	-1.70	3.02E-06
NM_153251	ZDHHC20	ZDHHC20,FLJ25952,MGC126005	-1.71	8.37E-11
A_24_P93321	A_24_P93321	A_24_P93321	-1.71	0.00E+00
NM_018685	ANLN	ANLN,Scraps,ANILLIN,DKFZp779A055	-1.71	5.55E-26
A_24_P383660	A_24_P383660	A_24_P383660	-1.71	9.09E-10
Y00706	COL4A1	COL4A1,arresten	-1.71	3.28E-06
NM_014290	TDRD7	TDRD7,KIAA1529,PCTAIRE2BP,RP11-508D10.1	-1.71	2.00E-05
NM_173473	C10orf104	C10orf104,FLJ33728,bA570G20.3	-1.71	5.73E-14
A_24_P584463	A_24_P584463	A_24_P584463	-1.71	9.40E-14
A_24_P6850	A_24_P6850	A_24_P6850	-1.71	2.45E-19
BC028735	LOC401431	LOC401431	-1.71	1.55E-10
AL109708	AL109708	AL109708	-1.72	9.00E-05
ENST00000305049	ENST00000305049	ENST00000305049	-1.72	1.05E-08
ENST00000333197	ENST00000333197	ENST00000333197	-1.72	6.91E-12
A_24_P264293	A_24_P264293	A_24_P264293	-1.72	5.23E-18
AF117819	BDKRB1	BDKRB1,B1R,BKR1,B1BKR,BKB1R,BRADYB1	-1.72	4.00E-05
NM_001151	SLC25A4	SLC25A4,T1,ANT,ANT1,PEO2,PEO3	-1.72	1.63E-19
NM_007173	PRSS23	PRSS23,SIG13,SPUVE,ZSIG13,MGC5107	-1.72	1.83E-17
NM_021197	WFDC1	WFDC1,PS20	-1.72	1.73E-07

NM_007085	FSTL1	FSTL1,follistatin-like 1	-1.72	1.77E-10
NM_002534	OAS1	OAS1,OIAS,IFI-4,OIASI	-1.72	8.00E-05
ENST00000320079	ENST00000320079	ENST00000320079	-1.72	1.39E-12
AK024926	DDAH1	DDAH1,dimethylarginine dimethylaminohydrolase 1	-1.72	7.09E-03
AF086541	LOC92196	LOC92196	-1.72	5.50E-04
NM_006106	YAP1	YAP1,YAP,YAP2,YAP65	-1.73	2.20E-04
A_32_P140501	A_32_P140501	A_32_P140501	-1.73	2.64E-09
Z97068	CYR61	CYR61,CCN1,GIG1,IGFBP10	-1.73	0.00E+00
A_24_P7021	A_24_P7021	A_24_P7021	-1.73	1.42E-13
NM_020826	SYT13	SYT13,KIAA1427	-1.73	2.11E-09
AK001616	FNBP1	FNBP1,FBP17,KIAA0554,MGC126804	-1.73	2.07E-10
NM_016571	GLULD1	GLULD1,LGS	-1.73	9.08E-03
AL831830	RAB11FIP4	RAB11FIP4,FLJ00131,KIAA1821,MGC11316,MGC126566,RAB11-FIP4	-1.73	1.36E-06
A_32_P193166	A_32_P193166	A_32_P193166	-1.73	2.07E-03
NM_001554	CYR61	CYR61,cysteine-rich, angiogenic inducer, 61	-1.73	1.20E-28
AK057293	TMEM76	TMEM76,FLJ22242,FLJ32731,DKFZp686G24175	-1.74	1.65E-08
NM_018475	TPARL	TPARL,TMPT27	-1.74	1.72E-43
BC042853	LOC645923	LOC645923	-1.74	6.56E-03
THC1852481	THC1852481	THC1852481	-1.74	9.34E-15
A_24_P306704	A_24_P306704	A_24_P306704	-1.74	5.75E-31
A_24_P341546	A_24_P341546	A_24_P341546	-1.74	2.02E-14
AF010447	MR1	MR1,HLALS	-1.74	1.28E-17
ENST00000333983	ENST00000333983	ENST00000333983	-1.74	1.63E-12
NM_012155	EML2	EML2,ELP70,EMAP2,EMAP-2	-1.74	1.16E-08
NM_057089	AP1S1	AP1S1,AP19,CLAPS1,SIGMA1A	-1.74	5.69E-20
NM_153012	TNFSF12	TNFSF12,APO3L,DR3LG,TWEAK,MGC20669,MGC129581	-1.74	9.46E-11
A_24_P358406	A_24_P358406	A_24_P358406	-1.75	1.93E-28
AK026668	UHMK1	UHMK1,KIS,Kist	-1.75	3.42E-24
NM_004318	ASPH	ASPH,BAH,HAAH,JCTN,junctin,CASQ2BP1	-1.75	1.13E-27
NM_002451	MTAP	MTAP,methylthioadenosine phosphorylase	-1.75	2.82E-26
NM_002006	FGF2	FGF2,fibroblast growth factor 2 (basic)	-1.75	8.93E-13
AK092522	ACOT4	ACOT4,PTE1B,PTE2B,PTE-Ib	-1.75	4.16E-06
A_24_P169843	A_24_P169843	A_24_P169843	-1.76	3.38E-19
AF131814	NPAL3	NPAL3,DJ462O23.2,RP3-462O23.3,DKFZp686E22155	-1.76	4.18E-03
ENST00000327852	ENST00000327852	ENST00000327852	-1.76	4.36E-11
XM_015334	XM_015334	XM_015334	-1.76	1.50E-22

NM_198473	NM_198473	NM_198473	-1.76	1.72E-26
A_24_P161827	A_24_P161827	A_24_P161827	-1.76	4.35E-06
NM_004481	GALNT2	GALNT2,UDP-N-acetyl-alpha-D-galactosamine:polypeptide N-acetylgalactosaminyltransferase 2 (GalNAc-T2)	-1.76	1.12E-26
NM_014506	TOR1B	TOR1B,DQ1,MGC4386	-1.76	1.53E-12
A_24_P7750	A_24_P7750	A_24_P7750	-1.76	1.34E-14
NM_004815	ARHGAP29	ARHGAP29,PARG1,RP11-255E17.1	-1.76	1.29E-13
THC1855826	THC1855826	THC1855826	-1.76	2.00E-06
NM_004293	GDA	GDA,CYPIN,GUANASE,MGC9982,NEDASIN,KIAA1258	-1.76	6.77E-12
A_24_P843309	A_24_P843309	A_24_P843309	-1.76	2.87E-22
AF003114	CYR61	CYR61,CCN1,GIG1,IGFBP10	-1.76	3.73E-39
NM_024956	TMEM62	TMEM62,FLJ23375	-1.76	2.71E-10
BC030949	PTPN11	PTPN11,CFC,NS1,SHP2,BPTP3,PTP2C,PTP-1D,SH-PTP2,SH-PTP3,MGC14433	-1.77	0.00E+00
AK095896	LOC340061	LOC340061	-1.77	1.54E-21
AF161372	HSPC254	HSPC254	-1.77	2.34E-06
A_24_P195974	A_24_P195974	A_24_P195974	-1.77	3.92E-14
THC1869247	THC1869247	THC1869247	-1.77	8.55E-03
NM_006402	HBXIP	HBXIP,XIP,MGC71071	-1.77	1.21E-22
THC1958020	THC1958020	THC1958020	-1.78	8.92E-16
AL834493	TMEM135	TMEM135,FLJ22104	-1.78	2.41E-13
NM_145306	C10orf35	C10orf35	-1.78	2.15E-08
NM_017855	ODAM	ODAM,APIN,FLJ20513	-1.78	4.63E-03
NM_175834	KRT6L	KRT6L,FLJ26646	-1.78	1.51E-17
NM_006793	PRDX3	PRDX3,peroxiredoxin 3	-1.78	2.10E-15
NM_003544	HIST1H4B	HIST1H4B,H4/I,H4FI	-1.78	1.94E-10
A_24_P890995	A_24_P890995	A_24_P890995	-1.78	9.68E-10
THC1953344	THC1953344	THC1953344	-1.79	2.97E-11
BC040993	KIAA1458	KIAA1458,FLJ21611	-1.79	5.21E-10
A_24_P15973	A_24_P15973	A_24_P15973	-1.79	2.15E-19
AK075319	FAM63B	FAM63B,KIAA1164	-1.79	2.67E-09
A_24_P358474	A_24_P358474	A_24_P358474	-1.79	9.45E-23
A_24_P247074	A_24_P247074	A_24_P247074	-1.80	2.92E-13
BM926140	BM926140	BM926140	-1.81	1.40E-04
THC1901760	THC1901760	THC1901760	-1.81	3.87E-06
NM_020373	TMEM16B	TMEM16B,C12orf3,DKFZp434P102	-1.81	2.00E-05
A_24_P306644	A_24_P306644	A_24_P306644	-1.81	3.20E-24
NM_004925	AQP3	AQP3,GIL	-1.82	0.00E+00

NM_139241	FGD4	FGD4,FRABP,FRABIN,ZFYVE6,MGC57222,DKFZp313E1818	-1.82	5.34E-10
NM_002195	INSL4	INSL4,EPIL,PLACENTIN	-1.82	2.28E-06
NM_004074	COX8	COX8,cytochrome c oxidase subunit VIII	-1.83	1.05E-20
NM_020216	RNPEP	RNPEP,DKFZP547H084	-1.83	8.10E-19
THC1972202	THC1972202	THC1972202	-1.83	5.70E-03
NM_012137	DDAH1	DDAH1,DDAH,FLJ21264,FLJ25539	-1.83	9.34E-07
X07109	PRKCB1	PRKCB1,PKCB,PRKCB,PRKCB2,MGC41878,PKC-beta	-1.83	2.47E-02
NM_012342	NMA	NMA,putative transmembrane protein	-1.84	1.01E-12
BC032478	MAP2K3	MAP2K3,MEK3,MKK3,MAPKK3,PRKMK3	-1.84	7.51E-12
BC052560	LOC387763	LOC387763	-1.84	1.04E-06
NM_006120	HLA-DMA	HLA-DMA,major histocompatibility complex, class II, DM alpha	-1.84	1.15E-10
NM_014583	LMCD1	LMCD1	-1.84	2.20E-12
NM_153290	FAM10A4	FAM10A4	-1.85	1.91E-15
NM_032578	MYOP	MYOP,sarcomeric protein myopalladin, 145 kDa	-1.85	4.66E-03
NM_005576	LOXL1	LOXL1,LOL,LOXL	-1.85	8.40E-04
NM_016203	PRKAG2	PRKAG2,AAKG,WPWS,AAKG2,H91620p	-1.86	0.00E+00
A_24_P375076	A_24_P375076	A_24_P375076	-1.86	8.86E-19
BC038556	BC038556	BC038556	-1.86	3.87E-21
A_24_P315594	A_24_P315594	A_24_P315594	-1.86	7.70E-10
NM_020151	STARD7	STARD7,GTT1	-1.87	2.12E-25
ENST00000301446	ENST00000301446	ENST00000301446	-1.87	2.96E-18
D13540	PTPN11	PTPN11,CFC,NS1,SHP2,BPTP3,PTP2C,PTP-1D,SH-PTP2,SH-PTP3,MGC14433	-1.87	2.98E-11
NM_138453	RAB3C	RAB3C	-1.87	2.03E-06
NM_152420	C9orf41	C9orf41,FLJ25795	-1.87	2.39E-10
NM_138444	KCTD12	KCTD12,PFET1,C13orf2,KIAA1778	-1.87	2.92E-30
NM_003480	MAGP2	MAGP2,Microfibril-associated glycoprotein-2	-1.87	7.76E-11
THC1914617	THC1914617	THC1914617	-1.88	1.00E-05
NM_033664	CDH11	CDH11,OB,CAD11,CDHOB,OSF-4	-1.88	3.68E-07
NM_015176	FBXO28	FBXO28,Fbx28,FLJ10766,KIAA0483	-1.89	4.07E-03
NM_152330	FRMD6	FRMD6,EX1,Willin,C14orf31,MGC17921,c14_5320	-1.89	1.12E-21
NM_000218	KCNQ1	KCNQ1,LQT,RWS,WRS,LQT1,SQT2,ATFB1,JLNS1,KCNA8,KCNA9,Kv1.9,Kv7.1,KVLQT1,FLJ26167	-1.89	1.71E-10
NM_016619	PLAC8	PLAC8,C15,onzin	-1.89	7.97E-16
NM_005590	MRE11A	MRE11A,ATLD,HNGS1,MRE11,MRE11B	-1.89	3.38E-09
AL117511	C14orf125	C14orf125,MGC72028,DKFZp781E083	-1.89	1.53E-03
AK092716	PRKAG2	PRKAG2,AAKG,WPWS,AAKG2,H91620p	-1.89	2.21E-25
ENST00000324460	ENST00000324460	ENST00000324460	-1.90	2.39E-11

BC029662	C20orf142	C20orf142,MGC30135,dJ881L22.2	-1.91	4.83E-22
XM_372991	LOC391540	LOC391540	-1.91	6.36E-30
NM_152344	LSM12	LSM12,FLJ30656,MGC104211	-1.91	0.00E+00
M86492	GMFB	GMFB,GMF	-1.92	2.17E-09
NM_004105	EFEMP1	EFEMP1,EGF-containing fibulin-like extracellular matrix protein 1	-1.92	1.84E-17
BC010946	TAGLN	TAGLN,SM22,SMCC,TAGLN1,WS3-10,DKFZp686P11128	-1.92	1.42E-07
AF188611	HSPA5	HSPA5,BIP,MIF2,GRP78,FLJ26106	-1.92	9.98E-13
BC015977	BC015977	BC015977	-1.93	1.35E-06
THC1808546	THC1808546	THC1808546	-1.93	6.16E-24
XM_208058	LOC283247	LOC283247	-1.93	2.82E-02
NM_021101	CLDN1	CLDN1,CLD1,SEMP1,ILVASC	-1.93	4.68E-16
NM_024636	STEAP4	STEAP4,TIARP,STAMP2,TNFAIP9,FLJ23153,DKFZp666D049	-1.95	7.50E-08
NM_199324	OTUD4	OTUD4,HIN1,HSHIN1,KIAA1046,DKFZp434I0721	-1.95	3.20E-04
NM_002017	FLI1	FLI1,Friend leukemia virus integration 1	-1.95	1.57E-09
AK057075	TPD52	TPD52,D52,N8L,PC-1,PrLZ,hD52	-1.95	4.12E-08
NM_024628	SLC12A8	SLC12A8,CCC9,FLJ23188,DKFZp686L18248	-1.96	9.95E-15
NM_145110	MAP2K3	MAP2K3,MEK3,MKK3,MAPKK3,PRKMK3	-1.96	4.00E-10
AK057669	PURB	PURB,PURBETA,MGC126784,MGC126786	-1.96	1.34E-31
NM_003330	TXNRD1	TXNRD1,thioredoxin reductase 1	-1.96	0.00E+00
A_32_P149416	A_32_P149416	A_32_P149416	-1.97	2.31E-27
NM_003186	TAGLN	TAGLN,transgelin	-1.97	6.21E-03
AK024669	WDR26	WDR26,MIP2,FLJ21016	-1.97	2.12E-18
AK000311	CRKL	CRKL	-1.98	5.53E-28
AB028952	SYNPO	SYNPO,KIAA1029	-1.98	2.83E-07
NM_152780	FLJ14503	FLJ14503,MGC104944,RP11-393H10.2	-1.98	2.63E-06
NM_017977	AIM1L	AIM1L,FLJ10040	-1.98	1.00E-05
ENST00000332472	ENST00000332472	ENST00000332472	-1.99	5.18E-37
AK026351	PRKAR2A	PRKAR2A,PKR2,PRKAR2,MGC3606	-1.99	4.83E-30
NM_012242	DKK1	DKK1,SK,DKK-1	-1.99	4.67E-11
NM_021213	PCTP	PCTP,STARD2	-2.02	3.86E-08
BC018117	TPD52	TPD52,D52,N8L,PC-1,PrLZ,hD52	-2.02	1.59E-17
NM_014452	TNFRSF21	TNFRSF21,DR6,BM-018,MGC31965	-2.02	4.37E-10
AF228738	PFN2	PFN2,PFL,D3S1319E	-2.02	2.36E-09
NM_005610	RBBP4	RBBP4,NURF55,RBAP48	-2.02	1.74E-09
M12996	G6PD	G6PD,G6PD1	-2.02	1.10E-13
NM_001299	CNN1	CNN1,SMCC,Sm-Calp	-2.03	2.90E-02

NM_001956	EDN2	EDN2,endothelin 2	-2.05	1.76E-02
NM_002543	OLR1	OLR1,oxidised low density lipoprotein (lectin-like) receptor 1	-2.06	7.00E-05
NM_021102	SPINT2	SPINT2,serine protease inhibitor, Kunitz type, 2	-2.07	3.58E-03
BC018548	FBXL17	FBXL17,Fbl17,Fbx13,FBXO13,DKFZp434C1715	-2.07	3.12E-09
NM_021955	GNGT1	GNGT1,GNG1	-2.08	2.80E-45
AB002445	DCP2	DCP2,NUDT20,FLJ33245	-2.08	2.24E-07
NM_014766	SCRN1	SCRN1,SES1,KIAA0193	-2.08	1.56E-11
NM_012095	AP3M1	AP3M1,MGC22164	-2.09	4.49E-16
AF088076	AF088076	AF088076	-2.10	1.28E-06
AK025336	MYO5B	MYO5B,myosin,KIAA1119	-2.12	1.48E-18
X92098	TMED2	TMED2,P24A,RNP24,FLJ21323	-2.12	7.79E-20
NM_005556	KRT7	KRT7,keratin 7	-2.13	0.00E+00
NM_007236	CHP	CHP,SLC9A1BP	-2.15	1.35E-09
NM_018662	DISC1	DISC1,SCZD9,KIAA0457	-2.15	3.89E-07
NM_032837	FAM104A	FAM104A,FLJ14775	-2.15	3.21E-31
NM_001979	EPHX2	EPHX2,epoxide hydrolase 2, cytoplasmic	-2.15	2.15E-16
NM_006148	LASP1	LASP1,MLN50,Lasp-1	-2.15	3.43E-36
AF068868	TNFRSF21	TNFRSF21,DR6,BM-018,MGC31965	-2.16	2.87E-23
NM_152331	ACOT4	ACOT4,PTE1B,PTE2B,PTE-Ib	-2.16	1.65E-34
NM_004661	CDC23	CDC23,CDC23 (cell division cycle 23, yeast, homolog)	-2.17	0.00E+00
THC1900459	THC1900459	THC1900459	-2.17	1.04E-03
NM_002354	TACSTD1	TACSTD1,tumor-associated calcium signal transducer 1	-2.17	5.88E-03
NM_018050	MANSC1	MANSC1,FLJ10298,LOH12CR3,9130403P13Rik	-2.18	2.48E-36
NM_006815	TMED2	TMED2,P24A,RNP24,FLJ21323	-2.20	1.36E-12
AK022936	CNIH	CNIH,CNIL,CNIH1,TGAM77,MGC117156	-2.20	4.94E-13
NM_012106	BART1	BART1,binder of Arl Two	-2.20	3.09E-28
THC1820486	THC1820486	THC1820486	-2.21	4.18E-17
NM_003280	TNNC1	TNNC1,TNC,TNNC	-2.21	1.90E-04
M13975	PRKCB1	PRKCB1,PKCB,PRKCB,PRKCB2,MGC41878,PKC-beta	-2.22	2.27E-03
NM_022917	NOL6	NOL6,NRAP,UTP22,FLJ21959,MGC14896,MGC14921,MGC20838,bA311H10.1	-2.23	1.10E-33
AI970688	TAGLN	TAGLN,SM22,SMCC,TAGLN1,WS3-10,DKFZp686P11128	-2.23	5.33E-22
NM_016399	TRIAP1	TRIAP1,WF-1,P53CSV,HSPC132	-2.25	6.90E-36
NM_001613	ACTA2	ACTA2,actin, alpha 2, smooth muscle, aorta	-2.25	3.40E-02
NM_012219	MRAS	MRAS,M-RAs,RRAS3,R-RAS3	-2.25	1.59E-40
AF077199	LYPLA1	LYPLA1,LPL1,APT-1,LYSOPLA	-2.26	0.00E+00
AK057223	LOC647589	LOC647589	-2.27	4.69E-02

X89674	OR1C1	OR1C1,OR1-42,TPCR27,HSTPCR27	-2.31	4.64E-02
NM_173216	ST6GAL1	ST6GAL1,CD75,SIAT1,ST6Gall,MGC48859,ST6Gal I	-2.32	4.73E-20
THC1851133	THC1851133	THC1851133	-2.32	5.40E-04
NM_199511	CCDC80	CCDC80,URB,DRO1,SSG1,MGC131805,MGC134851	-2.32	2.60E-21
AL080111	NEK7	NEK7	-2.36	1.71E-29
NM_004124	GMFB	GMFB,GMF	-2.36	4.73E-24
NM_000359	TGM1	TGM1,LI,LI1,TGK,ICR2,TGASE	-2.39	6.58E-14
BC011813	SHC1	SHC1,SHC,p66,SHCA,p52SHC,p66SHC,FLJ26504	-2.40	4.27E-06
AK074567	FLJ90086	FLJ90086	-2.41	3.55E-17
NM_004433	ELF3	ELF3,ERT,ESX,EPR-1,ESE-1	-2.42	1.89E-22
NM_053025	MYLK	MYLK,myosin, light polypeptide kinase	-2.44	9.37E-13
NM_152588	TMTC2	TMTC2,DKFZp762A217	-2.51	2.84E-26
NM_153687	IKIP	IKIP,FLJ31051	-2.58	0.00E+00
A_32_P199736	A_32_P199736	A_32_P199736	-2.62	9.45E-06
NM_019556	MOSPD1	MOSPD1,DJ473B4	-2.65	1.22E-32
NM_001562	IL18	IL18,interleukin 18 (interferon-gamma-inducing factor)	-2.69	4.26E-32
NM_003881	WISP2	WISP2,WNT1 inducible signaling pathway protein 2	-2.70	3.98E-11
A_24_P853366	A_24_P853366	A_24_P853366	-2.71	2.94E-13
NM_032405	TMPRSS3	TMPRSS3,DFNB8,DFNB10,ECHOS1,TADG12	-3.02	1.68E-15
AK098698	EID3	EID3	-3.13	2.56E-16
NM_005130	HBP17	HBP17,heparin-binding growth factor binding protein	-3.23	1.19E-11
NM_019000	FLJ20152	FLJ20152,hypothetical protein FLJ20152	-3.49	2.92E-28
NM_003029	SHC1	SHC1,SHC (Src homology 2 domain containing) transforming protein 1	-3.63	6.34E-03
NM_005025	SERPINI1	SERPINI1,serine (or cysteine) proteinase inhibitor, clade I (neuroserpin), member 1	-4.02	1.27E-31

Table 6-4. qRT-PCR results table. List showing the real-time quantitative values (RQ) and significance analysis of 10 genes selected for further experimental verification. Values are graphically represented in Figure 3-25.

Sample name	Gene	RQ 1	RQ 2	RQ 1 Min	RQ 1 Max	RQ 2 Min	RQ 2 Max	Mean RQ	SE	p-value[a]
HeLa + *C. trachomatis*	TEK	1.000	1.000	0.588	1.702	0.542	1.844	1.000	0.000	n.d.
HeLa + *C. trachomatis*	BMF	1.000	1.000	0.506	1.975	0.654	1.530	1.000	0.000	0.028
HeLa + *C. trachomatis*	EGR1	1.000	1.000	0.581	1.721	0.528	1.895	1.000	0.000	0.877
HeLa + *C. trachomatis*	FST	1.000	1.000	0.620	1.613	0.697	1.435	1.000	0.000	0.346
HeLa + *C. trachomatis*	PHLDA	1.000	1.000	0.422	2.371	0.534	1.873	1.000	0.000	0.015
HeLa + *C. trachomatis*	CXCL1	1.000	1.000	0.562	1.781	0.632	1.583	1.000	0.000	0.183
HeLa + *C. trachomatis*	DKK1	1.000	1.000	0.725	1.379	0.771	1.297	1.000	0.000	0.003

HeLa + *C. trachomatis*	SDC4	1.000	1.000	0.813	1.231	0.759	1.318	1.000	0.000	0.976
HeLa + *C. trachomatis*	MAP2K3	n.d.	1.000	n.d.	n.d.	0.615	1.627	n.d.	n.d.	n.d.
HeLa + *C. trachomatis*	FLI1	1.000	1.000	1.000	1.000	0.506	1.976	1.000	0.000	0.003
HeLa - *C. trachomatis*	TEK	0.329	n.d.	0.220	0.493	n.d.	n.d.	n.d.	n.d.	n.d.
HeLa - *C. trachomatis*	BMF	2.853	2.308	2.084	3.906	0.994	5.361	2.581	0.273	0.028
HeLa - *C. trachomatis*	EGR1	0.496	1.354	0.365	0.674	0.412	4.453	0.925	0.429	0.877
HeLa - *C. trachomatis*	FST	0.288	0.928	0.216	0.384	0.390	2.207	0.608	0.320	0.346
HeLa - *C. trachomatis*	PHLDA	0.729	0.651	0.534	0.994	0.229	1.848	0.690	0.039	0.015
HeLa - *C. trachomatis*	CXCL1	0.753	0.917	0.510	1.113	0.567	1.486	0.835	0.082	0.183
HeLa - *C. trachomatis*	DKK1	0.168	0.252	0.109	0.257	0.116	0.548	0.210	0.042	0.003
HeLa - *C. trachomatis*	SDC4	1.465	0.502	1.262	1.702	0.298	0.844	0.984	0.482	0.976
HeLa - *C. trachomatis*	MAP2K3	n.d.	n.d.	n.d.	n.d.	n.d.	n.d.	n.d.	n.d.	n.d.
HeLa - *C. trachomatis*	FLI1	0.293	0.214	0.213	0.402	0.122	0.376	0.253	0.039	0.003
HeLa SHC1KD + *C. trachomatis*	TEK	1.000	1.000	0.550	1.819	0.201	0.664	1.000	0.000	0.152
HeLa SHC1KD + *C. trachomatis*	BMF	1.000	1.000	0.545	1.834	0.787	2.647	1.000	0.000	0.021
HeLa SHC1KD + *C. trachomatis*	EGR1	1.000	1.000	0.542	1.844	2.299	7.815	1.000	0.000	0.003
HeLa SHC1KD + *C. trachomatis*	FST	1.000	1.000	0.545	1.834	0.773	2.600	1.000	0.000	0.674
HeLa SHC1KD + *C. trachomatis*	PHLDA	1.000	1.000	0.530	1.887	1.319	4.697	1.000	0.000	0.038
HeLa SHC1KD + *C. trachomatis*	CXCL1	1.000	1.000	0.388	2.577	0.650	4.319	1.000	0.000	0.372
HeLa SHC1KD + *C. trachomatis*	DKK1	1.000	1.000	0.831	1.203	0.788	1.141	1.000	0.000	0.008
HeLa SHC1KD + *C. trachomatis*	SDC4	1.000	1.000	0.869	1.151	0.588	0.779	1.000	0.000	0.277
HeLa SHC1KD + *C. trachomatis*	MAP2K3	1.000	1.000	0.583	1.715	0.717	2.108	1.000	0.000	0.213
HeLa SHC1KD + *C. trachomatis*	FLI1	1.000	1.000	0.612	1.634	0.246	0.656	1.000	0.000	0.398
HeLa Luci KD + *C. trachomatis*	TEK	0.890	0.715	0.404	1.265	0.147	0.462	0.802	0.087	0.152
HeLa Luci KD + *C. trachomatis*	BMF	0.402	0.195	0.099	0.384	0.143	0.555	0.298	0.103	0.021
HeLa Luci KD + *C. trachomatis*	EGR1	0.383	0.314	0.215	0.457	0.912	1.938	0.348	0.035	0.003
HeLa Luci KD + *C. trachomatis*	FST	0.397	1.208	0.670	2.177	0.951	3.086	0.802	0.406	0.674
HeLa Luci KD + *C. trachomatis*	PHLDA	0.519	0.680	0.495	0.934	1.232	2.326	0.599	0.080	0.038
HeLa Luci KD + *C. trachomatis*	CXCL1	0.694	0.980	0.551	1.741	0.924	2.917	0.837	0.143	0.372
HeLa Luci KD + *C. trachomatis*	DKK1	1.823	1.688	1.195	2.384	1.133	2.260	1.756	0.068	0.008
HeLa Luci KD + *C. trachomatis*	SDC4	2.377	1.266	0.818	1.959	0.554	1.326	1.822	0.556	0.277
HeLa Luci KD + *C. trachomatis*	MAP2K3	1.872	1.250	0.618	2.527	0.760	3.107	1.561	0.311	0.213
HeLa Luci KD + *C. trachomatis*	FLI1	1.926	1.029	0.658	1.610	0.264	0.646	1.478	0.448	0.398

[a] p-value according to Student's *t* test

6.2 Abbreviations

5(6)-TAMRA, 5-(and 6)-carboxytetramethylrhodamine; A, activation; AC, cytoplasmic ancillary proteins; ADT, AutoDockTools; AIDA, Advanced Image Data Analyzer; $A_{\lambda\ [nm]}$, absorbance; APAF-1, apoptosis activating factor-1; ATCC, American Type Culture Collection; b-FA, *Chlamydia*-derived branched fatty acid; bp, basepair; BSA, bovine serum albumin; CagA, cytotoxicity associated gene A; cDNA, complementary DNA; CH1, collagen-homology domain 1; CK18, cytokeratin 18; CL, cardiolipin; COX2, cyclooxygenase 2; cPLA2, cytosolic phospholipase A2; CRLS1, cardiolipin synthase 1; Cy, cyanine; Da, Dalton; DAG, diacylglycerol; ddH_2O, double-distilled H_2O; ΔG, free energy of binding; DHSM, dihydrosphingomyelin; DMEM, Dulbecco's modified Eagle's medium; E, biomacromolecular target; E, expression; EB, elementary body; EGF, epidermal growth factor; eGFP, enhanced green fluorescent protein; EGFR, EGF receptor; EMBL-EBI, European Bioinformatics Institute; EPEC, enteropathogenic *Escherichia coli*; ERK, extracellular signal-regulated kinase; ESI, electrospray ionization; F_0, background fluorescence; FASL, FAS ligand; FCS, fetal calf serum; F_{max}, maximum fluorescence at saturation; F_{obs}, observed fluorescence; GC, guanine-cytosine content; GRB2, growth factor receptor-bound protein 2; GST, glutathione S-transferase; HEPES, 4-(2-hydroxyethyl)-1-piperazineethanesulfonic acid; HM, host membrane; HPLC, high-performance liquid chromatography; HRP, horseradish peroxidase; Hsp60, heat shock protein 60; I, ligand; IFNγ, interferon gamma; IFU, inclusion forming unit; IgG, immunoglobulin G; IL-8, interleukin-8; IM, bacterial inner membrane; IPA, Ingenuity Pathway Analysis; K_D, equilibrium dissociation constant; KD, knockdown; KEGG, Kyoto Encyclopedia of Genes and Genomes; Lda, lipid droplet-associated protein; LGV, Lymphogranuloma venereum; LO, localization; LPC, lysophosphatidylcholine; Luci, luciferase; MALDI-TOF, matrix-assisted laser desorption/ionization time-of-flight; MAPK, mitogen-activated protein kinase; MB, group/complex membership; MEK, MAPK/ERK kinase; MOI, multiplicity of infection; mRNA, messenger RNA; MS, mass spectrometry; MTOC, microtubule-organizing center; MVB, multivesicular body; m/z, mass-to-charge ratio; NC, needle complex; NCBI, National Center for Biotechnology Information; NCK, non-catalytic region of tyrosine kinase adaptor protein; n.d., not determined; NF-κB, nuclear factor κB; NK cell, natural killer cell; OM, bacterial outer membrane; OMP1, outer membrane protein 1; P, phosphorylation/dephosphorylation; PA, phosphatidic acid; PAGE, polyacrylamide gel electrophoresis; PARP, poly (ADP-ribose) polymerase; PB, persistent body; PBS, phosphate buffered saline; PC, phosphatidylcholine; PD, protein-DNA binding; PDB, Protein Data Bank; PE, phosphatidylethanolamine; [pep], peptide concentration; PFA, paraformaldehyde; PG, phosphatidylglycerol; *p.i.*, *post infectionem*; PI, phosphatidylinositol; PI3K, phosphatidylinositol 3-kinase; PID, pelvic inflammatory disease; PKCδ, protein kinase Cδ; PL,

phospholipid; PLA1, phospholipase A1; PP, bacterial periplasm; PP, protein-protein binding; PS, phosphatidylserine; PTB, phosphotyrosine binding; qRT-PCR, quantitative real-time polymerase chain reaction; RB, regulation of binding; RB, reticulate body; RBD, RAS binding domain; RQ, real-time quantitative value; RT, room temperature; RTK, receptor tyrosine kinase; SD, standard deviation; SDS, sodium dodecyl sulfate; SE, standard error; SH2, SRC homology 2; SH3, SRC homology 3; SHC, SRC homology-containing; siRNA, small interfering RNA; SM, sphingomyelin; SOCS, suppressors of cytokine signaling; SPG buffer, sucrose phosphate glutamate buffer; SRC, sarcoma; STAT, signal transducers and activator of transcription; STD, sexually transmitted disease; T, transcription; TAG, triacylglycerol; Tarp, translocated actin-recruiting phosphoprotein; Tarp $L2_1$, singly phosphorylated Tarp L2; Tarp $L2_2$, doubly phosphorylated Tarp L2; TC, tip complex; Tir, translocated intimin receptor; TLC, thin-layer chromatography; T_m, melting temperature; TNFα, tumor necrosis factor alpha; TNFR1, TNF receptor 1; TR, translocation; Tr, translocator complex; TUNEL, terminal deoxynucleotidyl transferase dUTP nick end labeling; v/v, volume per volume; vol., volume; vs., versus; w/v, weight per volume.

6.3 List of figures

6.4 List of tables

6.5 Acknowledgments

First of all, I am most grateful to Prof. Dr. Thomas F. Meyer for giving me the excellent opportunity to work under his supervision and for scientific discussions, helpful suggestions and critical evaluation of my work.

I am deeply indebted to Dr. Adrian Mehlitz for his constant supervision, numerous fruitful discussions and ideas, and his motivating support in becoming an independent scientist.

I would like to thank Dr. Michele Lunelli (Department of Cellular Microbiology) for assistance in performing the docking simulations, Dr. Hans-Joachim Mollenkopf and Ina Wagner (Microarray Core Facility) for help with the DNA microarray experiments, and Dr. Beate Fuchs, PD Dr. Jürgen Schiller, and Rosmarie Süß (Institute of Medical Physics and Biophysics, University of Leipzig) for conducting the lipid measurements.

I am very grateful to Dr. Mirjana Kessler and Dr. Lesley A. Ogilvie for proofreading the manuscript.

Furthermore, I want to thank Prof. Dr. Mark R. Philips (Department of Cell Biology, NYU Langone Medical Center) for giving me the opportunity to visit his lab and providing me with the technique for monitoring RAS activation.

Finally, I want to express my sincere thanks to all my colleagues and friends in the Department of Molecular Biology for their support, scientific input, and the friendly and inspiring working atmosphere.

6.6 Publications

Banhart S.*, Mehlitz A.*, Mäurer A.P., Kaushansky A., Gordus A.G., Zielecki J., MacBeath G., Meyer T.F. 2010. Tarp regulates early *Chlamydia*-induced host cell survival through interactions with the human adaptor protein SHC1. *J Cell Biol*. 190(1):143-57. (* equal contribution)

Mehlitz A., **Banhart S.**, Hess S., Selbach M., Meyer T.F. 2008. Complex kinase requirements for *Chlamydia trachomatis* Tarp phosphorylation. *FEMS Microbiol Lett*. 289(2):233-40.

Banhart S., Mehlitz A., Fuchs B., Schiller J., Heuer, D., Meyer, T.F. Global lipid analysis reveals essential role of cardiolipin synthase 1 for *Chlamydia* replication. (in preparation)

Mehlitz A., **Banhart S.**, Rudel T., Meyer T.F. Tarp/PLCγ interaction and its role during *Chlamydia* infection. (in preparation)

Berlin, September 2011 Sebastian Banhart

6.7 Selbständigkeitserklärung

Hiermit erkläre ich, dass ich die vorliegende Arbeit selbständig und nur mit den angegebenen Hilfsmitteln erstellt habe.

Berlin, September 2011 Sebastian Banhart